KU LEUVEN

ARENBERG DOCTORAL SCHOOL
Faculty of Engineering Science

Machine learning approaches for ambulatory electrocardiography signal processing

Alexander Alexeis Suárez León

Supervisors:
Prof. dr. ir. Carlos Román Vázquez Seisdedos
Prof. dr. ir. Sabine Van Huffel

Dissertation presented in partial fulfillment of the requirements for the degree of Doctor of Engineering Science (PhD)

December 2018

Machine learning approaches for ambulatory electrocardiography signal processing

Alexander Alexeis SUÁREZ LEÓN

Examination committee:
Prof. dr. ir. Patrick Wollant, chair
Prof. dr. ir. Carlos Román Vázquez Seisdedos, supervisor
Prof. dr. ir. Sabine Van Huffel, supervisor
Prof. dr. MD. Rik Willems
Prof. dr. ir. Lieven De Lathauwer
Prof. dr. ir. Enrique Juán Marañón Reyes
Prof. dr. ir. Jef Vandemeulebroucke
(Department of Electronics and Informatics, Vrije Universiteit, Brussel)

Dissertation presented in partial fulfillment of the requirements for the degree of Doctor of Engineering Science (PhD)

December 2018

© 2018 KU Leuven – Faculty of Engineering Science
Uitgegeven in eigen beheer, Alexander Alexeis Suárez León, Kasteelpark Arenberg 10 box 2446, B-3001 Leuven (Belgium)

Alle rechten voorbehouden. Niets uit deze uitgave mag worden vermenigvuldigd en/of openbaar gemaakt worden door middel van druk, fotokopie, microfilm, elektronisch of op welke andere wijze ook zonder voorafgaande schriftelijke toestemming van de uitgever.

All rights reserved. No part of the publication may be reproduced in any form by print, photoprint, microfilm, electronic or any other means without written permission from the publisher.

Acknowledgments

First and foremost I want to thank my promotors Sabine Van Huffel and Carlos R. Vázquez Seisdedos, who had the patience to support me during the Ph.D. I also want to thank all biomedians - guys, thanks a lot. Now, I would like to thank three persons who made this thesis possible: Caro, muchas gracias por todo, siempre estuviste ahí para ayudar, para dar el consejo y el apoyo oportuno. Griet, thank you very much for your support. You were my first buddy in BioMed. I will never forget your help in those hard days. Yiss... ¿Qué puedo decir? Sólo agradecer todo, la compañía, el apoyo y sobre todo haber compartido estas aventuras.

Agradecer a todos mis profesores, desde el pre-escolar hasta la universidad. I also want to thank my professors in KU Leuven: Prof. dr. MD. Rik Willems and from the Biomedical Data Processing II course, Prof. dr. ir. Lieven De Lathauwer and Prof. dr. ir. Bart Vanrumste.

Un agradecimiento especial para mis compañeros de trabajo en la universidad. Y a todas las personas que han puesto un mínimo de su esfuerzo para ayudar.

Finalmente, a mamá y papá, porque por ellos y para ellos soy. A mis hermanitas por el cariño. A Say, el Potato, Alexa y Alena. A Daguito. A mis poquititos pero inmensos amigos, Alex, Kike, Puig, Kiro, FRCC, NAR. Para el final dejo a mi muchacha mona la vampira damita (MMVD). Sí bebe, en esta tesis estás tú por todas partes y no me sorprende. Desde hace mucho tiempo eres así de importante en mi vida. Gracias por ser mi compañera de aventuras, mi guerrera y las luz sobre mis sombras.

Abstract

The ambulatory electrocardiography (AECG) records the ECG while the patient is doing real-life activities. It allows the study of transient phenomena and cases of fatal arrhythmic events, including sudden cardiac death. However, noise and artifacts can corrupt the AECG signal which downgrades the underlying diagnostic information. This research focuses on the development of new machine-learning-based methods for improving the processing of the AECG signal. The relevance of this topic resides on the fact that improved processing steps may lead to reliable markers, thereby decreasing the risk of an incorrect diagnostic.

The first topic addressed in this book is the problem of ectopic heartbeat detection in the AECG as preprocessing step for heart rate variability or QT interval analyses. In this context, supervised learning algorithms based on support vector machines were evaluated. The new algorithms use tensors and tensor decompositions to deal directly with multi-lead AECG recordings. This approach is effective and saves training time since only one classifier is trained for each record. Furthermore, high performances were obtained considering only small training sets.

The next step covered in this work is the detection of the T-wave end in the AECG. Here, supervised learning algorithms based on neural networks and support vector machines were evaluated. Then, a novel algorithm based on support vector machines is presented for detecting the T-wave end. The new approach does not require large datasets for training and includes a robust and effective algorithm for selecting the training set. Moreover, extended evaluation and comparison of the proposed approach against state-of-the-art techniques are presented and discussed. The results showed that the proposed algorithm outperforms the state-of-the-art methods.

Finally, this research presents a software tool for the analysis of the QT interval in the AECG. The software was developed for cardiologists and specialists,

and no programming skilss are needed. Since QT markers are related to risk stratification of suffering life-threatening arrhythmias and sudden cardiac death, this tool constitutes a useful input to QT analysis. In this context, it will be useful for supporting the research on ventricular repolarization analysis.

List of Abbreviations

Acc	Accuracy.
AECG	Ambulatory electrocardiogram.
APV	Active prototype vector.
AV	Atrioventricular.
BR	Bayesian regularization.
BW	Baseline wander.
CPD	Canonical polyadic decomposition.
CSA	Coupled simulated annealing.
CVD	Cardiovascular diseases.
DCT	Discrete cosine transformation.
DWT	Discrete wavelet transform.
ECG	Electrocadiogram.
EHB	Premature/Ectopic heartbeat detection block.
EW	Exponential weighting.
FIR	Finite impulse response.
FN	False negative.

FP	False positive.
FS-LSSVM	Fixed-size least-squares support sector machines.
GUI	Graphical user interface.
HR	Heart rate.
HRV	Heart rate variability.
IDWT	Inverse discrete wavelet transform.
IQR	Inter quartile range.
LQTS	Long QT syndrome.
LS-SVM	Least-squares support sector machines.
LW	Linear weighting.
MI	Myocardial infarction.
MLP	Multilayer perceptron.
MLSVD	Multilinear singular value decomposition.
MRE	Mean relative error.
MSE	Mean squared error.
NN	Neural networks.
P+	Positive predictive value.
PCA	Principal components analysis.
PNS	Parasympathetic nervous system.
PV	Prototype vector.
QTd	QT dispersion.
RES	Resampling i.e. downsampling.

SA Sinoatrial.

SCD Sudden cardiac death.

Se Sensitivity.

SNS Sympathetic nervous system.

Sp Specificity.

SQA Signal quality assessment.

SSE Sum of squared error.

ST-MLSVD Sequentially truncated multilinear singular value decomposition.

SVEB Supraventricular ectopic beat.

SVM Support vector machine.

TdP Torsade de Pointes.

TKMEANS Trimmed k-means.

TWA T-wave alternans.

VEB Ventricular ectopic beat.

VI Voting index.

VIav VI absolute value.

List of Symbols

δ_{ij}	Kronecker delta
μ_e	Sample mean of the Te error (Accuracy)
σ_e	Sample standard deviation of the Te error (Precision)
σ	Kernel RBF parameter
γ	Regularization parameter
$a, b, \alpha, \lambda, \ldots$	Scalars
$\mathbf{a}, \mathbf{b}, \ldots$	Vectors
$\mathbf{A}, \mathbf{B}, \ldots$	Matrices
$\mathcal{A}, \mathcal{B}, \ldots$	Tensors
$x[k], y[k], \ldots$	Discrete sequence
$\mathbf{A}(z), \mathbf{B}(z), \ldots$	Discrete transfer functions

Contents

Abstract iii

List of Abbreviations vii

Contents xi

List of Figures xv

List of Tables xix

1 Introduction 1

1.1 Relevance of cardiac monitoring 1

1.1.1 The surface electrocardiogram 2

1.1.2 Hearth rhythms 7

1.1.3 ECG clinical applications 9

1.2 Ambulatory ECG monitoring 10

1.2.1 Noise, interferences and artifacts in ambulatory electrocardiogram 11

1.2.2 Stages in processing and analysis of AECG 13

1.3 Analysis of time intervals in the ECG 14

1.3.1 Heart rate variability 14

1.3.2 QT interval analysis 15
1.4 Problem statement and objectives 16
1.5 Chapter-by-chapter overview and personal contribution 18
1.6 Collaborations 20
1.7 Conclusions 20

2 Machine learning methods **23**
2.1 Introduction 23
2.2 Feature extraction 24
2.2.1 Resampling 24
2.2.2 Discrete cosine transformation 25
2.2.3 Principal component analysis 25
2.2.4 Tensor and tensor decomposition 26
2.3 Unsupervised machine learning. Clustering 31
2.3.1 k-means algorithm 31
2.3.2 Truncated k-means algorithm 32
2.3.3 Heterogeneous clustering algorithm 32
2.4 Supervised machine learning 35
2.4.1 Neural networks 35
2.4.2 Support vector machines 36
2.4.3 Least-squares support vector machines 39
2.4.4 Fixed-size LSSVM 40
2.4.5 Hyper-parameter tuning 42
2.5 Conclusions 45

3 Premature heartbeat detection using tensors **47**
3.1 Introduction 47
3.2 Premature heartbeat detection using CPD 50

3.2.1 Materials and methods 50
3.2.2 Results 52
3.2.3 Discussion 56
3.2.4 Conclusions 58
3.3 Premature heartbeat detection using ST-MLSVD 58
3.3.1 Materials and methods 59
3.3.2 Results 61
3.3.3 Discussion 62
3.3.4 Conclusions 63
3.4 Conclusions 64

4 T-wave end detection using machine learning 65

4.1 Introduction 65
4.2 T-wave end detection using neural networks 67
4.2.1 Materials and methods 68
4.2.2 Results 69
4.2.3 Discussion 71
4.2.4 Conclusions 71
4.3 T-wave end detection using neural networks and support vector machines 72
4.3.1 Materials and methods 72
4.3.2 Results 79
4.3.3 Discussion 83
4.3.4 Conclusions 88
4.4 Conclusions 89

5 Tool for the analysis of ventricular repolarization 91

5.1 Introduction 91

5.2 Materials and methods 92
5.2.1 QTVI and QT dynamicity modules 96
5.3 Results 98
5.3.1 Tool test 103
5.4 Conclusions 110

6 Conclusions and future work **111**
6.1 Conclusions 111
6.2 Future work 113

A Examples of T-wave end detection in QTDB **115**

Bibliography **121**

Curriculum **135**

List of publications **137**

List of Figures

1.1 The heart's conduction system. (L/R)A is left/right atrium and (L/R)V corresponds to left/right ventricle [130]. 3

1.2 The normal ECG, waves and intervals. 4

1.3 An example of 12-lead ECG. The strip was extracted from the record I01 of the St. Petersburg INCART 12-lead Arrhythmia Database [38]. The first 6 seconds are shown using the LightWAVE software from Physionet. 5

1.4 Placement of electrodes for recording precordial leads. 6

1.5 Ectopic beats and arrhythmia examples (a) supraventricular ectopic beat (SVEB), the P wave is inverted in the highlighted area, (b) ventricular ectopic beat (VEB), (c) atrial flutter and (d) ventricular flutter. 8

1.6 Noise, interferences and artifacts that affect AECG, (a) baseline wander, (b) electrode motion artifacts, (c) power line interference and (d) EMG noise. 12

1.7 Simplified block diagram for an ambulatory ECG signal processing system. 13

1.8 Schematic chapter overview. 19

2.1 Decimation system structure, where d is the decimation factor and f_s is the original sampling frequency. 24

2.2 Cannonical polyadic decomposition (CPD) 28

2.3 ST-MLSVD approximation diagram, (a) ST-MLSVD given the core tensor and the processing order and (b) core tensor truncation procedure for different processing orders. 30

2.4 TKMEANS and TCLUST comparisson. 33

2.5 Multilayer perceptron (MLP) architecture 36

2.6 Different separating surfaces. 37

2.7 Support vector machine hyperplane in $\mathbb{R}^2$ space. Dashed lines represent cannonical hyperplanes. Circled objects corresponds to the support vectors. 38

2.8 Fixed-Size LSSVM construction stages. 41

3.1 A general approach for classifying heartbeats using the ECG. . 48

3.2 *Tensorization* process for a 12-lead ECG. 49

3.3 Heartbeat classification scheme using CPD and SVM. 50

3.4 Mean relative errors in a rank-R CPD ($1 \leq R \leq 20$), for all records in the database. Both dashed-lines represent the MRE average curve $\pm$ the sample standard deviation of the MRE for a given R. 52

3.5 Plot of feature components extracted from two recordings of the INCART database, h_1, h_2, h_3 correspond to the feature components in the heartbeat mode factor matrix, $\mathbf{H}$ (a) record 33 and (b) record 34. 56

3.6 Fragments of recordings with several PAC heartbeats (a) record 33 and (b) record 34. 57

3.7 Proposed approach for detecting premature heartbeats using ST-MLSVD. 59

4.1 Heartbeat segmentation method for detetcting the T wave end. 68

4.2 General description of the experiment using MLP-based Te detectors. 68

4.3 Distribution of the precision in the evaluation set for each feature extraction method. 70

4.4 General workflow for training and testing for the Te detection algorithm. 72

4.5 Criteria for selecting the number of input units, (a) total mean squared error (MSE) in the reconstruction of the data using u components and (b) and trade-off Complexity-MSE ($C(u)$). In order to clarify the interval of interest only the first 50 values of both, MSE(u) and $C(u)$ criteria are drawn. 75

4.6 DCT reconstruction of an annotated beat from QTDB (record sel102, first heartbeat) using 13 components (a) segment of interest for detecting Te (b) the original segment (gray continuous line) and the 13-components DCT reconstructed segment (black dash-dotted line). 76

4.7 Performance of MLP based Te detection algorithms with random, k-means, trimmed k-means (TKMEANS) and TCLUST training set selection strategies, (a) accuracy and (b) precision. 80

4.8 Precision for TKMEANS (white) and TCLUST (black) algorithms with respect to (a) the number of clusters and (b) the training set size. 81

4.9 Performance indexes for random (white) and Rényi entropy (black) selection strategies, (a) accuracy and (b) precision . . . 82

4.10 Comparison between methods, TKMEANS+MLP, TCLUST+MLP and RE + FS-LSSVM, (a) accuracy and (b) precision. 86

5.1 PyECG general workflow. Preprocessing and lead selection stages of the software. SQA and EHB are the signal quality assessment and the ectopic heartbeats detection blocks respectively. 93

5.2 Voting index (VI) based on the relative values of the six quality indexes from both leads. The sign indicates the lead as follows, (+) lead A and (-) lead B. The absolute value corresponds to the difference in the voting process, (6) unanimity, (4) majority, (2) minimum majority and (0) tie. 95

5.3 QTVI module workflow. 97

5.4 QT dynamicity analysis module workflow. 97

5.5 PyECG user interface, main menu and toolbar. 99

5.6 R-peak detection results using the built-in algorithm in a 300 s segment. The panels to the right include the time positions of possibly missing or incorrectly detected points. The user can navigate directly to these positions by clicking on them. The popup menu shows the available options for the current point. . 100

5.7 QTVI analysis window, the options panel shows information on the current template heartbeat (thick dashed yellow line). 101

5.8 QT dynamicity analysis window, the panel at the bottom shows the available parameters. The user can select the profile and a time lag in seconds (only for linear and exponentially weighted profiles). 102

5.9 SQA block test with synthetically generated signals. Lead A was contaminated with noise and baseline drift (see the text), lead B is the clean signal. To the right, the QTVI tutorial points out lead B as the best one. 104

5.10 Results of the QT dynamicity analysis on the synthetic signal generated with the model (see Table 5.1). Scatter plot QT/RR and results panel of the QT dynamicity analysis. The first profile (QT depends on the previous RR) was used, so blue triangles represent the coordinates (RR_{i-1}, QT_i) for the i-th heartbeat. Ten models are accessible through the combo box. The model parameters (alpha and beta) are shown below the QT/RR scatter plot. Here, alpha is the slope of the regression line (in white) and beta is the y-intercept. The Pearson correlation coefficient is also available. The parameters for the linear model are given to the right. 109

A.1 T-wave end detection in a noisy recording, the interval corresponds to the recording "sel48.dat" from QTDB. 116

A.2 T-wave end detection for a low amplitude T-wave, the interval corresponds to the recording "sel31.dat" from QTDB. 117

A.3 T-wave end detection where U-wave is present, the interval corresponds to the recording "sel50.dat" from QTDB. 118

A.4 T-wave end detection for biphasic waves, the interval corresponds to the recording "sel301.dat" from QTDB. 119

A.5 T-wave end detection in an "unintuitive" case, the interval corresponds to the recording "sele0409.dat" from QTDB. 120

List of Tables

2.1 Different kernel functions and parameters 39

3.1 Global confusion matrix for all classifiers. 53

3.2 Global performance indexes for all classifiers. 53

3.3 Global confusion matrix for the classifiers tested in the balanced group (15 records) 53

3.4 Performance indexes for the classifiers tested in the balanced group (15 records). 53

3.5 Global confusion matrix for the classifiers tested in the imbalanced group (59 records) 54

3.6 Performance indexes for the classifiers tested in the imbalanced group (59 records). 54

3.7 Confusion matrix for the classifier trained and tested with record 36 (imbalanced dataset). 54

3.8 Performance indexes for the classifier trained and tested with record 36 (imbalanced dataset). 54

3.9 Confusion matrix for the classifier trained and tested with record 31 (balanced dataset). 55

3.10 Performance indexes for the classifier trained and tested with record 31 (balanced dataset). 55

3.11 Confusion matrix for the classifier trained and tested with record 33. 55

3.12 Performance indexes for the classifier trained and tested with record 33. 55

3.13 Confusion matrix for the classifier trained and tested with record 34. 55

3.14 Performance indexes for the classifier trained and tested with record 33. 56

3.15 Global confusion matrix for the classifiers tested in the balanced group excluding records 33 and 34. 56

3.16 Performance indexes for the classifiers tested in the balanced group excluding records 33 and 34. 56

3.17 Global performance indexes for INCARTDB. 61

3.18 Global performance indexes for MITDB. 61

3.19 Confusion matrix for the classifier trained and tested with record 33 using ST-MLSVD. 61

3.20 Performance indexes for the classifier trained and tested with record 33 using ST-MLSVD. 61

3.21 Confusion matrix for the classifier trained and tested with record 34 using ST-MLSVD. 62

3.22 Performance indexes for the classifier trained and tested with record 34 using ST-MLSVD. 62

4.1 Best results for each feature extraction method, μ is the sample mean error and σ is the sample standard deviation of the error. 69

4.2 Comparison with algorithms for detecting the Te on the ECG, μ is the sample mean error and σ is the sample standard deviation of the error. 70

4.3 Performance comparison using unique set measures and the testing set 83

4.4 Te detection algorithms performance comparison. The worst case is considered for the proposed approach (bold-faced). 84

4.5 QTDB Recording stratification according to Te accuracy and precision for Lead 1, (T): amount of records in each group, (%): percentage with respect to the total amount of records (103). Boldfaced values represent the best results for each group . . . 85

4.6 QTDB recording stratification according to Te accuracy and precision for both leads, (T): amount of records in each group, (%): percentage with respect to the total amount of records (103). 85

5.1 McSharry et. al. [71] model parameters for two experiments, the SQA evaluation and the QT dynamicity analysis. 104

5.2 Segments of 15 min from different Holter recordings for the evaluation of the EHB. 105

5.3 Evaluation of the ectopic heartbeat detection block using the signals from Table 5.2. Here, R is the number of detected heartbeats, TP, FP, FN and TN are the number of true positives, false positives, false negatives and true negatives respectively. Moreover, sensitivity (Se), specificity (Sp), positive predictive value (P+) and accuracy (Acc) performance metrics are included. 106

5.4 Evaluation of the Toff and Qon detectors using a subset of the QT database. MAT is the original MATLAB© implementation of the respective algorithms. 107

5.4 Evaluation of the Toff and Qon detectors using a subset of the QT database. MAT is the original MATLAB© implementation of the respective algorithms. 108

5.5 QT analysis on synthetic signals using the linear model and the profile where the QT depends on the previous RR interval. QT/RR regression line parameters given for both, contaminated and clean signals. Here α is the slope, β is the y-intercept and R.E. stands for relative error. 110

Chapter 1

Introduction

This chapter introduces the main topics on the processing and analysis of the ambulatory electrocardiography signal. It is organized as follows. The first section briefly introduces cardiac diagnostic techniques, the heart physiology as the underlying mechanism of the electrocardiogram, and the clinical applications of this signal. Section 1.2 focuses on the features of the ambulatory monitoring, the main disturbances that may affect the signal and the general approach for processing it. Then, section 1.3 provides a survey on both, heart rate variability and QT analyses and their clinical interest. Furthermore, the global aim of the thesis and specific objectives are discussed in section 1.4. The overview of the dissertation and the personal contributions are clearly stated in section 1.5. Finally, collaborations are indicated in section 1.6 and the chapter ends with conclusions in section 1.7.

1.1 Relevance of cardiac monitoring

Cardiovascular diseases (CVD) are the major cause of death worldwide. The World Health Organization (WHO) reported that 31% of all global deaths in 2015 were due to CVD [132]. CVD include a group of disorders of the heart and blood vessels such as the coronary heart disease (CHD), peripheral artery disease (PAD), the cerebrovascular disease (CBVD), heart arrhythmia, among others. Moreover, CVD have been associated with some risk factors as smoking, unhealthy diet and physical inactivity. Besides, CVD has also been associated to poverty since over 80% of related deaths take place in low-and middle-income countries.

In CVD early detection methods are crucial in order to improve treatments and prevent life-threatening events [67]. Hence, several cardiac diagnostic tests have been established in the medical practice. These methods can be classified into two main groups, invasive and non-invasive tests. On the one hand, cardiac catheterization or coronary angiogram is an example of invasive test. Coronary angiogram is indicated when coronary artery disease (CAD) is suspected or when the heart muscle function must be evaluated [36]. On the other hand, non-invasive tests include magnetic resonance imaging (MRI) of the heart [47], cardiac computed tomography (CT) scan [9], echocardiography [77] [56], electrocardiography and others. The electrocardiogram (ECG) is both, the simplest and the cheapest method among the non-invasive techniques for cardiac diagnostics.

1.1.1 The surface electrocardiogram

The electrocardiogram (ECG) is the recording of the electrical activity of the heart. Such activity is obtained from the body surface with an electrocardiograph. The ECG has a prominent role in the screening and diagnosis of cardiovascular diseases [1], metabolic disorders [106] and predisposition to sudden cardiac death (SCD) [32]. It is also indicated in cases of chest pain (angina) and/or hypertension. Below, a brief overview of heart's physiology and the electrocardiographic signal is presented.

Heart physiology

The heart is a muscular organ which is located in the chest, behind the sternum in the mediastinal cavity, between the lungs, and in front of the spine. The heart contains two pumps, the right and the left pump, and four chambers, the left and right atria and the left and right ventricles, see Figure 1.1. The right pump includes the right atrium and the right ventricle. The right atrium receives deoxygenated blood returning from the body and completes the filling process (atrial systole) of the right ventricle. Then, the right ventricle pumps the blood to the lungs where it is again oxygenated. The left atrium receives oxygenated blood from the lungs and during the atrial systole it finishes the filling process of the left ventricle. The left ventricle pumps the oxygenated blood to the rest of the body.

Contraction (systole) and relaxation (dyastole) processes of atria and ventricles are fired by electrical impulses generated by the heart [80]. Such impulses excite the muscle which produce the mechanical response. In a normal heart, there is a region where the electrical impulse is generated i.e. the pacemaker of the heart.

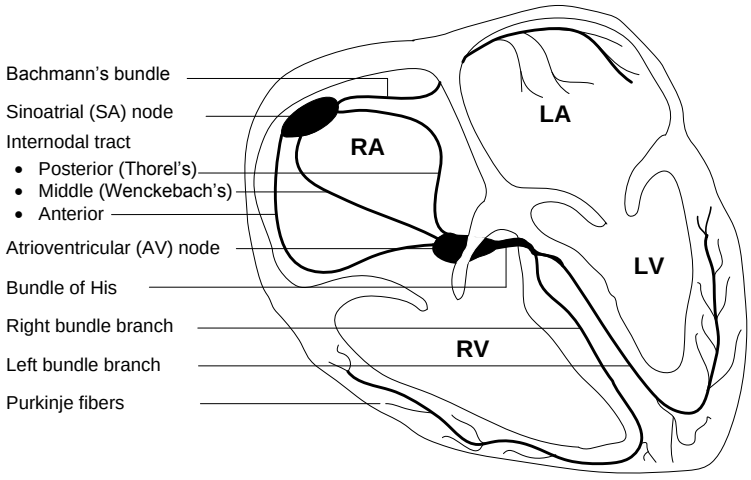


Figure 1.1: The heart's conduction system. (L/R)A is left/right atrium and (L/R)V corresponds to left/right ventricle [130].

The natural pacemaker of the heart is the sinoatrial (SA) node. The SA node can fire at a rate of 60 to 100 impulses per minute. The electrical impulse generated at SA node travels through the internodal tract to atrioventricular (AV) node. In the AV node, the electrical impulse is delayed by 0.04 s approximately. This pause assures that ventricles fill up completely. Then, the depolarization wave runs through both branches of the Bundle of His up to Purkinje fibers. The impulse travels faster through the left branch than through the right branch. This difference allows that both ventricles contract simultaneously [41], see Figure 1.1.

The ECG is the recording of the previously described electrical activity measured on the body surface. The ECG signal has characteristic waves and intervals [44] which are outlined below and depicted in Figure 1.2.

The **P wave** is the first deflection of a normal ECG waveform. It represents the atrial depolarization started at the SA node as well as the conduction of the electrical impulse through the atria. Normal P waves precede QRS complexes and last 60 ms to 120 ms. In most leads, normal P waves are rounded and upright with amplitudes from 0.2 mV to 0.3 mV.

The **PR/PQ interval** corresponds to the travel of the electrical impulse from its generation in the SA node through the internodal tract, AV node, the bundle of His and left and right bundle branches. Normal PR interval is located from

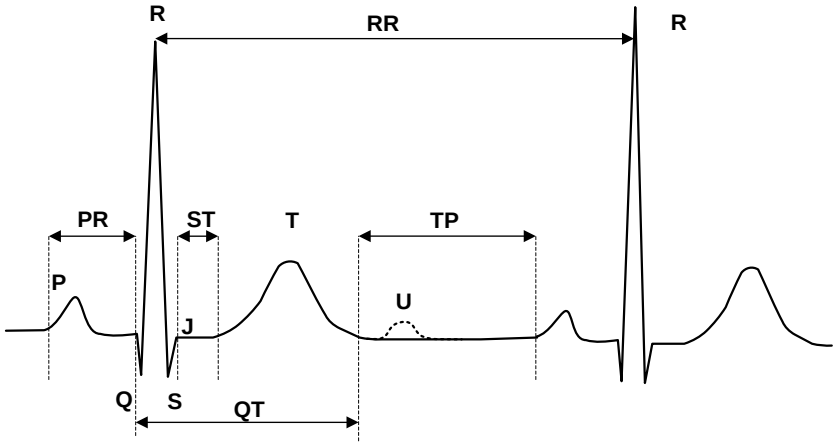


Figure 1.2: The normal ECG, waves and intervals.

the beginning of the P-wave to the beginning of the Q wave and lasts typically 120 ms to 200 ms.

The **QRS complex** represents the depolarization of the ventricles. It is composed of three waves, the Q wave, the R wave and the S wave. Not all of these waves have to be present in a normal QRS. The QRS complexes follow the PR intervals and their amplitudes may vary depending on the lead used. The QRS is measured from the beginning of the Q wave to the end of the S wave (the J point) and lasts in the range of 60 ms to 100 ms.

The **ST segment** represents the interval between the end of the ventricular depolarization and the beginning of the ventricular repolarization. Normal ST segments start at the J point and are usually isoelectric.

The **T wave** corresponds to the ventricular repolarization. Normal T wave follows the S wave and its amplitude varies depending on the lead. A non-pathological T wave is typically round and smooth as shown in Figure 1.2.

The **U wave** when it is present follows the T wave. Although the U wave genesis has been associated to several hypotheses its origin remains unclear. It has been observed in hypokalemia and hypercalcemia but also in young athletes.

On the one hand, the **QT interval** is the time elapsed from the beginning of the ventricular depolarization (Q onset) to the end of the ventricular repolarization (T offset). On the other hand, the **RR interval** is the time between two consecutive R peaks. The analysis of both intervals has found several applications in medical practice. This topic is discussed in more detail

further in the chapter.

The 12-lead ECG

The 12-lead ECG records information from 12 different views of the heart, see Figure 1.3. These views are the leads or channels. The leads provide a view of the electrical activity of the heart between two points or poles. One is the positive pole while the other one is the negative pole. There are two types of leads depending on their placement, the limb leads and the precordial (chest) leads.



Figure 1.3: An example of 12-lead ECG. The strip was extracted from the record I01 of the St. Petersburg INCART 12-lead Arrhythmia Database [38]. The first 6 seconds are shown using the LightWAVE software from Physionet.

Lead I provides a view of the heart that shows current moving from right to left. The positive electrode for this lead is placed on the left arm while the negative

one is placed on the right arm. For lead II, the positive electrode is on the patient left leg and the negative one on the right arm. Since the current travels down and to the left in this lead, it tends to produce a positive, high-voltage deflection. In lead III, the positive electrode is placed on the left leg while the negative one is placed on the left arm. Lead I is helpful in monitoring atrial rhythms while lead II is commonly used for routine monitoring and for detecting sinus node and atrial arrhythmias. On the other hand, lead III is convenient for detecting changes associated with an inferior wall myocardial infarction.

The lead axis is the imaginary line that lies between both poles of the lead. It represents the direction of the current moving through the heart. The axes of the three bipolar limb leads (I, II, and III) form the Einthoven's triangle. The augmented leads, aVR , aVL, and aVF are unipolar leads where the positive pole is in the right arm, left arm and left foot respectively. The negative pole is a combination of the other two limb electrodes called Goldberger's central terminal.

The precordial lead V1 electrode is placed on the right side of the sternum at the fourth intercostal rib space. It is common to use it in monitoring ventricular arrhythmias, ST-segment changes, and bundle-branch blocks. Lead V2 is placed at the left of the sternum at the fourth intercostal rib space while lead V4 is placed at the fifth intercostal space at the midclavicular line. Lead V3 goes between V2 and V4. Lead V5 is placed at the fifth intercostal space at the anterior axillary line. It can show changes in the ST segment or T wave. Lead V6 is placed level with V4 at the midaxillary line, see Figure 1.4.

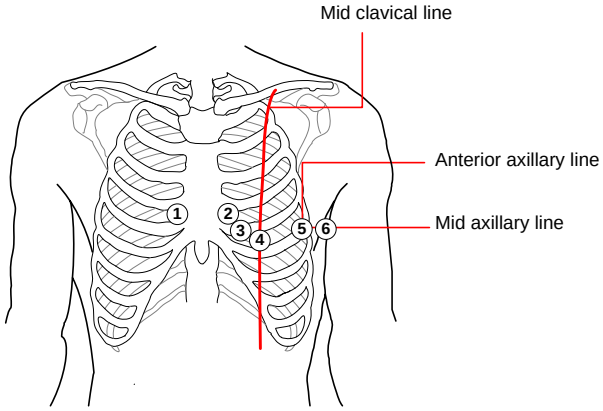


Figure 1.4: Placement of electrodes for recording precordial leads.

Leads I, II, III, aVL, aVF, V4, V5, and V6 produce positive deflections. Leads V1, V2, and V3 are biphasic, with both positive and negative deflections. aVR

produce negative deflections since the electrical activity of the heart moves away from this lead, see Figure 1.3

1.1.2 Hearth rhythms

As mentioned before, in a healthy heart, the rhythm is controlled by the SA node, and this rhythm is called normal sinus rhythm (NSR). The NSR has a rate between 60 and 100 beats/minute at rest. Although the NSR is regular, there are small variations on the heart rate (HR) caused by the interaction of both branches of the autonomic nervous system (ANS) i.e. the symphatetic (SNS) and parasympathetic (PNS) branches of the ANS. The SNS increases the firing rate while the PNS decreases the HR. The dynamical behaviour of these variations is known as heart rate variability (HRV).

However, in certain conditions, the rhythm might appear disturbed by an underlying disease. The anomalies of the normal sinus rhythm are known as arrhythmias. Arrhythmias can occur due to several causes, for instance, the premature activation of other cells outside the SA node or the existence of conduction blocks. This irregular firing might occur because other regions of the heart can serve as pacemakers.

The cells surrounding the AV node can act as a pacemaker if no electrical impulse is received from the SA node. These cells, called junctional tissue, can fire at a rate of 40 to 60 times per minute. Pacemaker cells can also be found at Purkinje fibers which are able to discharge at a rate of 20 to 40 times per minute. Such pacemaker cells can be activated when higher pacemakers (SA or AV nodes) are not generating the impulse or the conduction system through the bundle of His becomes blocked. An ectopic heartbeat is any beat generated outside the SA node, e.g. in one of the aforementioned pacemakers. Depending on the location of the focus, the ectopic heartbeat can be classified as supraventricular ectopic beat (SVEB) or ventricular ectopic beat (VEB). The former corresponds to a focus located in the atria, and the latter corresponds to an ectopic focus located in the ventricles, see Figures 1.5a-1.5b.

Either, an increase on the automaticity of the pacemaker-kind cells outside the SA node or a decrease on the automaticity of the SA node cells can lead to the occurrence of arrhythmias. Another cause of arrhythmias is the reentry phenomenon, where adjacent cells have different refractory periods. Thus, part of the tissue can be normally depolarized but not the other. When the refractory period of the latter has finished they can depolarize and serve as a pathway back to the cells that firstly depolarized. In the case that cells with the normal refractory period have had time to recover they may be able to depolarize again closing the reentry circuit.

Depending on its origin, an arrhythmia can be classified either as atrial arrhythmia which corresponds to ectopic foci located in the atria or ventricular arrhythmia, for the ones that have their origin in the ventricles. Atrial arrhythmias include atrial tachycardia, atrial flutter, and atrial fibrillation. A similar criterion is used for ventricular arrhythmias.

On the one hand, atrial tachycardia is caused by one or several ectopic foci in the atria. The firing rate is usually in the range between 140 and 220 bpm. On the other hand, atrial flutter and atrial fibrillation are both reentrant arrhythmias. The former is more organized and the atria typically beat at a rate of 300 bpm, see Figure 1.5c. The atrial fibrillation exceeds this value with firing rates in the range between 400 and 700 bpm. Ventricular tachycardia consists of beats with VEB-like morphologies at a rate of 120 bpm. In ventricular flutter QRS complexes and T waves are no longer detectable, Figure 1.5d. Likewise, ventricular flutter is a rapid and organized rhythm with a variable amplitude over time. Ventricular flutter may derive into ventricular fibrillation, which is a life-threatening arrhythmia where the rhythm is totally unorganized.

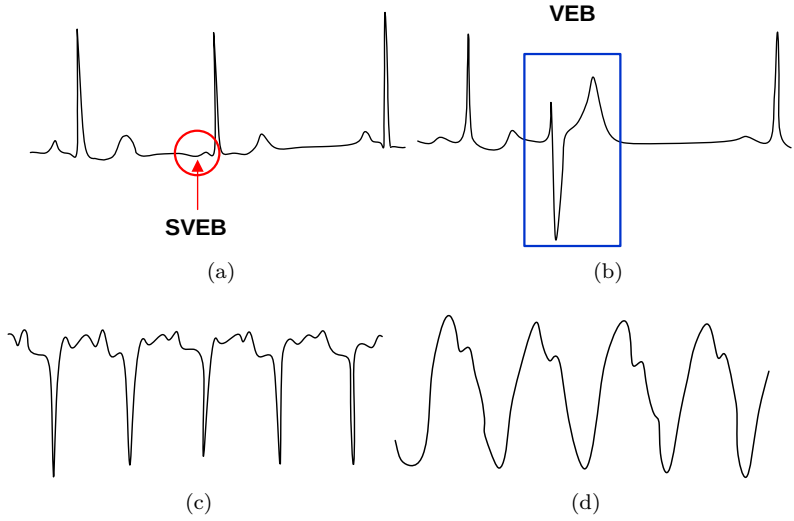


Figure 1.5: Ectopic beats and arrhythmia examples (a) supraventricular ectopic beat (SVEB), the P wave is inverted in the highlighted area, (b) ventricular ectopic beat (VEB), (c) atrial flutter and (d) ventricular flutter.

Arrhythmia detection systems aim to assess the type, location, and behavior of the abnormal rhythm by combining several processing/analysis techniques. Often, an stage for detecting and counting SVEB and VEB is involved. Other

tests focus on the variability of normal sinus rhythm. HRV and QT analyses correspond to the latter group. In this type of studies, SVEB and VEB should be detected as well. Here, the difference relies on the fact that such beats must be removed for the purposes of the analysis. This dissertation encourages this point.

1.1.3 ECG clinical applications

The ECG is one of the most used modalities in clinical practice and the most common tests are basal or resting ECG, intensive/coronary care unit (ICU/CCU) ECG, exercise or stress ECG, high-resolution ECG and ambulatory ECG. The basal ECG can detect certain heart conditions such as arrhythmias, ischemia, and myocardial infarction. The test takes about 5 minutes and no preparation is necessary. During resting ECG, the patient is lying on the back and the standard 12-lead ECG is recorded during 10 seconds.

The ECG of post-infarction patients is continuously monitored in the ICU and CCU. Despite the fact that patients in such conditions are normally at rest, the processing of the ECG signal in these circumstances is a challenging task. Of all clinical applications, this is the only one that requires real-time processing. Furthermore, ECG monitored in ICU or CCU is usually corrupted by noise and artifacts, which lead to numerous false alarms along with a severe decrease in the diagnostic performance.

Exercise ECG is normally indicated for the diagnostic assessment of coronary artery disease. In this test the ECG is recorded while the patient is performing exercises. The exercise equipment can be a treadmill or a cycle ergometer. The ECG is recorded continuously during exercise and during the recovery period. Myocardial ischemia can be assessed if deviation of the ST segment is present in the recording. Additionally, arrhythmias and conduction disturbances may occur during the process and must be considered in the final diagnostic.

The high-resolution ECG attempts to measure signals on the order of 1 μV by using signal averaging techniques. Likewise resting ECG, the signal is recorded at rest in supine position but for a longer period. Since high-frequency components are expected to appear during high-resolution ECG, this technique requires higher sampling rates (at least 1 kHz). One promising application of this method is the analysis of late potentials. The occurrence of late potentials has been associated with a high risk of suffering life-threatening arrhythmias in post-infarction patients.

Finally, ambulatory ECG (AECG) is used for studying transient phenomena that can be related to arrhythmias and other conditions. Since this thesis

focuses on the processing of the ambulatory ECG signal, the next section will cover it in more detail.

1.2 Ambulatory ECG monitoring

The AECG records the electrical activity of the heart during real-life activities. It allows the evaluation of cardiac electrical phenomena that can be transient. Moreover, the AECG is also used during the follow-up of patients that have suffered an acute myocardial infarction (AMI) or ischemia. The main goals of an AECG study, from diagnostic perspective, are summarized as follows [17]:

- Assessment of symptoms that may be related to disturbances of heart rhythm
- Assessment of risk in patients without symptoms of arrhythmia
- Efficacy of antiarrhythmic therapy
- Assessment of pacemaker and implantable cardioverter-defibrillator (ICD) function
- Monitoring for myocardial ischemia

There are two categories of AECG recorders: continuous and intermittent recorders. The continuous recorders are used to investigate symptoms and ECG events that are likely to occur in a period of 24 to 48 hours [52]. The intermittent recorders, on the other hand, are mainly used for longer periods of time that can be weeks or months. Such recorders are intended to investigate events that occur infrequently. Moreover, these do not record every heartbeat but only the cardiac activity around the time that the patient presses an event button which indicates the occurrence of symptoms. In order to avoid a potential loss of information, intermittent recorders are continuously registering the electrical activity of the heart in a time loop. Thus, they are also known as loop recorders. Furthermore, there are 2 types of loop recorders, the wearable external loop recorders (ELR) and the implantable cardiac monitors (ICM) [89], [90].

The Holter monitoring, named after Norman Holter who invented this method in 1960, is a medical test where the ECG is continuously recorded for a period of 24 to 48 hours. This AECG technique allows following the daily activities of the patient and the study of cases that can suffer life-threatening arrhythmic events and/or SCD. As mentioned before, this is not the only method of ambulatory ECG. However, it was historically the first and nowadays the term ambulatory

ECG is primarily associated with Holter monitoring. Thus, hereinafter in this document the terms Ambulatory ECG and Holter monitoring will be used interchangeably.

The ECG obtained in ambulatory conditions has the following features:

1. It covers a variety of situations such as physical and mental effort, rest, sleep, etc.
2. It allows studying arrhythmias and syncopes which can occur during the recording.
3. It is a low cost test with respect to other techniques such as high-resolution ECG.

1.2.1 Noise, interferences and artifacts in ambulatory electrocardiogram

Despite the previously mentioned advantages of the ambulatory ECG, there are several phenomena that affect the ECG obtained in ambulatory conditions and therefore its usefulness and reliability [60], [82]. Ambulatory ECG may be primarly affected by noise, interferences and artifacts. Noise and artifacts may be caused by both physiological and non-physiological sources. These disturbances may considerably alter the ECG. Hence, it is crucial to distinguish all of them from the real disease.

Baseline wander (BW), powerline interference and electrode motion artifacts are all disturbances in the ECG. Baseline wander or baseline drift is a low-frequency activity in the ECG, which may vary the signal drawn [13], [3], see Figure 1.6a. This may affect the clinical interpretation of the AECG. For example, the ECG measurements defined with reference to the isoelectric line cannot be computed because the isoelectric line is masked by the BW. There are several noise sources that can induce BW including perspiration, respiration, body movements, and poor electrode contact [108]. The BW spectral content, in normal conditions, is below 1 Hz except for some higher frequency components that may appear during exercise.

Electrode motion artifacts are mainly caused by the relative movement of the electrode with respect to the skin, which varies the impedance of the skin-paste interface [121], [105]. Although motion artifacts might seem similar to baseline wander, they are more difficult to deal with since their spectral content considerably overlaps the ECG spectrum. Usually, the spectral content of motion artifact noise ranges from 1 to 10 Hz. In the ECG, these artifacts

are manifested as large-amplitude waveforms that can be wrongly detected as QRS complexes. Electrode motion artifacts are particularly inconvenient in the context of ambulatory ECG monitoring where they constitute the main source of incorrectly detected heartbeats, Figure 1.6b.

Powerline interference (50/60 Hz) is caused by the improper grounding of the ECG equipment while interference is caused by near electronic equipment, see Figure 1.6c. Interference frequencies are normally outside the spectral range of the ECG meaningful spectrum, so they can be removed by means of linear or nonlinear filtering [7], [43].

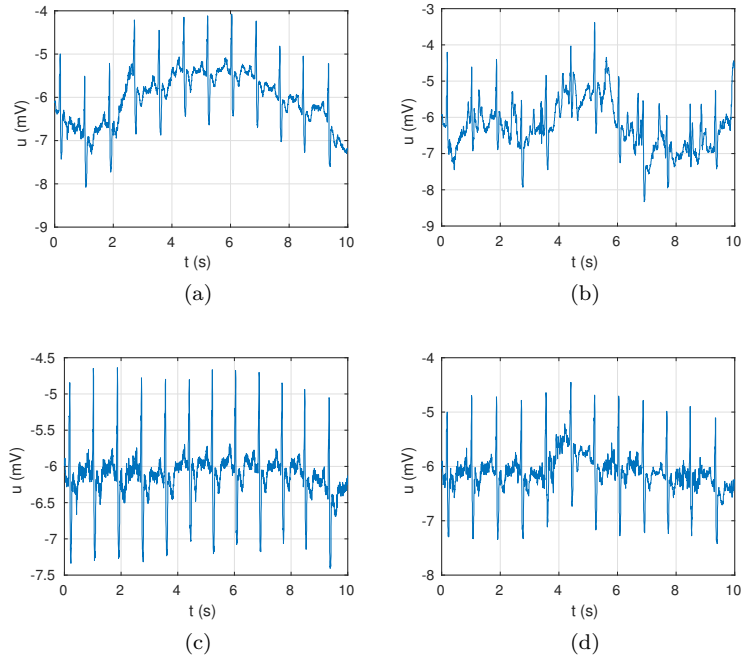


Figure 1.6: Noise, interferences and artifacts that affect AECG, (a) baseline wander, (b) electrode motion artifacts, (c) power line interference and (d) EMG noise.

Noise sources can also be of physiological origin or not. The electromyographic noise (EMG noise) for instance is caused by the electrical activity of the skeletal muscles during their contraction, Figure 1.6d. The frequency range of EMG noise extends to 10 kHz [82]. Thus, frequency components of EMG noise overlap with the ECG which affects the morphology of the signal [43]. Besides, there

could be noise due to the acquisition system, which is usually upper bounded by the manufacturer of the equipment.

Although the occurrence of ectopic heartbeats is associated with arrhythmias, they can also occur in healthy subjects. However, the use of these heartbeats in HRV or QT analysis should be avoided. A reason for this relies on the effect that ectopic beats have on the different markers of HRV, which might lead to incorrect diagnosis. Hence, ectopic heartbeats are considered artifacts of physiological origin. This topic will be addressed later in this dissertation.

1.2.2 Stages in processing and analysis of AECG

The analysis of ECG time series, either RR or QT, can be viewed as a three-cascade stages process, see Figure 1.7. The first stage corresponds to the pre-processing step. In this phase, the raw ECG signal is processed according to the requirements of the analysis. Normally, this stage should include filtering techniques that reduce baseline wander, interference, artifacts and assures a signal as clean as possible. Furthermore, this stage must include a step which deals with ectopic heartbeats.

In the second stage, fiducial points have to be extracted. Here all the characteristic points needed by the analysis should be accurately detected. For instance, in HRV analysis only R peaks are required while in QT analysis, besides the R peaks, the Q wave onset (Qon) and the end of the T wave (Te or Toff from T offset) are needed.

Finally, after determining the fiducial points, several markers can be computed, e.g., in HRV, temporal and spectral indexes might be obtained from the RR series, while in QT analysis the QTVI index or the QT dynamicity can be evaluated.

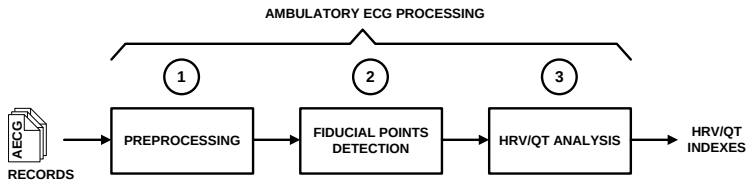


Figure 1.7: Simplified block diagram for an ambulatory ECG signal processing system.

1.3 Analysis of time intervals in the ECG

In the ECG two main groups of features provide diagnostic information. On one hand, the first group is related to the waves and intervals in the ECG and includes the waves length, its sequence and the lengths of the associated intervals. On the other hand, the second group is related to the amplitude and morphology of the signal. In this dissertation, morphological analysis is used for classifying heartbeats and for detecting the end of the T wave in the ECG (chapters 3 and 4). The analysis of time intervals, especially, the analysis of the QT interval is addressed in chapter 5.

1.3.1 Heart rate variability

It has been established that fluctuations on the heart rate (HR) in normal sinus rhythm are modulated by both, sympathetic (SNS) and parasympathetic (PNS) branches of the ANS [4]. Thus, the ANS modulates the depolarization-repolarization cycles of the heart cells in the so-called cardiac autonomic function. Evidence of this modulation can be found on indexes that quantify the variations of the HR signal [109].

The beat-to-beat variations in the RR interval is called Heart Rate Variability (HRV) [66], [99]. The HRV analysis in short periods of time (5 minutes) and long (up to 24 hours) can provide relevant information of some diseases and dysfunctions of both cardiovascular and non-cardiovascular origin [108]. Thus, a large number of applications using linear and/or nonlinear indexes of HRV have been reported in the literature. For instance, depressed HRV has been associated with left ventricular hypertrophy [92], recent myocardial infarction [8] and diabetes [98] [133]. Besides, it has been shown that a decrease in the parasympathetic cardiac control is an unfavorable prognosis in patients that suffered an acute myocardial infarction [49].

HRV has also been applied in epilepsy [97], stress assessment [48], risk stratification of cardiac death or ventricular arrhythmic events post-myocardial infarction [66] [8], detection and quantification of autonomic neuropathy in patients with diabetes mellitus [46] among others [122]. Moreover, recently HRV analysis has been suggested as marker in patients with heart failure [31] [99]. In summary, HRV has been thoroughly studied and its clinical significance has been well established on diagnosis and prognosis of several cardiovascular and non-cardiovascular conditions [30] [136].

1.3.2 QT interval analysis

The QT interval is mainly associated with the ventricular repolarization of the heart. Normal values of QT interval for males are around 450 ms, while, for healthy females, the mean value is 470 ms [39]. It is well known that QT interval is influenced by changes in heart rate and other factors like drug intake [79]. QT anomalies have been associated with the risk of suffering ventricular life-threatening arrhythmias and sudden cardiac death. For instance, in both congenital and acquired Long QT Syndrome (LQTS) there is a risk of developing Torsade de Pointes (TdP), a kind of polymorphic ventricular tachycardia which may result into SCD [135] [137]. Several markers have been proposed for the assessment of ventricular repolarization instability. The most relevant ones include QT variability indexes, QT dynamicity, QT dispersion (QTd) and T-Wave alternans (TWA).

QT variability (QTV) is the quantification of the slight changes in the QT beat to beat. One of the most accepted QTV temporary indexes is the QTVI proposed by Berger [6] [5]. QTVI is the log ratio between the QT and HR variances normalized with respect to their respective squared mean values. QTVI has been studied in different populations, such as dilated cardiomyopathy (DCM) patients, post-Myocardial Infarction (MI) subjects, healthy controls, patients with ICD devices [27] and more recently, patients that suffered spinal cord injury [101].

QT interval is influenced by various factors such as heart rate, sympathovagal balance, metabolic status or drugs. The evaluation of QT adaptation to changes in heart rate has gained relevance in sudden death risk stratification. The analysis of dynamic behavior of repolarization is called QT adaptation or QT dynamicity. Different methods exist to assess repolarization dynamicity, also known as adaptation or hysteresis. A well-known method estimates QT/RR slope, i.e., the slope of the linear regression between QT and RR intervals. Steeper QT/RR may indicate either excessive lengthening of QT at slow rates or excessive shortening at fast rates. Both of these processes may contribute to the occurrence of a malignant ventricular arrhythmia and consequently to SCD. Although there is no global consensus on the normal values of QT/RR slope, small values are in general associated with healthy people whereas higher values correspond to pathological subjects [91] [85].

Other relevant markers include QT dispersion (QT_d) and T-Wave Alternans (TWA). QT_d is defined as the difference between the maximum and minimum QT in a standard 12-lead ECG [20], [110]. Nowadays, it is known that spatial heterogeneity of ventricular repolarization is linked to a higher probability for the occurrence of malignant ventricular arrhythmias. QT_d mainly reflects

regional variations in ventricular repolarization. Thus, excessive time dispersion of repolarization results in a prolongation of the vulnerable period and increased susceptibility to malignant arrhythmias. However, there is still uncertainty on the ability of QT_d to identify patients at high risk of SCD [57]. Moreover, it requires a standard 12-lead ECG and is not available on routine used monitoring systems, but could be indirectly derived from Holter systems. TWA is a beat-to-beat alternation in the morphology and amplitude of the ST-segment or the T wave. It reflects spatiotemporal heterogeneity in the repolarization and has been proposed as a marker for risk stratification of ventricular tachycardia (VT) - ventricular fibrillation (VF) and SCD [73] [84].

1.4 Problem statement and objectives

From the technological point of view, a challenge for ambulatory ECG studies and particularly for the HRV and QT analysis is the loss of relevant information caused by the disturbances mentioned above. Since the signal quality is not always stable along the Holter recording, algorithms to extract ECG fiducial points often fail due to baseline drifts and artifacts. The latter causes false positives and false negatives in the time series of the ECG signal. False positives are artifacts or ectopic heartbeats incorrectly detected as normal ones. False negatives are normal heartbeats not detected or skipped by the algorithm. Both, false positives and false negatives affect the markers (indexes) used for the diagnosis.

Furthermore, in the AECG, a large amount of data should be processed. Typically, there could be more than 100,000 heartbeats per channel. Since visual analysis of such amount of data is a time-consuming task, many computer-based methods for automatic ECG analysis have been proposed [11], [123]. However, ECG classification in Holter recordings is a difficult problem because ECG waveforms may significantly differ even for the same heartbeat class taken from the same patient.

Besides, the interval time series analysis in ambulatory ECG studies assumes a correct selection of normal heartbeats as a requirement. For instance, HRV will be reliable if and only if all the considered beats follow the normal conduction system of the heart, i.e. a normal beat starts at the sinoatrial (SA) node, no AV blockades are present and the electric impulse travels along the right and left bundle of His branches ending at the Purkinje fibers [66]. In any other case, the heartbeat should be excluded from the analysis. Spurious waves caused by the movement of the electrodes or noise should be removed as well. Similar conditions are needed for most of the ventricular repolarization analysis. For

instance, in QTVI computation a clean signal is mandatory and ectopic beats should represent less than 5% of the total number of heartbeats under analysis. On the other hand, in QT dynamicity analysis, ectopic beats are not allowed and the signal should be as clean as possible. The latter points out that it is necessary to perform a manual or automated morphological recognition of heartbeats, in order to identify the normal beats and reject the invalid ones (abnormal or premature beats).

Artifact rejection and ectopic heartbeat detection are classification problems where it is necessary to classify the current heartbeat in one of two classes, normal or abnormal. The normal class groups all normal heartbeats which satisfy all the conditions for a subsequent HRV or QT analysis. Ectopic beats, QRS-like artifacts, and noisy heartbeats compose the abnormal class. Even though there are many studies on ECG signal classification that use supervised learning based classifiers, there are still many challenges that need to be tackled to achieve an optimal performance. For instance, supervised classifiers have not been extensively applied in practice [129]. Perhaps, because patient-independent approaches have not demonstrated to be more effective than unsupervised methods [58] [23] [45]. Thus, other alternatives like hybrid patient-independent/patient-adapting algorithms [24] and active learning methods have been propossed [129].

Another issue arises in QT interval analysis. Since the variability of the QT interval is small in healthy and pathological subjects, it is crucial to determine the T-wave end with high accuracy and precision. Besides, accurate and precise T-wave end detection might allow for discriminating among small margins of variability, therebyincreasing the reliability of the analysis. In the last years, several unsupervised methods have been proposed [128] [70] [138] [69]. Most of these methods use threshold criteria which may increase the sensitivity to noise, interferences, and artifacts. Unsupervised approaches may be suitable for short-term analysis. Nevertheless, it is not the case for long-term recordings where both, signal quality and morphology may change. Since these variations are a plausible scenario in ambulatory recordings, a considerable amount of time might be spent in correcting the T-wave end detection errors of unsupervised approaches. The adjust (tuning) of the parameters of unsupervised methods is not always possible neither intuitive. Moreover, the possibility of tuning an algorithm does not ensure better results.

In Cuba, the analysis software of the EXCORDE E3C ambulatory monitoring system [15] has been improved through the years. However, this software still has the following limitations: (1) errors in the classification of heartbeats, and therefore in the subsequent analysis, (2) errors in the estimation and removal of baseline wander causing failures in detection of characteristic points, (3) the QT time series analysis is very limited and does not include T-wave alternans,

(4) it does not include spectral indexes of HRV analysis and (5) some indexes are not robust to the presence of false positives (FP) and false negatives (FN) in RR time series.

Hence, the overall objective of this Ph.D. research is to propose new machine-learning-based methods for improving the processing of ambulatory electrocardiography signal. The relevance of this topic resides on the fact that improved processing steps may lead to reliable markers, thereby decreasing the risk of an incorrect diagnostic.

The specific objectives of this research are the following:

- To characterize and improve machine-learning-based methods for premature heartbeat recognition.
- To characterize and improve machine-learning-based methods for fiducial point detection in the ECG, particularly the T-wave end.
- To develop and evaluate new tools for ambulatory ECG signal processing and analysis.

1.5 Chapter-by-chapter overview and personal contribution

This book follows the structure mentioned in section 1.2.2. Chapter 2 describes the different machine learning methods used in this research. In addition, each chapter corresponds to one specific objective, see Figure 1.8. Chapter 3 presents two new methods for detecting premature heartbeats using different tensor decompositions, both methods have been published in [113] and [111].

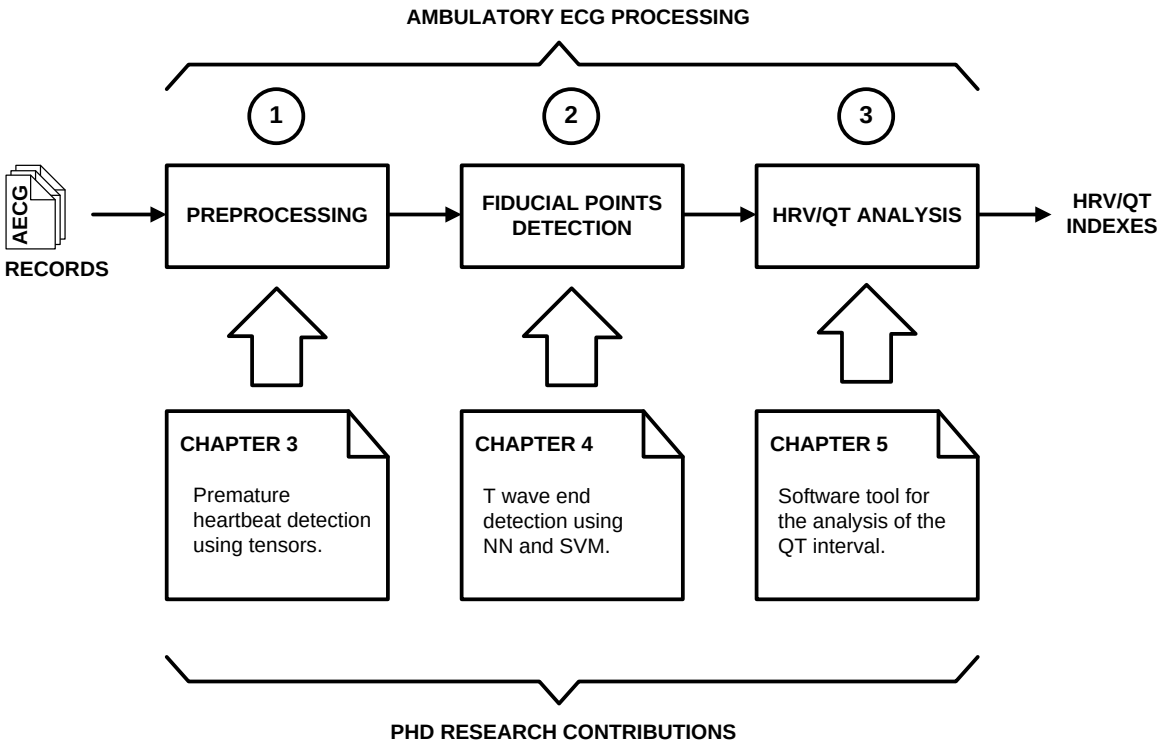


Figure 1.8: Schematic chapter overview.

Chapter 4 deals with the detection of the T-wave end using neural networks (NN) and support vector machines (SVM). This chapter shows an evaluation of NN and SVM as regression algorithms in the context of fiducial point detection. The results of this work have been published in [114] and in [112]. Finally, in chapter 5 a tool for the analysis of the QT interval is shown. This tool has been developed using the free software language Python. The individual contribution of the author in the publications is in correspondence with his position as the first author in all of them.

1.6 Collaborations

This research was done in close collaboration with professors and researchers from the biomedical data processing research group (BioMed), STADIUS Center for Dynamical Systems, Signal Processing, and Data Analytics, Department of Electrical Engineering (ESAT), KU Leuven, Belgium. Within this group I worked with Carolina Varon and Griet Goovaerts.

Regarding the advice from medical doctors, professor Rik Willems, from UZ Leuven, Belgium, provided the necessary feedback during the discussions on heartbeat classification and T-wave end detection. On the other hand, the group led by professors José Ramón Malleuve Palancar and Carlos Angulo Elers from Hospital Provincial Clínico Quirúrgico Saturnino Lora, Santiago de Cuba, Cuba, provided feedback and support. From this group, I collaborated with M.D. Leuken Rojas Hernández and M.D Lenar Beatón Pérez.

This research has been partially supported by the Belgian Development Cooperation through VLIR-UOS (Flemish Interuniversity Council-University Cooperation for Development) in the context of the Institutional University Cooperation programme with Universidad de Oriente.

1.7 Conclusions

In this chapter, the physiology of the cardiovascular system, particularly the heart as the origin of the electrocardiographic signal was described. The latter served as a motivation for introducing the main concepts related to the ECG signal interpretation and analysis. An overview of the different ambulatory ECG techniques was given along with its main features and applications. Moreover, the main factors that significantly limit Holter monitoring analysis were presented. Furthermore, the main medical applications of HRV and QT

analyses were described. Finally, the chapter-by-chapter overview, personal contribution and collaborations were summarized.

Chapter 2

Machine learning methods

This chapter introduces the main aspects of machine learning methods used in the thesis. The chapter has been divided into three main parts. First, some feature extraction techniques are discussed. Then, the focus moves to unsupervised learning (clustering) algorithms. Finally, supervised methods are further discussed. The whole structure is as follows, section 2.2 is an overview of the feature extraction algorithms used in this dissertation including tensor decompositions. Section 2.3 is dedicated to the unsupervised machine learning algorithms, particularly cluster analysis using k-means and robust clustering methods. Section 2.4 provides details on supervised machine learning algorithms including Multilayer Perceptron (MLP) and different Support Vector Machine (SVM) formulations. Finally, the conclusions of the chapter are given in section 2.5.

2.1 Introduction

Machine learning methods are broadly applied nowadays. Such methods have the ability to "learn" from input data. Here, the term "learn" is used in the sense of increasing its performance on a given task. This increase is sometimes supported by a training process. Several fields of knowledge such as statistics and computer science converge in machine learning. Furthermore, machine learning methods can be classified in supervised learning and unsupervised learning. In supervised learning, the training data include examples of the input vectors and their corresponding target vectors. In unsupervised learning, the training data consists of the set of input vectors and there is no additional

information available. Problems like classification and regression belong to the supervised class of algorithms. Other problems such as feature extraction, clustering, and density estimation correspond to unsupervised learning. In this thesis, several algorithms from both supervised and unsupervised approaches are used.

2.2 Feature extraction

Feature extraction methods process raw input data producing a new data representation where redundancies have been eliminated. Feature extraction is an essential step before using machine learning algorithms in order to reduce the dimensionality of the input data while keeping the relevant information. Below, all feature extraction methods used in this thesis are briefly discussed.

2.2.1 Resampling

The resampling operation in digital signal processing is the process of changing the sampling rate of a signal. There are two types of resampling operations: the upsampling and the downsampling or decimation. The upsampling process increases the signal rate whereas decimation reduces the number of components that represents a vector (signal). Therefore, the latter may be used as feature extraction stage. The decimation applied to a given sequence produces the approximation of the sequence that would have been obtained by sampling the signal at a lower rate. The decimation consists of two functional blocks, an anti-aliasing filter, and the downsampler, Figure 2.1.

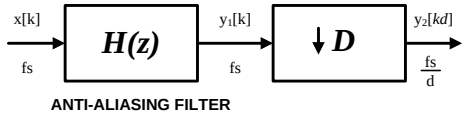


Figure 2.1: Decimation system structure, where d is the decimation factor and f_s is the original sampling frequency.

The decimation processs can be expressed as follows,

$$x[k] = x[kd],\ d \in \mathbb{N}_{>0} \tag{2.1}$$

where d is the decimation factor.

First, the signal has to be band-limited. Nyquist theorem imposes that the maximum frequency in the downsampled signal must be $f_c = fs/2d$. Thus, the antialiasing filter is designed to meet this specification. Normally, finite impulse response (FIR) filters are used rather than infinite impulse response (IIR) filters mainly due to linear phase properties of the former.

2.2.2 Discrete cosine transformation

The discrete cosine transformation (DCT) $y(k), k = 0, 1, \ldots, L-1$ of a data sequence $x(n), n = 0, 1, \ldots, L-1$ is defined as,

$$\begin{aligned} y(0) &= \frac{\sqrt{2}}{L} \sum_{n=0}^{L-1} x(n) \\ y(k) &= \frac{2}{L} \sum_{n=0}^{L-1} \left(x(n) \cos\left(\frac{(2n+1)k\pi}{2L} \right) \right), \end{aligned} \tag{2.2}$$

where L is the length of the data sequence $x(n)$.

The DCT is a data independent transformation which has high energy-packing efficiency, i.e., the DCT has the property of compacting the energy into a few coefficients. It has been widely used in compression algorithms [2], [93] and also as feature extraction method in ECG morphological recognition [126].

2.2.3 Principal component analysis

The principal component analysis (PCA) is defined as an orthogonal transformation which turns a set of observations of possibly correlated variables into a set of values of linearly uncorrelated variables. Given the matrix $\mathbf{X} \in \mathbb{R}^{m \times n}$ of centered observations where the rows are observations and the columns are variables describing these observations, the PCA problem involves finding the row factor scores under the following constraints:

- The factor scores ($\mathbf{F}$) "explain" as much of the variance of $\mathbf{X}$ as possible.
- The set of factors are pairwise orthogonal.

The problem above can be expressed as the following factorization,

$$\mathbf{F} = \mathbf{XP}, \tag{2.3}$$

subject to

$$\mathbf{F}^T\mathbf{F} = \mathbf{D}, \quad \mathbf{P}^T\mathbf{P} = \mathbf{I}, \tag{2.4}$$

where $\mathbf{D}$ is a diagonal matrix and $\mathbf{I}$ is the identity matrix. The expressions above formulate an optimization problem which reduces to the following eigenvalue problem,

$$\mathbf{X}^T\mathbf{XP} = \mathbf{\Lambda P}. \tag{2.5}$$

Since $\mathbf{X}^T\mathbf{X}$ is a positive semi-definite matrix, $\mathbf{P}$ is a matrix of orthonormalized eigenvectors and $\mathbf{\Lambda}$ is a diagonal matrix of eigenvalues. The matrix of factor scores can be obtained by,

$$\mathbf{F} = \mathbf{P}\mathbf{\Lambda}^{\frac{1}{2}}. \tag{2.6}$$

A truncated version of the factor score matrix can be obtained by removing the eigenvectors associated to the smallest eigenvalues,

$$\hat{\mathbf{F}} = \mathbf{X}\hat{\mathbf{P}} \tag{2.7}$$

PCA transforms data in a new orthogonal (uncorrelated) dataset. It is an optimal transformation with respect to the variance of the data. Therefore, it has been widely used as feature extraction stage in signal processing applications and particularly in ECG signal processing [28] [68].

2.2.4 Tensor and tensor decomposition

A tensor is a multidimensional (multiway) array of numbers, i.e., tensors can be viewed as a generalization of vectors and matrices to higher dimensions. With the emergence of big data science, recent years have witnessed an increased interest in the applications of multilinear algebra and in tensor-based methods [14]. Besides, tensor decompositions have also found many applications in modern signal processing/analysis and machine learning algorithms [102], [104], [53], [103]. Particularly in machine learning applications, tensor decompositions have been used as feature extraction in classification algorithms [100], [103].

Before applying tensor methods in signal processing, signals have first to be transformed into tensors. Nowadays, several signals such as RGB images and video are indeed tensors. Besides, there are methods that allow constructing tensors from data. Tensor generation methods are usually problem-dependent and there are many ways to do so. The process of creating a tensor from data of lower dimension is called *tensorization* [14]. This section briefly introduces basic tensor algebra and some tensor decompositions used in the thesis.

Basic tensor algebra

In this section, some necessary concepts from tensor algebra are presented. The contents of this section is based on [125].

The symbol $\otimes$ represents the outer product on tensors, e.g., $\mathcal{T} = \mathbf{a} \otimes \mathbf{b} \otimes \mathbf{c}$ implies that $t_{ijk} = a_i b_j c_k$.

The tensor unfolding operation is defined as follows: given a tensor $\mathcal{T} \in \mathbb{R}^{n_1 \times n_2 \times \cdots \times n_d}$, a mode-$k$ vector $\mathbf{v}$ is defined as the vector that is obtained by fixing all indices of $\mathcal{T}$ and varying the mode-k index as $\mathbf{v} = \mathcal{T}_{i_1,\ldots,i_{k-1},:,i_{k+1},\ldots,i_d}$ with i_j a fixed value. The mode-k vector space is the set of all mode-k vectors of $\mathcal{T}$.

The mode-k unfolding, or matricization of $\mathcal{T}$, denoted by $\mathbf{T}_{(k)}$, is an $n_k \times \prod_{i \neq k} n_i$ matrix whose columns are all possible mode-k vectors [125].

The multilinear rank of a tensor $\mathcal{T} \in \mathbb{R}^{n_1 \times \cdots \times n_d}$ is a d-tuple $(r_1, r_2, \ldots, r_d)$, wherein r_k is the dimension of the mode-k vector space, i.e., r_k is the column rank of $\mathbf{T}_{(k)}$.

The symbol $\times_k$ represents the multilinear multiplication in mode k. Let be $k \in [1, d]$, the multilinear multiplication with a matrix $\mathbf{M}$ is equivalent to multiply the mode-k vectors by $\mathbf{M}$. That is, if $\mathbf{M}$ is at position k in the tuple, then $\mathcal{T} = \mathcal{S} \times_1 \mathbf{I} \times \cdots \times_{k-1} \mathbf{I} \times_k \mathbf{M} \times_{k+1} \mathbf{I} \times \cdots \times_d \mathbf{I}$, where $\mathbf{I}$ is the identity matrix of suitable dimensions.

Canonical polyadic decomposition

Canonical polyadic decomposition (CPD), [42] [14], Figure 2.2, decomposes the tensor $\mathcal{T} \in \mathbb{R}^{n_1 \times n_2 \times n_3 \times \ldots \times n_N}$ as a minimal sum of R rank-1 tensors,

$$\mathcal{T} = \sum_{r=1}^{R} \lambda_r \mathbf{u}_r^{(1)} \otimes \mathbf{u}_r^{(2)} \otimes \ldots \otimes \mathbf{u}_r^{(N)} \tag{2.8}$$

where R is the rank of the tensor $\mathcal{T}$, N is the number of dimensions (order) and λ_r are arbitrary scale factors such that $\prod_{i=1}^{R} \lambda_i = 1$. Besides, the superscripts refer to the order while the subscripts correspond to the rank. The previous definition refers to a tensor of order N. For third order tensors ($N = 3$), the equation (2.8) can be written as follows,

$$\mathcal{T} = \sum_{r=1}^{R} \lambda_r \mathbf{a}_r \otimes \mathbf{b}_r \otimes \mathbf{c}_r \ . \tag{2.9}$$

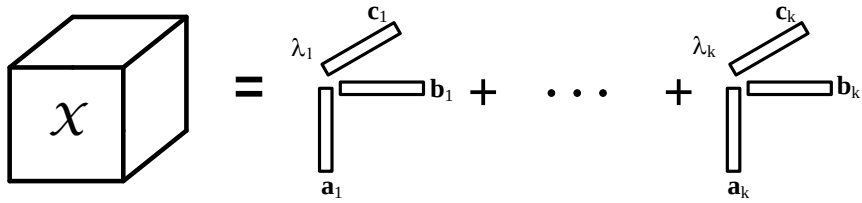


Figure 2.2: Cannonical polyadic decomposition (CPD)

Multilinear singular value decomposition

A multilinear singular value decomposition (MLSVD) [25] of a rank-(r_1, r_2, r_3) tensor $\mathcal{T} \in \mathbb{R}^{n_1 \times n_2 \times n_3}$ is a decomposition of the form

$$\mathcal{T} = \mathcal{S} \times_1 \mathbf{U}^{(1)} \times_2 \mathbf{U}^{(2)} \times_3 \mathbf{U}^{(3)}, \tag{2.10}$$

where

1. the matrices $\mathbf{U}^{(1)} \in \mathbb{R}^{n_1 \times n_1}, \mathbf{U}^{(2)} \in \mathbb{R}^{n_2 \times n_2}$ and $\mathbf{U}^{(3)} \in \mathbb{R}^{n_3 \times n_3}$ are orthogonal,
2. the tensor $\mathcal{S} \in \mathbb{R}^{n_1 \times n_2 \times n_3}$ is all orthogonal and ordered

The all-orthogonality condition for the core tensor is defined as,

$$\left(\sum_{i_2=1}^{n_2}\sum_{i_3=1}^{n_3} s_{i_1 i_2 i_3} s_{j_1 i_2 i_3}\right)^{\frac{1}{2}} = \sigma_{i_1}^{(1)} \delta_{i_1 j_1} \tag{2.11}$$

$$\left(\sum_{i_1=1}^{n_1}\sum_{i_3=1}^{n_3} s_{i_1 i_2 i_3} s_{i_1 j_2 i_3}\right)^{\frac{1}{2}} = \sigma_{i_2}^{(2)} \delta_{i_2 j_2} \tag{2.12}$$

$$\left(\sum_{i_1=1}^{n_1}\sum_{i_2=1}^{n_2} s_{i_1 i_2 i_3} s_{i_1 i_2 j_3}\right)^{\frac{1}{2}} = \sigma_{i_3}^{(3)} \delta_{i_3 j_3} \tag{2.13}$$

$$\tag{2.14}$$

where $\sigma_{i_k}^{(k)}$ are the mode-k singular values and δ_{ij} denotes the Kronecker delta ($\delta_{ij} = 1$ if $i = j$ and $\delta_{ij} = 0$ if $i \neq j$). The columns of $\mathbf{U}^{(1)}, \mathbf{U}^{(2)}$ and $\mathbf{U}^{(3)}$ are called mode-1, mode-2 and mode-3 singular vectors respectively.

Sequentially truncated MLSVD

Sequentially truncated multilinear singular value decomposition (ST-MLSVD) [125] is a method for reducing a tensor $\mathcal{T} \in \mathbb{R}^{n_1 \times n_2 \times \cdots \times n_d}$ to a lower multilinear rank one $\hat{\mathcal{T}}_p \in \mathbb{R}^{r_1 \times r_2 \times \cdots \times r_d}, r_i \leq n_i, \forall i = 1, \ldots, d$ as follows,

$$\mathcal{T} \approx \hat{\mathcal{S}} \times_1 \hat{\mathbf{U}}_1 \times_2 \hat{\mathbf{U}}_2 \times \cdots \times_d \hat{\mathbf{U}}_d = \hat{\mathcal{T}}_p \in \mathbb{R}^{r_1 \times r_2 \times \cdots \times r_d}, \tag{2.15}$$

where $\hat{\mathbf{U}}_k \in \mathbb{R}^{n_k \times r_k}$ are factor matrices with orthonormal columns, $\hat{\mathcal{S}}$ is the truncated core tensor, d is the number of dimensions and p is the processing order, see Figure 2.3a.

ST-MLSVD computes a sequence of approximations, $\hat{\mathcal{S}}_0, \hat{\mathcal{S}}_1, \ldots, \hat{\mathcal{S}}_d$, such that the multilinear rank of $\hat{S}_k$ equals the desired dimension of the corresponding vector space for the first k modes. Let be p, any permutation of the first d numbers, $i = [1, 2, \ldots, d]$ and $k = p(i)$. Each tensor approximation is obtained in two steps: (1) the compact singular value decomposition (SVD) of the mode-k vector space (mode-k matrix unfolding) is computed and (2) the energy in the tensor is re-ordered by projecting onto the span of the matrix of left singular vectors $\hat{\mathbf{U}}_k \in \mathbb{R}^{n_k \times r_k}$, where n_k is the mode-k dimension and r_k is the preselected rank in the current mode. This process is repeated d times. Since the result of each projection depends on the previous ones it is noticeable that

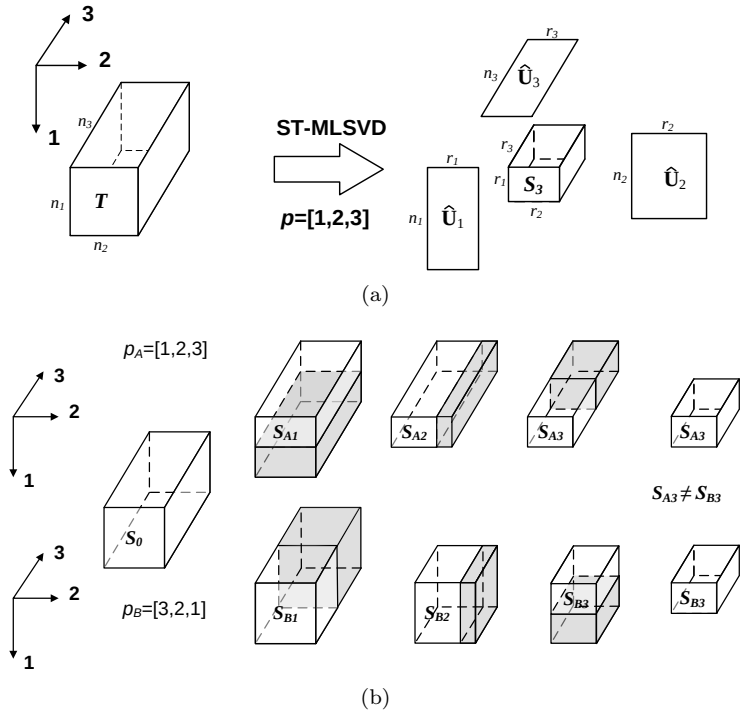


Figure 2.3: ST-MLSVD approximation diagram, (a) ST-MLSVD given the core tensor and the processing order and (b) core tensor truncation procedure for different processing orders.

given the same core size and multilinear ranks, two different processing orders will yield distinct core tensors and factor matrices, see Figure 2.3b.

Figure 2.3b shows two runs of the algorithm for the tensor $\mathcal{S}_0$. The top of Figure 2.3b shows the process for the processing order p_A where $\mathcal{S}_{A1}, \mathcal{S}_{A2}, \mathcal{S}_{A3}$ are the different core tensors after each truncation. On the other hand, the bottom of Figure 2.3b shows the algorithm using a different processing order p_B. It starts with the same tensor $\mathcal{S}_0$ but a different sequence $\mathcal{S}_{B1}, \mathcal{S}_{B2}, \mathcal{S}_{B3}$ is followed. Despite the fact that S_{A3} and S_{B3} have the same dimensions they are not equal since the different processing orders.

2.3 Unsupervised machine learning. Clustering

In unsupervised machine learning algorithms, the aim is to infer a function which describes the hidden structure from non categorized or unlabeled data. One specific type of unsupervised machine learning algorithms is cluster analysis. In cluster analysis, the goal is to partition a set of objects into groups/clusters that capture the natural structure of the data. The clustering process is based only on the information provided by the data. This information describes the objects and their relationships, therefore, similarity measures can be used in order to group objects that are similar in the same cluster. This document focuses on algorithms from cluster analysis, particularly in k-means versions. First, the classic k-means is briefly screened and then two robust versions are discussed.

2.3.1 k-means algorithm

The k-means clustering is an unsupervised learning algorithm which aims to find groups (clusters) in the data. The number of groups is represented by the variable k. The algorithm iteratively assigns each data point to one of k groups based on feature similarity. Since a similarity measure is required, normally the Euclidean distance is used. The output of the algorithm include, the centroids of the k clusters and the class membership labels for each point in the training data. The algorithm consists of two main steps.

1. Data assigment step: each data point is assigned to its nearest centroid based on the squared Euclidean distance $d(\cdot,\cdot)^2$. Let $M = (\mathbf{m}_1^l, \mathbf{m}_2^l, \ldots, \mathbf{m}_k^l)$ be the set of k centroids, then each data point $\mathbf{x}$ is assigned to a cluster based on

$$\mathbf{x} \in S_i : \arg\min\ d(\mathbf{m}_i^l, \mathbf{x})^2, \quad i = 1, \ldots, k \tag{2.16}$$

   where S_i is the set of vectors associated to the centroid $\mathbf{m}_i^l$ and l is the iteration number.

2. Centroid update step: New centroids are computed using the mean of all data points assigned to the given centroid's cluster.

$$\mathbf{m}_i^{l+1} = \frac{1}{\#S_i} \sum_{\mathbf{x}_j \in S_i} \mathbf{x}_j,\ j = 1, \ldots, \#S_i \quad \forall\, i = 1, \ldots, k, \tag{2.17}$$

   where $\#S_i$ is the number of vectors in S_i

The algorithm repeats both steps until a stopping criteria is met.

2.3.2 Truncated k-means algorithm

The trimmed k-means algorithm (TKMEANS) allows that in a given dataset there could be vectors which cannot be assigned to any cluster (outliers) [19], [33]. The algorithm requires two parameters: the number of clusters (k) and the percentage of trimmed observations (α), see algorithm 1.

Algorithm 1 Trimmed k-means (TKMEANS)

Input: A set of observations $\mathbf{X} = \{\mathbf{x}_1, \mathbf{x}_2, \ldots, \mathbf{x}_n\}$, the number of clusters $k \geq 2$, and the percentage of outliers α.

Output: k centroids and n cluster membership labels of $k+1$ clusters.

1: Initialize k random centers, $\mathbf{m}_j^0$, where $j = 1, \ldots, k$

2: Build the set $\mathbf{H}$ which includes the $n(1-\alpha)$ vectors closest to the centers, where (n) is the number of observations.

3: Divide $\mathbf{H}$ into k subsets where, $\mathbf{H}_j$ contains the vectors in $\mathbf{H}$ closer to the center $\mathbf{m}_j$ than to the other centers.

4: Update centers $\mathbf{m}_j^{l+1}$ such that each $\mathbf{m}_j^{l+1}$ is the sample mean of the vectors in $\mathbf{H}_j$.

5: Repeat steps 1-4 $Q = 15$ times (default value), keeping the best solution in the sense of minimizing the function,

$$\arg\min_{\mathbf{H}} \min_{\mathbf{m}_1,\ldots,\mathbf{m}_k} \sum_{\mathbf{x}_i \in \mathbf{H}} \|\mathbf{x}_i - \mathbf{m}_j\|^2. \tag{2.18}$$

6: **stop**

2.3.3 Heterogeneous clustering algorithm

Since trimmed k-means is defined using the Euclidean distance, it assumes a spherical distribution for each cluster. Notwithstanding, in certain problems this assumption might not be valid, i.e., one or more clusters might have different scatter structures, see Figure 2.4. For these types of problems, heterogeneous clustering would yield better results.

TCLUST belongs to the class of heterogeneous clustering algorithms, and it is based on the probabilistic framework proposed in [119] and [120]. It requires three parameters: the number of clusters (k), the proportion of trimmed observations (α) and the upper bound of the ratio between the largest (M_n)

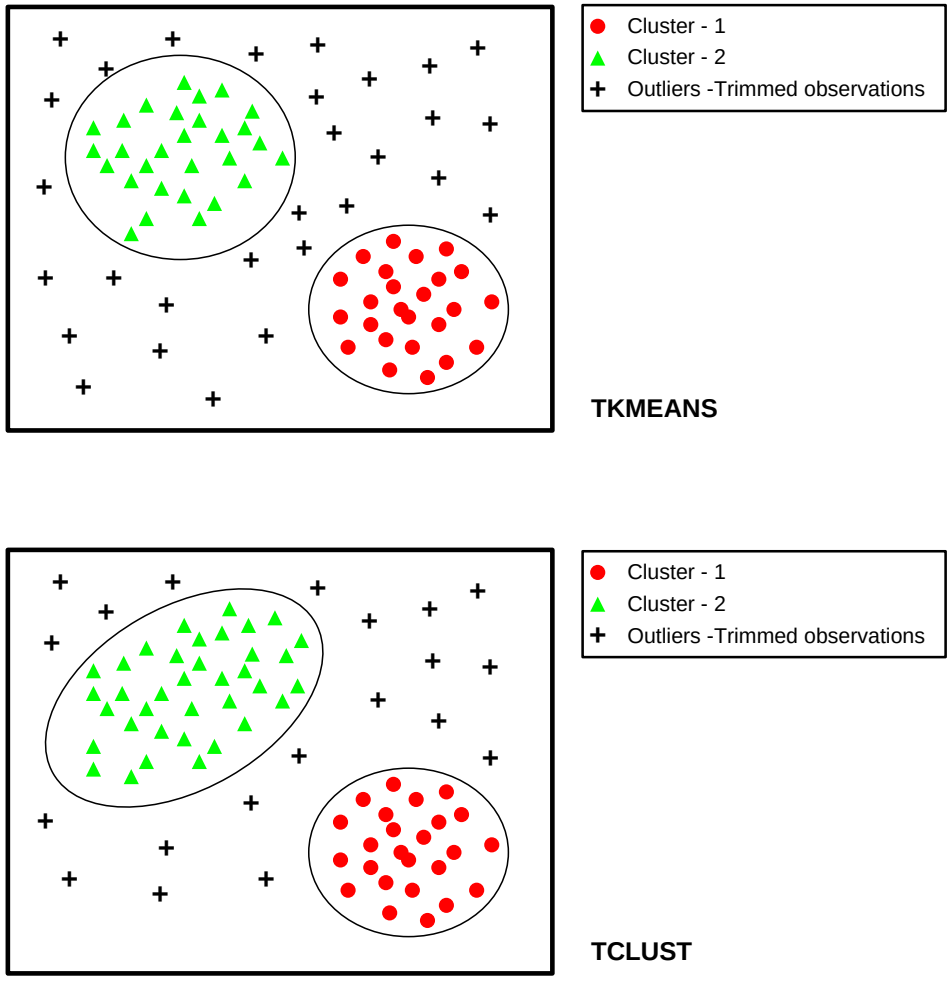


Figure 2.4: TKMEANS and TCLUST comparisson.

and the smallest (m_n) eigenvalue of all covariance matrices (c). The algorithm is described in detail below.

Algorithm 2 Heterogeneous clustering (TCLUST)

Input: A set of observations $\mathbf{X} = \{\mathbf{x}_1, \mathbf{x}_2, \ldots, \mathbf{x}_n\}$, the number of clusters $k \geq 2$, the percentage of outliers α and the upper bound of the ratio between the largest (M_n) and the smallest (m_n) eigenvalue of all covariance matrices (c).

Output: k centroids and n cluster membership labels of $k+1$ clusters.

1: Initialize k random centers ($\mathbf{m}_j^0$), covariance matrices (Σ_j^0) and weights, (π_j^0), where $j = 1, \ldots, k$.

2: Build the set $\mathbf{H}$ which includes the $n(1-\alpha)$ vectors with the largest values for the function,

$$\max_{j=1,\ldots,k} \pi_j^l f\left(\mathbf{x}; \mathbf{m}_j^l, \Sigma_j^l\right). \tag{2.19}$$

where $f(\cdot, \mathbf{m}, \mathbf{\Sigma})$ is the probability density function of the multivariate normal distribution with mean $\mathbf{m}$ and covariance matrix $\mathbf{\Sigma}$.

3: Divide $\mathbf{H}$ into k subsets where $\mathbf{H}_j$ contains the vectors in $\mathbf{H}$ such that the maximum value of the function (2.19) is attained to this j.

4: Update centers $\mathbf{m}_j^{l+1}$, covariance matrices Σ_j^{l+1}, and weights π_j^{l+1} with the sample mean, the sample covariance matrices, and the proportion of vectors in $\mathbf{H}_j$ respectively.

5: Compute

$$\begin{cases} M_n = \max\limits_{j=1,\ldots,k} \max\limits_{l=1,\ldots,p} \lambda_l(\Sigma_j) \\ m_n = \min\limits_{j=1,\ldots,k} \min\limits_{l=1,\ldots,p} \lambda_l(\Sigma_j), \end{cases} \tag{2.20}$$

where $\lambda_l(\Sigma_j)$ are the eigenvalues of the covariance matrices.

6: **if** $M_n/m_n > c$

7: Solve a quadratic programming problem in order to force the constraint $c \geq M_n/m_n$

8: **end if**

9: Repeat steps 1-8 $Q = 15$ times (default value), keeping the best solution in the sense of minimizing the function,

$$\sum_{j=1}^{k} \sum_{\mathbf{x}_i \in \mathbf{H}_j} \log\left(\pi_j^l f\left(\mathbf{x}_i; \mathbf{m}_j^l, \Sigma_j^l\right)\right), \tag{2.21}$$

with $\# \cup_{j=1}^{k} \mathbf{H}_j = [n(1-\alpha)]$

10: **stop**

2.4 Supervised machine learning

A supervised machine learning algorithm learns a function which maps an input to an output. This procedure is based on examples of input-output pairs where the algorithm infers a function from this labeled training dataset. Generally, both input and output data are vectors. The algorithm analyzes the training input-output pairs and yields a function that can be used for inferring the output for new unseen data. In this document, several supervised machine learning algorithms were used. Below, all of them are briefly discussed.

2.4.1 Neural networks

Artificial neural networks are models inspired on the structure and function of the nervous system. A neuron is modeled as a black box which receives information from the outside or other neurons. Furthermore, the neuron produces an output in response to stimuli which is transmitted to other neurons. The standard neuron model is given below,

$$y_i(t) = f_i\left(\sum_{j=1}^{n} \omega_{ij} x_j(t) - \theta_i\right) \tag{2.22}$$

where f_i is the activation function, ω_i is the weighted path between the i-th neuron and the j-th neuron, from the biological point of view it represents the strength of the connection among both neurons, x_j is the j-th input and θ_i is the bias of the neuron or resting value of the neuron.

The architecture of a neural network is the structure or topological pattern of the connections among neurons. The architecture determines the neural network behavior. The neurons can be grouped in units called layers. There are three types of layers:

- Input layer includes the neurons that receive information directly from the outside
- Output layer groups neurons that yield the response of the neural network
- Hidden layer includes full-processing neurons which do not have a connection with the outside.

A multilayer perceptron (MLP) is a feedforward artificial neural network where each neuron is connected to all the neurons in the previous layer through

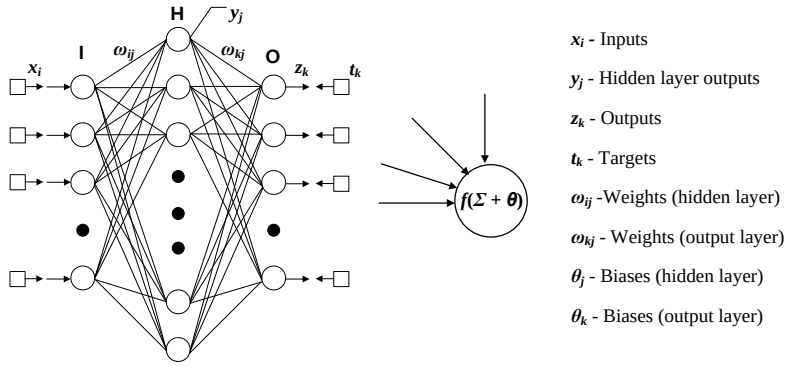


Figure 2.5: Multilayer perceptron (MLP) architecture

weighted paths. In this type of neural networks, there are layers in-between the input and output layers (hidden layers). The network consists of 3 or more layers that all together map data at the input to the output, Figure 2.5.

Multiple algorithms have been proposed for training the MLP. Here, the algorithm used for training is the Levenberg-Marquardt (LM) with Bayesian regularization (BR), the update rule for this algorithm is as follows,

$$\triangle\boldsymbol{\omega}(t) = -\left[\mathbf{J}(t)^T\mathbf{J}(t) + \mu\mathbf{I}\right]^{-1}\mathbf{J}(t)^T\mathbf{E}(t) \tag{2.23}$$

where $\mathbf{J}(t)$ is the Jacobian matrix, $\mathbf{E}(t)$ is the error or performance function which can be the mean squared error (MSE) or the sum of squared errors (SSE) and μ is a control parameter.

2.4.2 Support vector machines

Support vector machines (SVM) are a type of classifier proposed by Vapnik [16], [63] in the context of learning theory. The SVM constructs the hyperplane that best separates between two given classes. The best is in the sense of maximum margin between classes. Figure 2.6a shows two sets of objects of two different classes. There are infinite decision surfaces that can separate between both classes. Two of them are shown in dashed lines. However, the surface with the maximum margin between classes is shown in 2.6a. Here, the margin is the distance of the hyperplane H to both parallel hyperplanes S_0 and S_1 that contain the points nearest to H of both classes.

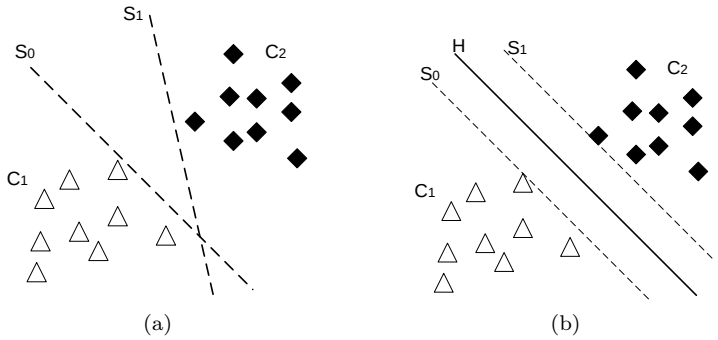


Figure 2.6: Different separating surfaces.

SVM aims to construct the hyperplane for classifying a given set of input-output pairs in the n-dimensional space. Let the set of input vectors $(\mathbf{x}_1, \mathbf{x}_2, \ldots, \mathbf{x}_n)$ all be labeled as follows,

$$\begin{aligned} y_i &= +1, \quad \mathbf{x}_i \in C_1 \\ y_i &= -1, \quad \mathbf{x}_i \in C_2 \end{aligned} \tag{2.24}$$

Given the linear discriminant,

$$g(\mathbf{x}) = \boldsymbol{\omega}^T \mathbf{x} + \omega_0, \tag{2.25}$$

with the decision rule,

$$\begin{aligned} \boldsymbol{\omega}^T \mathbf{x}_i + \omega_0 > 0 \Rightarrow \mathbf{x}_i \in C_1, y_i = +1 \\ \boldsymbol{\omega}^T \mathbf{x}_i + \omega_0 < 0 \Rightarrow \mathbf{x}_i \in C_2, y_i = -1 \end{aligned} \tag{2.26}$$

The set of training patterns will be correctly classified when,

$$y_i g(\mathbf{x}) = y_i(\boldsymbol{\omega}^T \mathbf{x} + \omega_0) > 0, \quad \forall\, i = 1, 2, \ldots, n. \tag{2.27}$$

Hence, the separating hyperplane is,

$$g(\mathbf{x}) = \boldsymbol{\omega}^T \mathbf{x} + \omega_0 = 0 \tag{2.28}$$

Figure 2.7 shows an example in $\mathbb{R}^2$. Here, the margin can be separately computed for each vector,

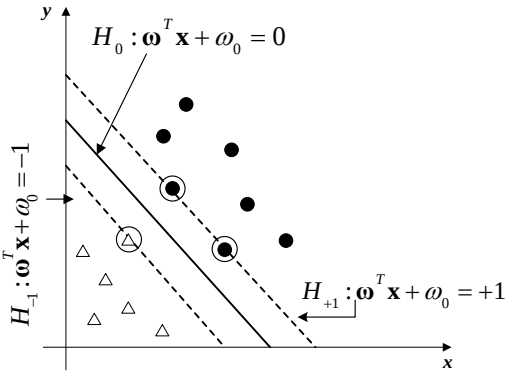


Figure 2.7: Support vector machine hyperplane in $\mathbb{R}^2$ space. Dashed lines represent cannonical hyperplanes. Circled objects corresponds to the support vectors.

$$m(\boldsymbol{\omega}, \omega_0) = \min_{\mathbf{x}_i \in C_1} d(\boldsymbol{\omega}, \omega_0; \mathbf{x}_i) + \min_{\mathbf{x}_j \in C_2} d(\boldsymbol{\omega}, \omega_0; \mathbf{x}_j) = \frac{2}{\sqrt{\boldsymbol{\omega}^T \boldsymbol{\omega}}} = \frac{2}{\|\boldsymbol{\omega}\|} \tag{2.29}$$

Maximizing $m(\boldsymbol{\omega})$ is equivalent to minimize the function,

$$\begin{aligned} &\min_{\boldsymbol{\omega}} J(\boldsymbol{\omega}) = \frac{1}{2} \boldsymbol{\omega}^T \boldsymbol{\omega}, \\ &\text{subject to} \\ &y_i(\boldsymbol{\omega}^T \mathbf{x} + \omega_0) \geq 1, \quad \forall\, i = 1, 2, \ldots, n. \end{aligned} \tag{2.30}$$

In order to relax the constraints slack variables can be introduced. Hence,

$$\begin{aligned} &\min_{\boldsymbol{\omega}, \xi} J(\boldsymbol{\omega}, \xi) = \frac{1}{2} \boldsymbol{\omega}^T \boldsymbol{\omega} + c \sum_{i=1}^{n} \xi_i, \\ &\text{subject to} \\ &y_i(\boldsymbol{\omega}^T \mathbf{x} + \omega_0) \geq 1 - \xi_i, \\ &\qquad \xi_i \geq 0 \quad \forall\, i = 1, 2, \ldots, n. \end{aligned} \tag{2.31}$$

A standard approach for solving the problem above is to apply the Lagrange method and the Karush-Kuhn-Tucker (KKT) conditions for optimality which result in,

$$\min_{\boldsymbol{\alpha}} L(\boldsymbol{\alpha}) = \sum_{i=1}^{n} \alpha_i - \frac{1}{2} \sum_{j=1}^{n} \sum_{i=1}^{n} \alpha_i \alpha_j y_i y_j \mathbf{x}_j^T \mathbf{x}_i$$

subject to (2.32)

$$\sum_{i=1}^{n} \alpha_i y_i = 0, \quad 0 \leq \alpha_i \leq c, \quad \forall\, i = 1, 2, \ldots, n.$$

The last expression is known as the dual form of the Lagrange function for the SVM. One relevant feature of the dual form is that the function is expressed in terms of the scalar product of both vectors. This fact can be exploited in order to extend the formulation to nonlinear SVM. This can be accomplished by replacing the normal scalar product by another nonlinear function which represents the scalar (inner) product in a higher dimensional space.

$$L(\boldsymbol{\alpha}) = \sum_{i=1}^{n} \alpha_i - \frac{1}{2} \sum_{j=1}^{n} \sum_{i=1}^{n} \alpha_i \alpha_j y_i y_j K(\mathbf{x}_j, \mathbf{x}_i), \tag{2.33}$$

where the function K is the kernel or the scalar product in a high (possibly infinite) dimensional space. Several functions have been proposed as inner products. Some of these are shown in table 2.1.

Table 2.1: Different kernel functions and parameters

Kernel	**Expression**	**Parameters**
Quadratic	$\langle \mathbf{x}_i, \mathbf{x}_j \rangle^2$	-
Polynomial	$(\langle \mathbf{x}_i, \mathbf{x}_j \rangle + p)^n$	p, n
Radial Basis Functions	$\exp(-\|\|\mathbf{x}_i - \mathbf{x}_j\|\|^2 / 2\sigma^2)$	σ
Hyperbolic tangent	$\tanh(\langle \mathbf{x}_i, \mathbf{x}_j \rangle + b)$	b

2.4.3 Least-squares support vector machines

Least-squares support vector machines (LS-SVM) is a formulation of SVM where the inequality constraints have been replaced by equality constraints [117], [116]. The new problem is written as follows,

$$J(\boldsymbol{\omega}, e) = \frac{1}{2}\boldsymbol{\omega}^T\boldsymbol{\omega} + \gamma \sum_{i=1}^{n} e_i^2,$$

$$\text{subject to} \tag{2.34}$$

$$y_i(\boldsymbol{\omega}^T\mathbf{x} + \omega_0) = 1 - e_i, \quad \forall\, i = 1, 2, \ldots, n.$$

This modification allows for solving the SVM through the solution of a set of linear equations [117] [116]. The LS-SVM dual model representation is as follows,

$$\left[\begin{array}{c|c} 0 & \mathbf{y}^T \\ \hline \mathbf{y} & \boldsymbol{\Omega} + \gamma^{-1}\mathbf{I} \end{array}\right] \begin{bmatrix} b \\ \boldsymbol{\alpha} \end{bmatrix} = \begin{bmatrix} 0 \\ \mathbf{1} \end{bmatrix}, \tag{2.35}$$

where $\mathbf{y}$ is the vector of outputs, $\boldsymbol{\alpha}$ and b are the dual model parameters, γ is the regularization parameter, $K(\cdot)$ is the kernel function, $\mathbf{1}$ is a column vector of ones and $\boldsymbol{\Omega}$ is the matrix whose elements are,

$$\Omega_{(i,j)} = y_i y_j K(\mathbf{x}_i, \mathbf{x}_j). \tag{2.36}$$

Depending on the kernel function there could be one or more parameters to adjust for this model.

2.4.4 Fixed-size LSSVM

Fixed-size least-squares support vector machines (FS-LSSVM) is a method for solving large-scale classification/regression problems. It takes advantage of the primal-dual LS-SVM formulations. Particularly in problems with large datasets, it could be of benefit to solve the SVM in the primal space [116] [21]. Such approach would require an explicit expression of the feature map or an approximation to this map. In order to efficiently obtain the approximation to the map, the Nyström method has been proposed [131].

The Nyström method uses a low rank approximation of the kernel matrix by selecting m rows or columns of this matrix. Figure 2.8 shows a general diagram for a FS-LSSVM construction.

The vectors for training are selected by using the active prototype vector (APV) selection method [116] [21]. This procedure searches for prototype vectors (PV)

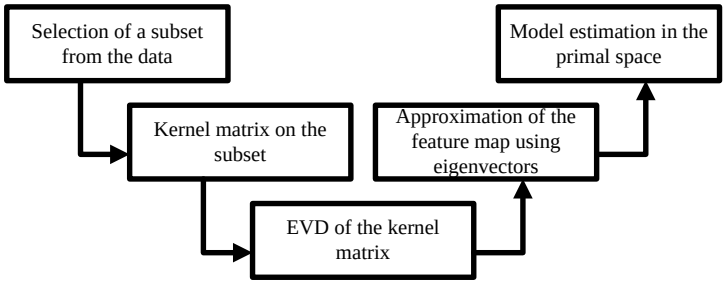


Figure 2.8: Fixed-Size LSSVM construction stages.

which maximize the quadratic Rényi entropy criterion ($H_{R2}^m(x)$). The formal definition of the quadratic Rényi entropy [29] is as follows,

$$H_{R2}^m(x) = -\log \int f(x)^2 dx, \tag{2.37}$$

where $f(\cdot)$ is the probability density function. In practice, the information potential ($\hat{H}_{R2}^m(\mathbf{X})$) is used. The latter is an estimator of $H_{R2}^m(\mathbf{X})$ determined by kernel density estimation methods. Here, the link between kernel principal component analysis (KPCA) and nonparametric density estimation is exploited [37],

$$\hat{H}_{R2}^m(\mathbf{X}) = -\log \left[\frac{1}{m^2} \mathbf{1}^T \cdot \mathbf{K} \cdot \mathbf{1} \right], \tag{2.38}$$

where $\mathbf{K}$ is the kernel matrix given by

$$\mathbf{K} = K(h_{R2}^m; \mathbf{x}_i, \mathbf{x}_j) \forall\, i, j, \tag{2.39}$$

where $K(\cdot)$ is the Radial Basis Functions kernel as defined in Table 2.1, h_{R2}^m is the kernel bandwidth, and m is the number of vectors. Using the eigenvalue decomposition of this matrix, the information potential can be estimated as [124],

$$\hat{H}_{R2}^m(\mathbf{X}) = -\log \left[\frac{1}{m^2} \sum_{i=1}^{m} \sum_{j=1}^{m} v_{ij}^2 \cdot \lambda_i \right], \tag{2.40}$$

where v_{ij} are the components of the i-th eigenvector and λ_i is the i-th eigenvalue of the following eigenvalue problem,

$$\mathbf{K} \cdot \mathbf{v}_i = \lambda_i \cdot \mathbf{v}_i, \quad i = 1, \ldots, m. \tag{2.41}$$

Below a slightly modified version of APV selection is presented in algorithm 3 [116] [21]. The main difference with respect to the algorithm proposed in [21] is that the algorithm 3 runs for a predefined number of iterations (m), which is equal to the number of support vectors.

Algorithm 3 APV selection for training

Input: A set of training set pairs $T_n = \{(\mathbf{x}_1, y_1), (\mathbf{x}_2, y_2), \ldots, (\mathbf{x}_n, y_n)\}$, n the total number of data points, $m \ll n$ the number of support vectors.

Output: A set of prototype vectors S_m where Rényi entropy is maximized.

1: Let the training set $T_n = \{(\mathbf{x}_1, y_1), (\mathbf{x}_2, y_2), \ldots, (\mathbf{x}_n, y_n)\}$.
Choose a subset of prototype vectors $S_m \subset T_n$ of size m at random and define the complement subset $S_{n-m} = (S_m)^{\mathrm{c}} \in T_n$.

2: **for** $i = 1$ **to** m

3: Randomly select one sample point from both subsets $\mathbf{x}^* \in S_m$ and $\mathbf{x}^+ \in S_{n-m}$, then
swap$(\mathbf{x}^*, \mathbf{x}^+)$

4: Compute

$$\begin{cases} E_1 = \hat{H}^m_{R2}(\mathbf{x}_1, \ldots, \mathbf{x}^+, \ldots, \mathbf{x}_m) \\ E_2 = \hat{H}^m_{R2}(\mathbf{x}_1, \ldots, \mathbf{x}^*, \ldots, \mathbf{x}_m) \end{cases} \tag{2.42}$$

5: **if** $E_1 > E_2$

6: $\mathbf{x}^+ \in S_m$ and $\mathbf{x}^* \notin S_m$, $\mathbf{x}^* \in S_{n-m}$,

7: **else**

8: $\mathbf{x}^* \in S_m$ and $\mathbf{x}^+ \notin S_m, \mathbf{x}^+ \in S_{n-m}$,

9: **end if**

10: **end for**

11: **stop**

2.4.5 Hyper-parameter tuning

Usually, both unsupervised and supervised machine learning methods have hyper-parameters that have to be tuned. For instance, the number of hidden layers and the number of neurons in each hidden layer are common hyper-parameters to adjust in neural networks. Another example of hyper-parameter

is the number of clusters in a clustering problem. There are several approaches to address the problem of hyper-parameter tuning, e.g., random selection, trial-and-error procedures, grid search, cross-validation, optimization among others [81].

In this document, mainly grid search and optimization methods have been used. The optimization method used here has been proposed in [50] and is based on both coupled simulated annealing (CSA) and Nelder-Mead simplex optimization algorithms. Below, a brief introduction to both algorithms is presented.

Coupled simulated annealing

Coupled simulated annealing (CSA) is a global optimization technique which consists of a set of simulated annealing [134] processes coupled to each other by a term in the acceptance probability function (a.p.f). Thus, a new term is included in the a.p.f as follows,

$$0 \leq A_{\Theta}(\xi, \mathbf{x}_i \rightarrow \mathbf{y}_i) \leq 1, \tag{2.43}$$

where $\mathbf{x}_i$ is the i-th current solution, Θ is the set of current solutions $\mathbf{x}_i \in \Theta$, $\forall i$, $\mathbf{y}_i$ is the i-th probing solution and ξ is the coupling term which is a function that depends on the cost of the solutions in Θ,

$$\xi = f(E(\mathbf{x}_1), E(\mathbf{x}_2), \ldots, E(\mathbf{x}_m)), \tag{2.44}$$

where m is the number of coupled simulated annealing processes.

There are several approaches to CSA which differ in the acceptance probability function and/or the coupling term used. Here the CSA modified with variance control (CSA-MwVC) [134] was used. The acceptance probability function of CSA-MwVC is as follows,

$$A_{\Theta}(\xi, \mathbf{x}_i \rightarrow \mathbf{y}_i) = \frac{1}{\xi} \exp\left(\frac{\hat{E}(\mathbf{x}_i)}{T_{ac}^k}\right), \tag{2.45}$$

where ξ is

$$\xi = \sum_{\mathbf{x}_i \in \Theta} \exp\left(\frac{\hat{E}(\mathbf{x}_i)}{T_{ac}^k}\right). \tag{2.46}$$

In both expressions $\hat{E}(\mathbf{x}_i)$ is defined as,

$$\hat{E}(\mathbf{x}_i) = E(\mathbf{x}_i) - \max_{\forall \mathbf{x}_i \in \Theta} E(\mathbf{x}_i). \tag{2.47}$$

The acceptance temperature schedule in CSA-MwVC is replaced by a variance control using the following rule,

$$T_{ac}^{k} = \begin{cases} T_{ac}^{k-1}(1-\upsilon), \text{ if } \sigma^2 < \sigma_D^2 \\ T_{ac}^{k-1}(1+\upsilon), \text{ if } \sigma^2 > \sigma_D^2 \end{cases}, \tag{2.48}$$

where T_{ac}^{k} is the acceptance temperature in the k-th step, υ is the rate of increase or decrease of the acceptance temperature and σ^2 and σ_D^2 are the variance and the desired variance of the process respectively. The latter can be computed as,

$$\sigma_D^2 = \hat{\sigma}^2 \left(\frac{m-1}{m^2} \right), \tag{2.49}$$

where $\hat{\sigma}^2$ is a suitable value of the variance and m is the number of coupled SA processes.

Nelder-Mead *simplex*

Nelder-Mead *simplex* is an unconstrained optimization algorithm for finding the minimum of a function of n variables [78], [54]. A *simplex* is a generalized triangle in n dimensions. The method consists of a pattern search that compares the target function values at the vertices (points) of a *simplex*. The largest value of the target function corresponds to the worst vertex which is rejected and replaced with a new one each iteration. Thus, a succesive approximation procedure is performed where the function values at the vertices get smaller after each iteration. Algorithm 4 describes the standard Nelder-Mead, for the sake of simplicity, only reaching the maximum number of iterations has been considered as termination criterion.

Algorithm 4 Standard Nelder-Mead *simplex*

Input: A function to minimize $f(\mathbf{x}) : \mathbf{x} \in \mathbb{R}^n$, $N_{\max}$, maximun number of iterations and $n+1$ vertices $(\mathbf{x}_1, \mathbf{x}_2, \ldots, \mathbf{x}_{n+1})$.

Output: $\hat{\mathbf{x}} = \text{argmin } f(\mathbf{x})$.

1: **for** i=1 **to** $N_{\max}$

2: Order the $n+1$ vertices to satisfy:

$(f(\mathbf{x}_1) \leq f(\mathbf{x}_2) \leq \cdots \leq f(\mathbf{x}_{n+1}))$

Algorithm 4 Standard Nelder-Mead *simplex*

Compute, *//Reflection step.*

$$\begin{cases} \overline{\mathbf{x}} = \frac{1}{n}\sum_{i=1}^{n}\mathbf{x}_i \\ [\mathbf{x}_r = \overline{\mathbf{x}} + (\overline{\mathbf{x}} - \mathbf{x}_{n+1}), f_r = f(\mathbf{x}_r)] \end{cases}, \tag{2.50}$$

if $f_1 \leq f_r \leq f_n$
  $\mathbf{x}_{n+1} = \mathbf{x}_r$
else if $f_r < f_1$ *//Expansion step.*
  Compute, $[\mathbf{x}_e = \overline{\mathbf{x}} + 2(\mathbf{x}_r - \overline{\mathbf{x}}), f_e = f(\mathbf{x}_e)]$
  if $f_e < f_r$
    $\mathbf{x}_{n+1} = \mathbf{x}_e$
  else
    $\mathbf{x}_{n+1} = \mathbf{x}_r$
  end if
else if $f_r \geq f_n$ *//Contraction step.*
  if $f_r < f_{n+1}$ *//Outside contraction.*
    Compute, $[\mathbf{x}_{oc} = \overline{\mathbf{x}} + 0.5(\mathbf{x}_r - \overline{\mathbf{x}}), f_{oc} = f(\mathbf{x}_{oc})]$
    if $f_{oc} \leq f_r$
      $\mathbf{x}_{n+1} = \mathbf{x}_{oc}$
    end if
  else *//Inside contraction*
    Compute, $[\mathbf{x}_{ic} = \overline{\mathbf{x}} - 0.5(\overline{\mathbf{x}} - \mathbf{x}_{n+1}), f_{ic} = f(\mathbf{x}_{ic}),]$
    if $f_{ic} < f_{n+1}$
      $\mathbf{x}_{n+1} = \mathbf{x}_{ic}$
    end if
  end if
else
  Compute $f(\mathbf{x})$ at $\mathbf{v}_i = \mathbf{x}_1 + 0.5(\mathbf{x}_i - \mathbf{x}_1)$
  Conform the next unordered set of vertices $(\mathbf{x}_1, \mathbf{v}_2, \ldots, \mathbf{v}_n)$
end if
end for
stop

2.5 Conclusions

This chapter presented an overview of the machine learning algorithms used in this thesis. All the algorithms presented will be used for AECG processing. Tensors and tensor decompositions are used in the context of premature heartbeat detection in Chapter 3. PCA, DCT and RES are all used in Chapter

4 as feature extraction stages for T-wave end detection algorithms. Clustering algorithms such as k-means and robust k-means are used for training set selection in Chapter 4. The different SVM formulations have been used in both, premature heartbeat detection and T-wave end detection in Chapter 3 and 4 respectively. Finally, MLP neural networks are used in Chapter 4 for detecting the T-wave end.

Chapter 3

Premature heartbeat detection using tensors

This chapter presents two methods for premature or ectopic heartbeat detection in the AECG. Since the reliability of HRV/QT analysis in a holter monitoring context might be affected by the inclusion of ectopic heartbeats, the aim is to provide a novel approach for constructing high performance classifiers for this application. Both algorithms are tensor-based methods. The chapter is divided in four sections. An introduction to the classification topic is included in section 3.1. Then, a first approach based on CPD and SVM is addressed in section 3.2. In section 3.3 the second method is presented and discussed. Final comments and conclusions are given in section 3.4. The contents of this chapter is based on two conference papers [113], [111].

3.1 Introduction

As stated above, the premature heartbeat detection task is essentially a classification problem. There are multiple approaches to ECG signal classification. However, most of them require basic steps that include signal filtering, R-peak (maximum of R wave) detection, classification and sometimes post-processing. Figure 3.1 shows a generic structure for ECG signal classification.

The filtering stage may include linear and/or nonlinear filtering techniques. The aim of digital filtering is to eliminate (or to reduce) the noise, the interferences

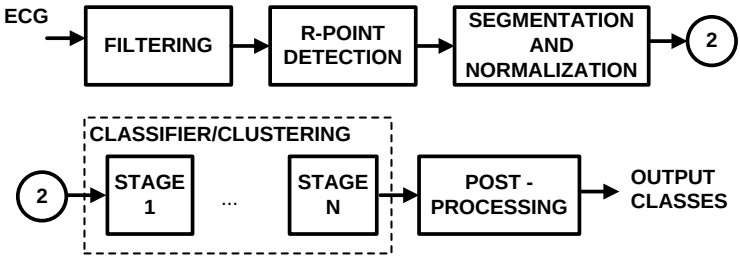


Figure 3.1: A general approach for classifying heartbeats using the ECG.

and the baseline drift that may contaminate the ECG signal. The R-point detection stage determines the R-peak position for each heartbeat with the smallest possible error. There are hundreds of papers that address the R-peak detection. For an extensive review, the reader is refered to [51]. Since the aim of this study is not the R-peak detection, the annotations provided with the database were used to evaluate the algorithms. Hence, the R peaks are known for all records on the database. This assures that the results depend on the classification methods regardless of the R-peak detection approach.

The segmentation of the signal allows obtaining fixed-length vectors. Two approaches are possible for the segmentation method. On one hand, an equal number of samples may be taken at both sides of the R-peak i.e. a symmetric window may be used. On the other hand, a different number of samples taken at both sides of the R-peak corresponds to an asymmetric window. The classification/clustering stage assigns a class or cluster to each heartbeat. Often this is a multi-stage block and there are several alternatives that make use of machine learning techniques. The post-processing stage interprets and qualifies the output of the classifier/clustering stage. Frequently, this stage includes decision rules to determine the final output.

The algorithms presented in this chapter follow the general diagram depicted in Figure 3.1 excluding the R-point detection stage. Here, a patient-dependent approach was taken. Thus, the training and testing processes are performed for each record. Other similarities will be outlined below. The main differences among algorithms are shown in sections 3.2.1 and 3.3.1 respectively.

Both algorithms have been evaluated using the database from the St.-Petersburg Institute of Cardiological Technics 12-lead Arrhythmia Database (INCARTDB) available at Physionet [38]. INCARTDB consists of 75 annotated recordings extracted from 32 Holter records. Each record is 30 minutes long and contains 12 standard leads. The sampling frequency in all cases is 257 Hz. INCARTDB is a highly imbalanced database, the normal class or sinus rhythm beats,

corresponds to 87.30% of the total number of beats while premature ventricular contraction (PVC) beats correspond to 11.38%. Any other beat type belongs to the remaining 1.32% of the total. The latter along with PVC beats compound the abnormal class.

The segmentation method is the same for both approaches. It consists of truncating the heartbeat using a window length of $\sim$ 510 ms which starts $\sim$ 195 ms before the current R-peak and ends $\sim$ 315 ms after. Since annotated signals are used, the R-peak locations are previously known. This assures that the results do not depend on the R-peak detection method. Each heartbeat was normalized by subtracting the average value and dividing by the standard deviation.

A segmented multi-lead heartbeat can be represented as a matrix where the rows are the different leads or channels. Similarly, the columns correspond to the samples of the segmented heartbeat. Thus, each heartbeat is a $L \times W$ matrix, where L is the number of leads and W is the length in samples of the heartbeat. Since both approaches use tensor decompositions and the signals are second order tensors (matrices) a *tensorization* process must take place ensuring the increase of the data order. The *tensorization* maps the set of $L \times W$ matrices to a third order tensor where each heartbeat (matrix) is stacked as frontal slices one after the other. This results in a third order tensor, $\mathcal{T} \in \mathbb{R}^{L \times W \times N}$, where N is the number of heartbeats in the record, Figure 3.2.

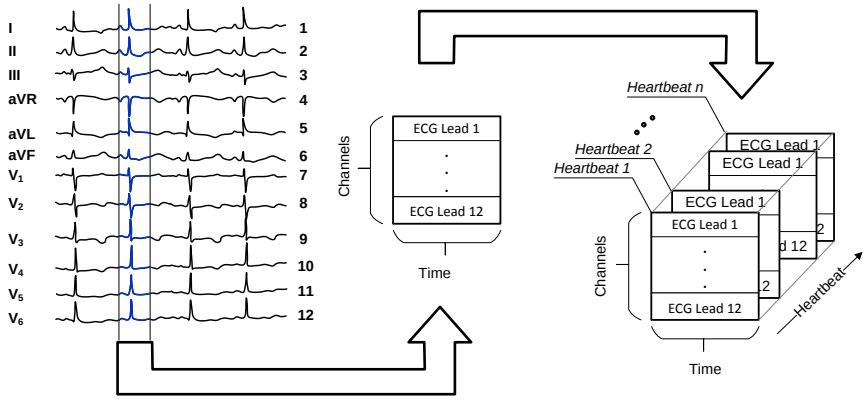


Figure 3.2: *Tensorization* process for a 12-lead ECG.

3.2 Premature heartbeat detection using CPD

This method uses a combination of *tensorization* and CPD to extract features from a multi-lead ECG. Next, these features are used as inputs to a classifier for detecting premature heartbeats. The classifier structure is shown in Figure 3.3.

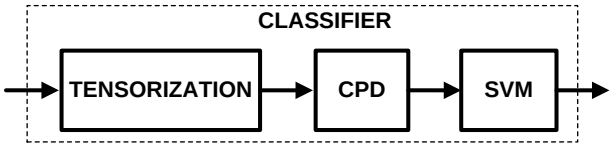


Figure 3.3: Heartbeat classification scheme using CPD and SVM.

3.2.1 Materials and methods

The filtering block is divided into two stages, i.e. (1) elimination of baseline wander and (2) high-frequency noise filtering. The first stage uses median-based filtering [22] and the second one uses a wavelet filter with a hard thresholding approach [72].

The median-based filter performs two passes with two different window sizes, 200 ms, and 600 ms. The first pass using the 200 ms window removes the P waves and the QRS complexes of each heartbeat. The second pass removes the T wave. After removing the physiological waves the resulting signal is considered the baseline wander. Thus, it is subtracted from the original ECG.

The second stage filters out the high-frequency noise. First, the discrete wavelet transform (DWT) of the signal is computed. This process decomposes the signal into four levels using the Daubechies 4 (db4) as the mother wavelet. After the signal decomposition, both detail coefficients of level 1 and 2 are filtered using thresholds for each level. First, estimates of the noise variance in each level are computed as follows,

$$\sigma_{d_j} = \frac{\text{med}\left(|d_j|\right)}{0.6745} \tag{3.1}$$

where d_j is either d_1 or d_2, i.e., the detail coefficients of level 1 and 2 respectively. Then, the thresholds can be obtained by,

$$T_{d_j} = \sigma_{d_j}\sqrt{2\log(N)}, \tag{3.2}$$

where N is the length of the signal. Next, the hard thresholding procedure is performed over $d_j[k]$ using,

$$\widehat{d}_j[k] = \begin{cases} d_j[k] & \text{if } |d_j[k]| \geq T_{d_j} \\ 0 & \text{if } |d_j[k]| < T_{d_j} \end{cases} \tag{3.3}$$

where $1 < k < N$. Finally, the signal is reconstructed using the inverse DWT (IDWT). The length of the segmentation window is equal to 131 samples including the R-peak. The segmentation window is asymmetric. It starts 50 samples (195 ms) before each R-peak and ends 80 samples (315 ms) after the R-peak.

After *tensorization*, the constructed tensor has three modes. The first mode is the space, i.e., the channels, the second one is the time course, and finally the last mode is the heartbeat. Before applying CPD, an appropriate rank value (R) must be selected. Here, the criterion for selecting rank is based on the mean relative error (MRE) among all records for a given rank (R value).

$$\underset{R=1,\cdots,20}{\text{MRE}(\%)} = 100\% \cdot \frac{1}{N_r} \sum_{i=1}^{N_r} \frac{\left\| \hat{\mathcal{T}}_i^R - \mathcal{T}_i \right\|_F}{\|\mathcal{T}_i\|_F} = 100\% \cdot \frac{1}{N_r} \sum_{i=1}^{N_r} \frac{\|\mathcal{E}_i^R\|_F}{\|\mathcal{T}_i\|_F}, \tag{3.4}$$

where $\hat{\mathcal{T}}_i^R$ is the rank-R tensor after the CPD and N_r is the number of records in the database. For each record the MRE was computed varying R in the range of 1 to 20. Figure 3.4 shows the average graph for the whole database. The figure was obtained by averaging the graphs of each individual recording. As expected, the mean relative error monotonically decreases with the rank of the CPD.

It is noticeable that the MRE drops below 20% when $R \geq 12$. However, MRE drop for $R \in [6, 12]$ is only 5%, and smaller for the range $[12, 20]$. On the contrary, the MRE decreases approximately 30% for $R \in [1, 5]$. Furthermore, the improvement in the MRE is below 5% when the number of rank-1 terms in the CPD increases from 3 to 4. The opposite of the latter are the first differences, 17.56% and 12.05% respectively. This suggests 3 as the appropriate number of rank-1 terms.

The rank-3 CPD yields three loading matrices corresponding to space (channel) $\mathbf{S} \in \mathbb{R}^{12\times3}$, time course ($\mathbf{T} \in \mathbb{R}^{131\times3}$) and heartbeat mode ($\mathbf{H} \in \mathbb{R}^{N\times3}$) respectively, where N is the number of heartbeats in the current recording. The heartbeat mode factor matrix ($\mathbf{H}$) is used as the input for the classifier. The

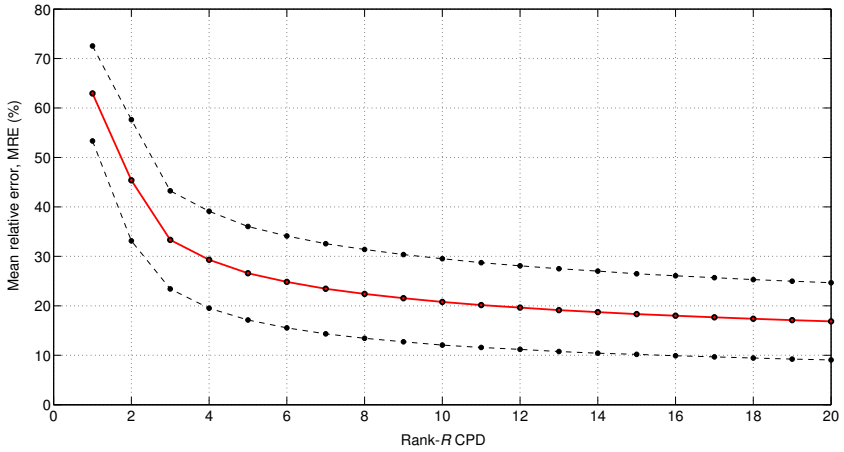


Figure 3.4: Mean relative errors in a rank-R CPD ($1 \leq R \leq 20$), for all records in the database. Both dashed-lines represent the MRE average curve $\pm$ the sample standard deviation of the MRE for a given R.

rows of $\mathbf{H}$ are the feature components extracted for each heartbeat. A binary linear SVM was used for the classification task. The linear classifier is chosen because it is simpler and faster than the nonlinear ones. The main drawback is that non-linearly separable datasets will be harder to separate affecting the overall performance. All the SVM-based classifiers were created, trained and tested using LIBSVM [12]. A very useful feature of LIBSVM is the inclusion of weighted SVM for dealing with imbalanced datasets. Since the balance ratio between classes in INCARTDB is $\cong 7$, a suitable weight value might be in the range of 3 to 7. The results below were obtained with a weight value of 5.

Here, a patient-specific approach is followed for selecting the training and testing sets. For each record, 2% of the beats are randomly selected for training while the ratio among classes is kept. This low percentage allows for a fast training set construction. The performance evaluation for the classifier was carried out by computing four indexes in the testing set: sensitivity (Se), specificity (Sp), positive predictive value (P+) and accuracy (Acc).

3.2.2 Results

Tables 3.1 and 3.2 show the global confusion matrix and the performance indexes of the classifiers respectively. The capital letter **N** stands for normal class whereas ectopic heartbeats are represented by the capital letter **A**. Table

3.2, was obtained by summing the confusion matrices from all recordings. Record 61 was omitted from the analysis since it contains only one premature heartbeat. Thus, it is not possible to build training and testing sets using the 2%-98% ratio.

Table 3.1: Global confusion matrix for all classifiers.

	A	**N**
A	20530	3421
N	1333	145666

Table 3.2: Global performance indexes for all classifiers.

Se(%)	**Sp**(%)	**P+**(%)	**Acc**(%)
93.90	97.70	85.72	97.22

Besides, the performance of the classifier was examined under two conditions, namely, imbalanced and balanced datasets. A balanced record would be any record in the database that has a ratio lower than three, e.g. (76%-24%), between the most represented class and the least represented class in the record. From the 75 records in the database, only 15 records fulfill this condition, the other 60 belong to the group of imbalanced records. The results in Tables 3.3 - 3.6 show the global performance for the two groups. As record 61 has been excluded the imbalanced group covers 59 records.

Table 3.3: Global confusion matrix for the classifiers tested in the balanced group (15 records)

	A	**N**
A	12457	2722
N	116	19904

Table 3.4: Performance indexes for the classifiers tested in the balanced group (15 records).

Se(%)	**Sp**(%)	**P+**(%)	**Acc**(%)
99.08	87.97	82.07	91.94

Table 3.5: Global confusion matrix for the classifiers tested in the imbalanced group (59 records)

	A	**N**
A	8073	699
N	1217	125762

Table 3.6: Performance indexes for the classifiers tested in the imbalanced group (59 records).

Se(%)	**Sp**(%)	**P+**(%)	**Acc**(%)
86.90	99.45	92.03	98.59

Next, specific cases were examined at record level in both groups (imbalanced and balanced datasets). The first example corresponds to the record 36 of the database. This record has 3449 (N)ormal and 462 (A)bnormal heartbeats yielding a balance ratio of 88%-12%. The test results for this record are shown in Tables 3.7 and 3.8.

Table 3.7: Confusion matrix for the classifier trained and tested with record 36 (imbalanced dataset).

	A	**N**
A	387	47
N	66	3333

Table 3.8: Performance indexes for the classifier trained and tested with record 36 (imbalanced dataset).

Se(%)	**Sp**(%)	**P+**(%)	**Acc**(%)
85.43	98.61	89.17	97.05

The second example corresponds to the record 31 which has 1844 normal and 1366 abnormal heartbeats yielding a balance ratio of 62%-42%, see Tables 3.9 and 3.10.

Table 3.9: Confusion matrix for the classifier trained and tested with record 31 (balanced dataset).

	A	**N**
A	1332	24
N	7	1783

Table 3.10: Performance indexes for the classifier trained and tested with record 31 (balanced dataset).

Se(%)	**Sp**(%)	**P+**(%)	**Acc**(%)
99.48	98.67	98.23	99.01

Finally, two examples from the balanced group are presented where negative results were obtained, record 33 (58%-32%) and record 34 (73%-27%), see Tables 3.11 - 3.14.

Table 3.11: Confusion matrix for the classifier trained and tested with record 33.

	A	**N**
A	580	1221
N	0	0

Table 3.12: Performance indexes for the classifier trained and tested with record 33.

Se(%)	**Sp**(%)	**P+**(%)	**Acc**(%)
100	0	32.20	32.20

Table 3.13: Confusion matrix for the classifier trained and tested with record 34.

	A	**N**
A	526	1401
N	0	0

Table 3.14: Performance indexes for the classifier trained and tested with record 33.

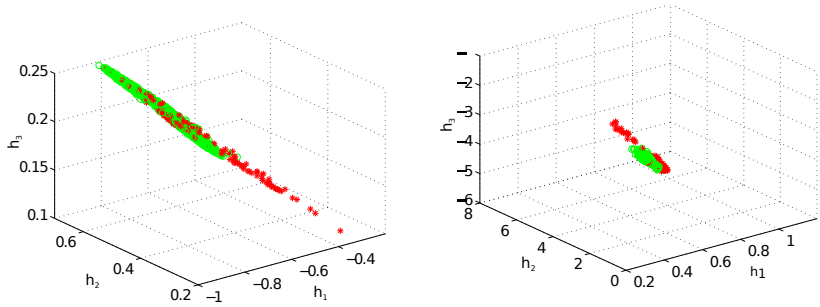
Se(%)	**Sp**(%)	**P+**(%)	**Acc**(%)
100	0	27.30	27.30

Table 3.15: Global confusion matrix for the classifiers tested in the balanced group excluding records 33 and 34.

	A	**N**
A	11351	100
N	116	19904

Table 3.16: Performance indexes for the classifiers tested in the balanced group excluding records 33 and 34.

Se(%)	**Sp**(%)	**P+**(%)	**Acc**(%)
98.99	99.50	99.17	99.31



(a) (b)

Figure 3.5: Plot of feature components extracted from two recordings of the INCART database, h_1, h_2, h_3 correspond to the feature components in the heartbeat mode factor matrix, **H** (a) record 33 and (b) record 34.

3.2.3 Discussion

As can be seen from Tables 3.1 and 3.2, the classifier has a high global performance. Comparing the performances in groups of imbalanced and balanced

recordings, one can see that in general terms, the performance is higher in the balanced group, see Tables 3.3-3.6. The latter is consistent with the fact that balanced datasets are likely to produce better training sets. However, the results for imbalanced datasets are still acceptable with a sensitivity above 85%.

Going deeper into the analysis, two examples where the method has shown the worst performance are given in Tables 3.11-3.14. This misbehavior arises in records with a majority of premature atrial contractions (PAC) such as records 33 (591 PAC) and 34 (536 PAC), see Figures 3.6a-3.6b. PAC heartbeats are originated somewhere outside the SA node but in the atria. Normally, the morphology of the P wave will change or might be completely absent in this class of heartbeats. However, the morphology of the heartbeat will not be extensively affected since the ventricular repolarization occurs normally. It is likely that the failure of the algorithm is due to the subtle morphological differences between normal and PAC heartbeats. Thus, it seems clear that the classifiers will not work effectively for these two records. Figures 3.5a-3.5b show the plot of the features extracted for both recordings. It is apparent that the points are not linearly separable and the linear SVM cannot effectively handle such conditions. Tables 3.15 and 3.16 show the confusion matrix and the performance indexes for the balanced group excluding records 33 and 34. Excluding these records, the performance is therefore clearly improved.

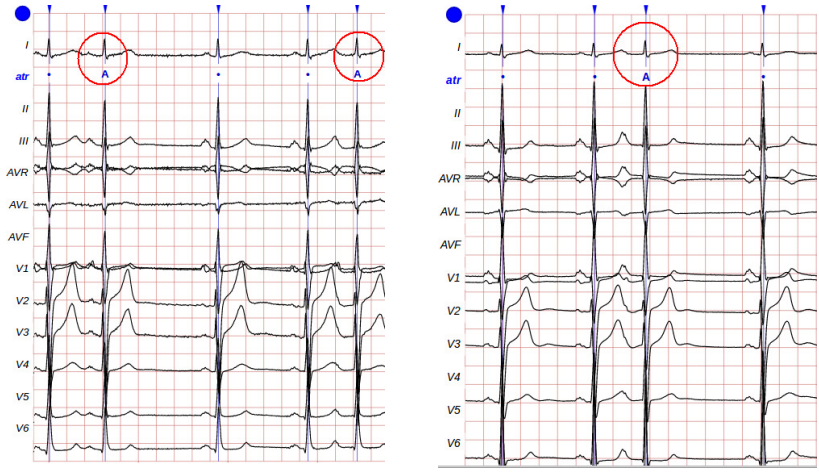


Figure 3.6: Fragments of recordings with several PAC heartbeats (a) record 33 and (b) record 34.

3.2.4 Conclusions

The findings of this study suggest that the use of tensors and CPD in combination with SVM is feasible for detecting ectopic heartbeats. Moreover, the algorithm deals with multi-lead ECG in a straightforward and natural approach. Besides, this algorithm allows building only one classifier regardless the number of leads in the record. The latter saves time and eliminates the need for decision rules. However, there are still some limitations in this approach that require attention in the future. The first limitation is the selection of the rank of the decomposition which strongly depends on the data. Thus, it demands no minor effort in tuning up the algorithm for a patient-specific approach. The latter is unacceptable from the perspective of practical implementations. The second limitation is the performance drop in records with PAC heartbeats. This limitation could be eliminated using nonlinear SVM. The last restriction is the lack of a clearly defined method for selecting the training set. In this approach, this process is implicitly based on prior knowledge of the underlying class distribution. However, this is not a plausible scenario in practice. The next section addresses all these issues.

3.3 Premature heartbeat detection using ST-MLSVD

In a system for AECG analysis, no prior knowledge of the underlying class distribution is available. Hence, there is no straightforward way to build balanced training sets neither a guarantee to achieve a predefined number of heartbeats of a certain class for training. Moreover, if the algorithm requires training e.g in a patient-specific approach, a very small training/testing size ratio is expected i.e. small training set sizes should be assumed by default because they are provided by manual annotations of the cardiologist.

Given the limitations mentioned above regarding the use of CPD as feature extraction method, another supervised learning approach for abnormal heartbeats detection is evaluated in this section. The proposed method focuses on building high-performance classifiers optimizing the training set selection process. The main points to keep in mind are (1) the underlying class distribution of the data is unknown and (2) the training sets have to be small. This approach uses another decomposition, namely, the Sequentially Truncated - Multilinear Singular Value Decomposition (ST-MLSVD). Figure 3.7 shows the general diagram of the new algorithm.

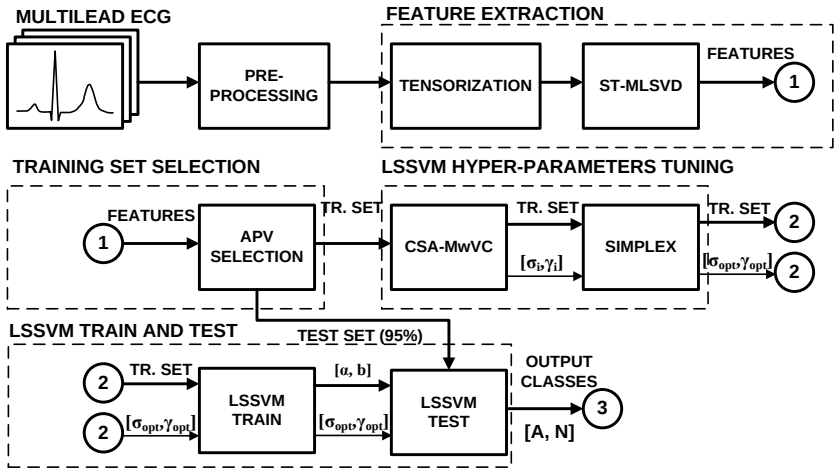


Figure 3.7: Proposed approach for detecting premature heartbeats using ST-MLSVD.

3.3.1 Materials and methods

The performance evaluation of the algorithm was carried out using two databases, the St.-Petersburg Institute of Cardiological Technics 12-lead Arrhythmia Database (INCARTDB), and the Massachusetts Institute of Technology - Beth Israel Hospital Arrhythmia database (MITDB) [38], [75]. MITDB consists of 48 30-min two-lead Holter recordings sampled at 360 Hz. Using two databases allows assessing the performance of the algorithm with different datasets.

The pre-processing stage uses a fourth order zero-phase band-pass Butterworth filter to deal with both, baseline wandering and high frequency noise. The cut-off frequencies are 0.5 Hz and 40 Hz for high-pass and low-pass respectively. This frequency interval corresponds to the power spectrum of the diagnostic ECG. Given the sample frequencies, the window length for MITDB is 184 samples. Again, each heartbeat is normalized subtracting the sample mean and dividing by the standard deviation in all leads.

Once the tensor has been constructed, a low-rank approximation to this tensor is obtained by Sequentially Truncated Multilinear Singular Value Decomposition (ST-MLSVD). This approximation is used to extract features for the training of the classifier. Given the definition and $d = 3$, there are two parameters to adjust, the multilinear rank of the approximation $R_{\boxplus} = (r_1, r_2, r_3)$ and the processing order p. Unfortunately, there are no general criteria for setting these

parameters. Below, a heuristic approach is used for selecting both of them.

Since there are two different databases, the dimensions of the generated tensors will be different. On one hand, the 12-lead INCARTDB generates tensors of dimension $12 \times 131 \times N$. On the other hand, MITDB generates tensors of dimension $2 \times 184 \times N$, where N is the number of heartbeats in the current record for each database. It is worth to note that N is different for each record in the database. Thus, N represents the number of heartbeats in a given recording regardless the database. The first criterion adopted is that independently of the generated tensor dimensions, the core tensor size is the same for both databases. The second criterion is to keep the multilinear rank as small as possible in order to increase the speed of the feature extraction stage. Since ST-MLSVD is based on truncated SVD, the number of singular values to compute depends on the multilinear rank. Consequently, the algorithm will run faster as the desired multilinear rank decreases.

Thus, the first rank is $(r_1 = 2)$ because it is the minimum of (2, 12). Following the speed criterion, the second rank is $r_2 = 2$. The r_3 value is upper-bounded by the previous two modes, i.e., $r_3 = [1, r_1 r_2]$. Considering that the third mode corresponds to the heartbeat dimension, it may be advisable to keep the maximum information possible. Therefore, the r_3 value is $r_3 = 4$.

In absence of any other information, it is recommended to select the processing order in the direction of increasing values of the mode size [125]. Thus, the processing order is $p = [1, 2, 3]$ due to the fact that for both databases $L < W < N$. Such approach minimizes the number of operations to perform and consequently speeds up the feature extraction stage. The feature vectors were obtained directly from the mode-3 factor matrix, $\hat{\mathbf{U}}_3 \in \mathbb{R}^{N \times 4}$ of the ST-MLSVD approximation.

The vectors for the training set are automatically selected using the APV selection algorithm presented in section 2.4.4. The training set size is fixed beforehand to 5% of the total number of heartbeats in the recording (N). Using small training set sizes is crucial because from the point of view of a practical implementation, the training set should be manually annotated by the cardiologist. Therefore, as the training set size increases, the effort in manually annotating it increases as well.

The LS-SVM dual model solution for a gaussian kernel requires the adjustment of two hyper-parameters, the regularization parameter γ and the kernel parameter σ. A combination of CSA and the standard Nelder-Mead *simplex* method is used to find optimal values for the duple (γ, σ) [50]. First, CSA searches for suitable starting values of these parameters. Then, the Nelder-Mead method is used in a refinement stage.

This study uses both, the CSA-MwVC and the *simplex* method included in the LS-SVMlabToolbox [50]. The default parameters are $\hat{\sigma}^2 = 0.995$, $m = 5$ and $\upsilon = 0.1$. The cost function is the misclassification rate in an V-fold ($V = 10$) cross validation.

3.3.2 Results

Tables 3.17 and 3.18 show the performance indexes for both databases using the test dataset (95%). The included metrics are the sensitivity (Se), specificity (Sp), the positive predictive value (P+) and the global accuracy (Acc). Furthermore, Table 3.17 compares the results of previous tensor-based algorithms with this approach. The method CPD+SVM is the one discussed in section 3.2.

Table 3.17: Global performance indexes for INCARTDB.

Study	**Se**(%)	**Sp**(%)	**P+**(%)	**Acc**(%)
Goovaerts et al. [40]	91.10	94.47	NR	NR
CPD+SVM	93.90	97.70	85.72	97.22
ST-MLSVD+LS-SVM	94.39	99.65	97.81	98.91

Table 3.18: Global performance indexes for MITDB.

Se(%)	**Sp**(%)	**P+**(%)	**Acc**(%)
96.27	99.55	99.03	98.49

As a reference, the output of the classifiers for the records 33 and 34 from INCARTDB are given.

Table 3.19: Confusion matrix for the classifier trained and tested with record 33 using ST-MLSVD.

	A	**N**
A	325	215
N	233	972

Table 3.20: Performance indexes for the classifier trained and tested with record 33 using ST-MLSVD.

Se(%)	**Sp**(%)	**P+**(%)	**Acc**(%)
58.24	81.89	60.19	74.33

Table 3.21: Confusion matrix for the classifier trained and tested with record 34 using ST-MLSVD.

	A	**N**
A	383	81
N	117	1286

Table 3.22: Performance indexes for the classifier trained and tested with record 34 using ST-MLSVD.

Se(%)	**Sp**(%)	**P+**(%)	**Acc**(%)
89.39	94.07	82.54	27.30

3.3.3 Discussion

The algorithm in [40] is an unsupervised approach, i.e., no training set is needed. This is a relevant advantage with respect to the supervised approach proposed here. However, in this study, the training set is small (5%). Therefore, a little additional effort in manually annotating the training set is required for better performance indexes.

From Table 3.17, it is clear that the performance indexes of this study are better than the ones previously obtained using CPD+SVM. The largest difference is in the predictive positive value which has improved with 12%. However, it is worth noting that the training set size in the CPD+SVM method (2%) is smaller than in the current study (5%). Thus, the observed differences might be the consequence of a larger training set. Nevertheless, the main advantage of this approach with respect to the CPD based method is that the training set selection is fully automatic. In contrast, the former assumes a previous knowledge of the classes' distribution in the record. This is unrealistic because in general, the cardiologist does not know in advance such distribution. Hence, the ST-MLSVD+LS-SVM approach succesfully deals with the third limitation mentioned above.

It is worth to mention that despite the fact that the method using ST-MLSVD+LS-SVM has more parameters to adjust than the alternative CPD, the heuristic approach adopted here is effective. The rank selection heuristics followed a minimalistic approach which encouraged the processing speed.

Tables 3.19-3.22 show the results in records with PAC heartbeats. Broadly speaking, the respective performances have been increased, specifically in record 34 where both the sensitivity and the positive predictive value are above

80%. Record 33 still shows a poorer performance with a sensitivity below 60%. However, an improvement is clearly visible in the specificity and the positive predictive value. This increase in performance might be explained by two main causes. Firstly, the introduction of nonlinear SVM that allows constructing nonlinear separation surfaces. Secondly, the training set (APV) selection strategy which led to better-selected heartbeats for training. It is worth to mention that there is still room for improvements on this topic since the performance indexes are not satisfactory yet.

Finally, the performance of the same approach in different datasets can be examined. From Tables 3.17 and 3.18 the major difference is in the sensitivity, the other indexes are almost the same. One possible cause is that in the case of tensors from MITDB, the mode-1 size is the same for both, the original and the multilinear approximation core tensor. The latter means that no information is discarded in the first truncation. Hence, this could lead to an improvement in the sensitivity value. Notwithstanding, a further study with special attention on this point is therefore suggested.

3.3.4 Conclusions

This second approach for detecting ectopic heartbeats using tensors addressed the main issues of the former method. The main points can be summarized as follows.

- The introduction of the ST-MLSVD instead of CPD for extracting features in multi-lead ECG along with a simple set of criteria for selecting the multilinear-rank led to a fast and unique decomposition.
- The use of nonlinear LS-SVM along with a method for tuning the hyper-parameters using optimization, particularly CSAwMV and the Nelder-Mead method led to a more effective construction process of the classifiers.
- The use of the APV methodology for the training set selection process allowed to construct small and relevant training sets.

Furthermore, the performance assessment showed that with such small training sets it is possible to train high precision classifiers for detecting ectopic heartbeats. Despite the fact that the algorithm was evaluated on two databases with a different number of leads and sampling frequencies, almost the same results were obtained for both cases. This demonstrates that the method has high performance even for very different datasets.

3.4 Conclusions

The premature heartbeat detection problem in Holter monitoring was addressed in this chapter. The attention was focused on the use of tensor-based methods and machine learning in this context. The evaluation of two methods resulted in global sensitivities, positive predictive values, and specificities above 93%. The method using ST-MLSVD outperformed the CPD-based method. Besides, the ST-MLSVD-based algorithm was evaluated in two databases with remarkable differences and similar results were obtained. Hence, the use of tensor methods along with machine learning techniques for ectopic heartbeat detection in ambulatory recordings is a feasible and efficient approach.

Chapter 4

T-wave end detection using machine learning

This chapter presents new algorithms for detecting the end of the T-wave (Te) using MLP and SVM. The first part of the chapter gives an introduction to the physiological meaning of the QT interval and its clinical applications. Furthermore, an overview of the most relevant studies in T wave end detection is presented. Next, the general approach of the algorithm and the dataset are described. Then, an exploratory study using MLP along with three feature extraction methods is presented. The latter serves as the basis for presenting new experiments using both, MLP and SVM. The results obtained with both approaches are compared and discussed. Finally, conclusions will be presented. The contents of this chapter has been published in [114] and [112].

4.1 Introduction

Torsades de pointes (TdP) is a specific electrocardiographic form of polymorphic ventricular tachycardia. Sustained or prolonged TdP can lead to ventricular fibrillation and SCD [137]. TdP has been associated with either, congenital or acquired Long QT Syndrome (LQTS). Congenital LQTS diseases are due to mutations of the genes that encode the functions of sodium (Na+) and potassium (K+) channels. On the other hand, the blockade of the inward potassium rectifier (IKr) channel due to the effects of pro-arrhythmic drugs intake is the main cause of acquired LQTS [76] [79].

The QT interval is associated to the ventricular repolarization of the heart. It starts at the beginning of the QRS complex (first deflection) and lasts till the end of the T-wave. It is also known that QT interval depends on the previous RR interval. Several formulas have been defined to correct the QT interval, leading to a family of corrected QT intervals (QTc) which includes Bazett, Fridericia, Frammighan among others. It has been demonstrated that the main factors associated with increased risk of QT prolongation and TdP include sex (females are more susceptible than males), advanced age, bradycardia, congestive heart failure, long QTc and others [137].

Long QTc (Bazett) has been defined as QTc$\leq$450 ms for men and QTc $\leq$ 460 ms for women. A severely prolonged QTc with an increased risk of TdP is defined as QTc$\leq$500 ms [94]. Normally, the T-wave end point (Te) is at baseline level of the ECG signal, which is usually contaminated by noise and interference in ambulatory ECG. Another issue is that there is no consensus on the leads and the number of them that should be used for assessing Tend. Thus, a gold-standard for the T wave end is difficult to define [74]. Nevertheless, proper T-wave end detection remains an open problem.

There are multiple approaches proposed in the literature for estimating Te. For instance, Vila et al. [128] presented a Te detection algorithm based on a mathematical model. An ECG delineation method was proposed in [70] using a quadratic spline wavelet and four dyadic scales. Other studies are based on area computation [138] [127]. Discrete wavelets, area-curve length index and thresholds were used for delineating the ECG in [35]. A mathematical model of skewed Gaussian functions combined with the trapezium's area method was described in [64]. Other methods include the partially collapsed Gibbs sampler [61], the phasor transform [69] and piecewise derivative Dynamic Time Warping [139].

One possible approach is to consider that Te location depends on the samples of the current beat. In other words, detecting the Te point can be formulated as the problem of finding a certain function which estimates the position of Te from the samples contained in a given interval, i.e., a regression problem. The problem is to find a $\mathbf{\Phi}(\mathbf{x})$ function which maps $\mathbf{x} \in \Re^d$ to $y \in \Re$, where $\mathbf{x}$ is a segment of the signal, d is the length of the segment and y is the location of the Te. From the point of view of the multivariate function regression analysis this is a heuristic approach. In [10] a similar approach was taken for modeling the Te using neural networks. However, the latter study focuses on the properties of the fitted model rather than on the detection problem itself. Up to our knowledge there are no previous studies that address and deeply analyze machine learning based Tend detection algorithms.

For the evaluation of the algorithms proposed in this chapter the QT Database

(QTDB) [55] will be used. QTDB is publicly available at Physionet [38]. It was designed for evaluating the performance of algorithms for event detection in ECG. It consists of short segments (15 min) extracted from 105 Holter recordings, each with two channels. All records have a sampling frequency of 250 Hz. Two cardiologists annotated the database: Cardiologist 1 (C1) annotated 3542 T-wave ends in 103 records, and Cardiologist 2 (C2) annotated 402 Te in 11 records. In this study, the set annotated by C1 was used.

4.2 T-wave end detection using neural networks

This section addresses the problem of detecting the T-wave end (Te) in the ECG using Multilayer Perceptron (MLP) neural networks. It shows the first approximation to this problem using different feature extraction stages.

Preprocessing

The pre-processing step includes three stages: filtering, R-peak detection, and heartbeat segmentation. The filter stage uses a fourth order zero-phase band-pass Butterworth filter to deal with both baseline wandering and high frequency noises. The cut-off frequencies are 0.5 Hz and 50 Hz for high-pass and low-pass respectively.

The next step detects the R peaks using an algorithm based on parabolic fitting [65]. The heartbeat segmentation is as follows: for each heartbeat, a 100 samples vector (400 ms) is extracted from a reference point (x_{ref}) at R + 50 samples (200 ms), where R is the R-peak location of the current heartbeat. This segmentation has two goals, (1) to select a relatively small interval which includes the Te and (2) to bypass the high energy and frequency content of the QRS complex, see Figure 4.1.

The Te location for the current heartbeat is given by the position of the x_{ref} point for the current heartbeat and an offset. The latter is the desired output of the regression function to estimate. Both, MLP and FS-LSSVM are used as regression algorithms. For MLP, the target vector is normalized dividing by 100 samples (400 ms) as follows,

$$t_i = \frac{Te_i - R_i - 50}{100}, \tag{4.1}$$

where t_i is the i-th component of the target vector, i.e. the offset of the i-th heartbeat selected for training, Te_i and R_i are the annotated Te and the R

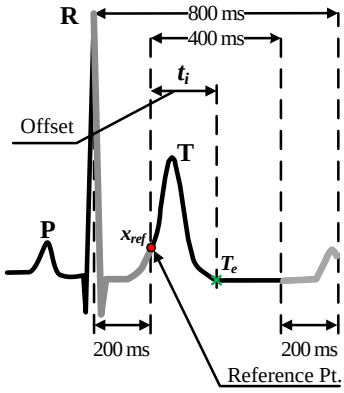


Figure 4.1: Heartbeat segmentation method for detetcting the T wave end.

point for the current heartbeat respectively. On the other hand, the division by 100 samples is not needed in FS-LSSVM, so only the numerator of (4.1) is used.

4.2.1 Materials and methods

The feature vectors were obtained using DCT, PCA, and resampling (RES). The MLP networks have three layers: input, hidden and output. For each feature extraction stage, a set of MLP networks were trained. The number of input neurons varies from 1 to 16, and the number of hidden neurons from 1 to 32, resulting in 512 topologies per method, see Figure 4.2.

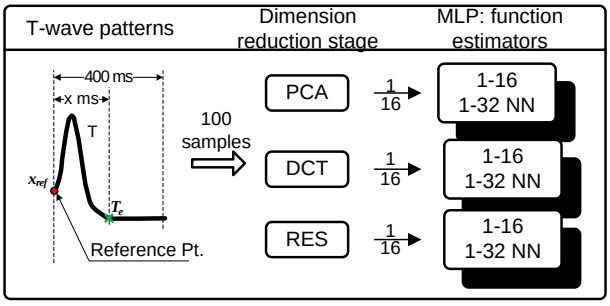


Figure 4.2: General description of the experiment using MLP-based Te detectors.

The activation functions for the hidden and output layers are the hyperbolic tangent (tanh) and linear function, respectively. The training function is

Backpropagation-Bayesian Regulation. The training error function used is:

$$E = \frac{1}{2}\sum_{i}^{N}(\hat{t}_i - t_i)^2 + \frac{1}{2}\sum_{i}^{N}\omega_i^2, \tag{4.2}$$

where $\hat{t}_i$ is the output of the neural network and ω_i is the weight decay regularizer. It represents all the weights and biases of the neural network.

In this first approximation, the channels in each recording are considered independent. Thus, for each annotated heartbeat there are two input-output pairs. Such procedure duplicates the available patterns. Furthermore, in order to prevent outliers in the training, the whole dataset was filtered using the following constraint: given a pair $P_i(\mathbf{x}_i, t_i)$ it will be eligible for training only if $t_i \in [-0.5, 1.5]$ i.e. the Te point is inside the 800 ms window. Using this criterion, 106 beats ($\sim 1.5\%$) were excluded.

A new training subset is randomly generated from the eligible dataset every time the number of input neurons changes. A fixed percentage (30%) of all annotated heartbeats in both leads was used as training set. Thus, the test set corresponds to 70%. The performance measure is the sample standard deviation of the Tend location error (precision, σ) in milliseconds for the test set.

4.2.2 Results

The precision in validation for each dimensional reduction method is distributed according to the following ranges (all values in milliseconds): $\sigma_{\mathrm{PCA}} = [35.22, 70.77]$ $\sigma_{\mathrm{DCT}} = [34.94, 117.63]$ and $\sigma_{\mathrm{RES}} = [33.43, 68.37]$. Figure 4.3 shows the distribution of the values of precision in 10 ms intervals.

Table 4.1: Best results for each feature extraction method, μ is the sample mean error and σ is the sample standard deviation of the error.

Method	**Topology**	**Error:** $\mu \pm \sigma$ (ms)
DCT	16-31-1	-0.06 ± 15.45
PCA	16-29-1	-0.50 ± 15.34
RES	16-19-1	-0.12 ± 15.06

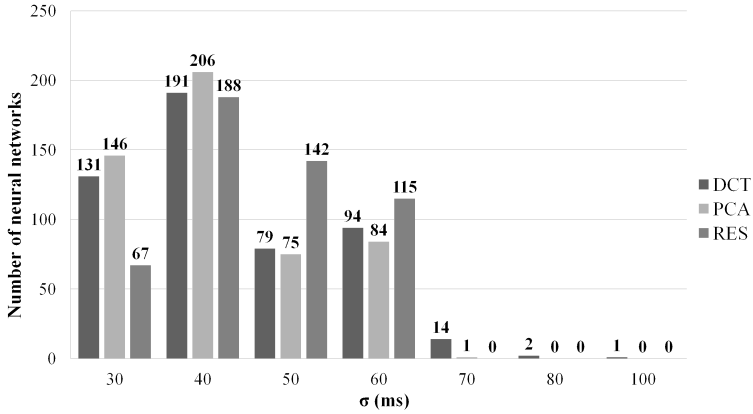


Figure 4.3: Distribution of the precision in the evaluation set for each feature extraction method.

Table 4.2: Comparison with algorithms for detecting the Te on the ECG, μ is the sample mean error and σ is the sample standard deviation of the error.

Algorithm	**Error:** $\mu \pm \sigma$ (ms)
Madeiro et al. [64]	2.80 ± 15.30
RES 16-29-1 (best precision)	-0.12 ± 15.06
Vázquez et al. (Trapezium) [127]	1.98 ± 16.90
Lin et al [61]	4.30 ± 20.80
A. Martínez et al. [69]	5.80 ± 22.70
Ghaffari et al. [35]	0.80 ± 10.70
Zhang et al. [138]	0.31 ± 17.43
DCT 16-31-1 (best accuracy)	-0.06 ± 15.45
Martínez et al. (Wavelet) [70]	-1.60 ± 18.10
Vila et al. [128]	0.80 ± 30.30

4.2.3 Discussion

Using as reference the 30-40 ms interval (344 neural networks with the best results), the approaches that use the DCT and PCA methods are the biggest group ($\sim 80\%$) on this interval. Conversely, RES does not reach 20% of the total. Hence, RES approach produces fewer architectures with acceptable performance ($\sigma < 40$ ms). This is because the effectiveness of the RES method heavily depends on keeping a high number of components (12 to 16). Also, the RES method shows the worst overall mean value of precision (51.17 ± 9.22 ms). Using DCT the mean value of precision is 45.65 ± 14.72 ms while for PCA the mean precision is 46.17 ± 9.48 ms.

The RES approach requires the use of a greater number of features, making it less effective in reducing the size of the network in comparison with the other two methods. However, this does not mean that the RES method cannot produce good results. Table 4.1 shows the evaluation of the best architectures for each approach using the criterion "best beat per cardiac cycle" [70].

The results of the Te detection algorithms reported in the literature are shown in Table 4.2. The proposed method allows building MLP-based Te detectors with performances comparable to those of the state of the art. The accuracy (mean error value) of the three MLP-based Te detectors is comparable to the accuracy of Zhang's method (the best). Meanwhile, the precision is in the range of the method of Madeiro et al. [64], the second best one after Ghaffari's method. Nevertheless, it must be emphasized that there is a relevant limitation in this approach. The main issue is that 30% is still a large number of patterns to be manually annotated, especially, if ambulatory recordings are considered. Thus, it is crucial to decrease the number of patterns needed for the training process.

4.2.4 Conclusions

This work revealed that is feasible to use MLP neural networks for detecting the end of the T wave end in the ECG. Since a supervised approach has been used for solving the involved regression problem, manual annotations would be required in a practical implementation. However, on one hand, considering the number of patterns the method becomes impracticable for ambulatory ECG processing. On the other hand, decreasing the number of training patterns might lead to overfitting problems, especially in neural networks. Hence, the training set should be decreased without compromising its diversity and therefore the generalization capabilities of the regression algorithm. The next section covers this issue exploring different algorithms for efficiently selecting the training set.

4.3 T-wave end detection using neural networks and support vector machines

This section evaluates MLP and LS-SVM for detecting the end of the T wave in the ECG. MLP and LSSVM are both supervised approaches that have been used in pattern recognition problems [83], [115]. In this study, both were considered in a context of a function approximation or regression problem.

4.3.1 Materials and methods

Here, the set annotated by Cardiologist 1 is used. The total number of available patterns in this set is $N_A = 3542$. The training step consists of selecting a subset of heartbeats in order to construct and tune the regression algorithm. The test step uses the trained algorithm to predict the end of the T-wave for beats which were not previously included in the training set, see Figure 4.4.

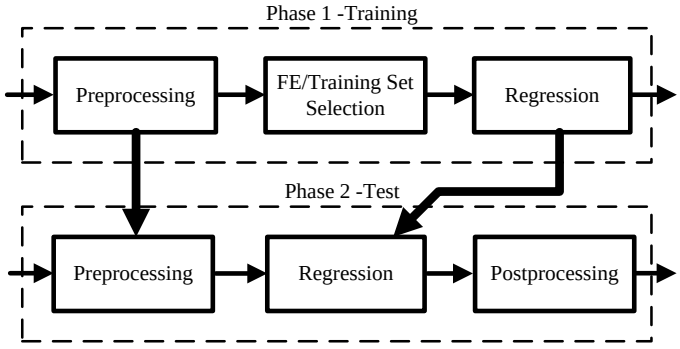


Figure 4.4: General workflow for training and testing for the Te detection algorithm.

Next sections explain in detail the training and testing phases and their respective stages.

Feature extraction and training set selection

The number of components of each vector is 100. This value is too large to be used as input to a regression algorithm. In order to reduce the size of the input vector for both, MLP and SVM approaches, a feature extraction algorithm must be used. Here, the DCT is used for reducing the dimension of the input

data. Nevertheless, it is not only desirable to decrease the dimensionality of the observations but also the size of the training set. Since a small size of the training set can lead to a strong negative impact on the performance of the regression algorithms, a selection procedure for training vectors should be implemented. The method could be based on multiple criteria. Here, random selection, clustering methods and the quadratic Rényi entropy criterion were evaluated.

The simplest method for clustering is the well-known k-means algorithm. However k-means is not robust in the presence of outliers. In fact, one extreme value can lead to the failure of the algorithm. Hence, robust clustering methods should be used. Here, two trimmed k-means based approaches where used: the trimmed k-means (TKMEANS) algorithm [19] and TCLUST [34]. Both algorithms were previously presented in sections 2.3.2 and 2.3.3.

The number of iterations for both algorithms (Q) was set to 15. Although the probability of an efficient clustering increases with the value of Q, the execution time also grows, especially in TCLUST. Several trials with values 10, 15 and 20 were performed for both algorithms, however, no evidence of better results was found for the values 10 and 20. In fact, a noticeable increased execution time for TCLUST was observed for ($Q = 20$). So, the default value ($Q = 15$) is kept.

MLP setup

The MLP neural networks used in this study have three layers: input, hidden and output. While the number of output units is given by the nature of the problem, choosing the number of input and hidden units is a critical step when configuring a neural network. This is because training the network is a problem with a large number of free parameters (weights and biases). The output for a general three layer network with N_I input units, N_H hidden neurons, and N_O output units is given by,

$$y_k = f_o \left[\sum_{j=1}^{N_H} w_{jk} f_h \left(\sum_{i=1}^{N_I} w_{ij} x_i + \theta_j \right) + \theta_k \right], \tag{4.3}$$

where f_o and f_h are, respectively, the hidden and output activation functions, w_{ij} is the weight from the input neuron i to the hidden unit j, w_{jk} is the weight from the hidden neuron j to the output unit k, x_i is the input i, θ_j and θ_k are the biases for the hidden and output units respectively, and the indexes $i = 1, \ldots, N_I$, $j = 1, \ldots, N_H, k = 1, \ldots, N_O$.

Normally $f_o(x) = x$, in this study $N_O = 1$ and $f_h = \tanh(\cdot)$. Thus, the expression (4.3) can be rewritten as,

$$y = \sum_{j=1}^{N_H} w_j \tanh\left(\sum_{i=1}^{N_I} w_{ij} x_i + \theta_j\right) + \theta. \tag{4.4}$$

The number of parameters to adjust (provided that $N_O = 1$) is given by,

$$N_p = N_H(N_I + 2) + 1. \tag{4.5}$$

Generally, neural networks need a high number of examples for training. There are several criteria for selecting the number of training patterns. Here, we examined training set sizes lower than the 30% of the dataset size. Given the number of parameters, a common criterion is to select the training set size q times the number of free parameters,

$$N_H(N_I + 2) + 1 \leq 0.3q^{-1}N_A, \tag{4.6}$$

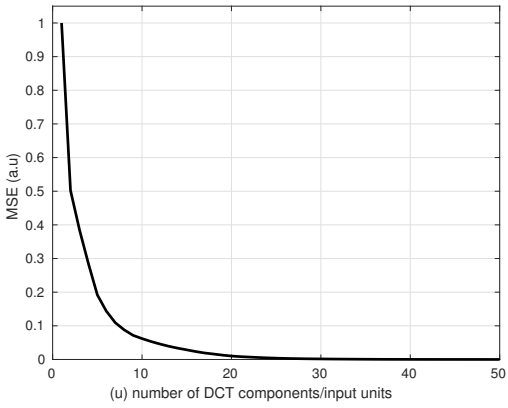
where $q \geq 2$. The expression (4.6) has three degree of freedom $(N_I; N_H; q)$. Although a well-known practical criterion suggests $q = 10$, given the amount of available patterns ($N_A = 3542$) the latter value for this criterion is impractical. So, we explore first the possible values of N_I and N_H, and then the value of q can be computed from (4.6).

From both values N_I and N_H, the number of input units (N_I) is the most relevant because it is equal to the number of the DCT components to keep (u) which is an expression of the grade of compression that we apply to the signal. On the other hand, N_H can be always upper-bounded as a multiple of N_I e.g. $N_H \leq 2N_I$. So, the problem of selecting the number of input units (N_I) is also the problem of selecting the number of DCT components to keep (u).

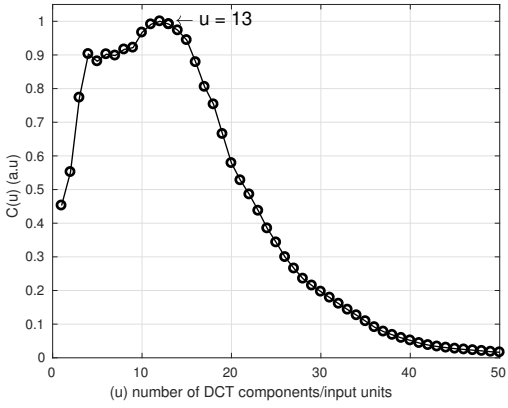
In order to satisfy (4.6), it is necessary to choose the lowest possible value for u since N_I is a multiplier term on the left side of (4.6). Appropriate values for u can be given by the total MSE in the reconstruction of the 30% of the dataset when u components are kept, see Fig. 4.5a. At first glance, appropriate values for u seem to be on the interval [30, 40], however, such values are not small enough, this is due to the fact that this criterion does not take into account (4.6). In Fig. 4.5b we have explored a criterion which is based on both, MSE and the number of parameters (N_p) as follows,

$$C(u) = \text{mse}(\mathbf{X}^u)N_p(u),\ u = 1, \ldots, L, \tag{4.7}$$

where $\mathbf{X}^u$ is the truncated $N_A \times u$ matrix of the dataset when the first u components of the DCT are kept, $N_p(u)$ is the number of parameters to adjust as defined in (4.5) considering $N_I = u$ and bounding N_H as $N_H \leq 2N_I = 2u$.



(a)

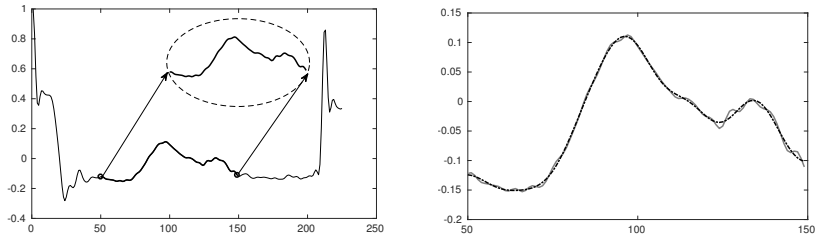


(b)

Figure 4.5: Criteria for selecting the number of input units, (a) total mean squared error (MSE) in the reconstruction of the data using u components and (b) and trade-off Complexity-MSE ($C(u)$). In order to clarify the interval of interest only the first 50 values of both, MSE(u) and $C(u)$ criteria are drawn.

The value $u = 13$ is selected since it is the first value for which the error decreases faster than the complexity grows, where the complexity is seen as the number of free parameters to adjust (N_p). Figures 4.6a-4.6b illustrate the

DCT reconstruction of an annotated heartbeat from QTDB using the first 13 components. Using (4.6), $N_I = u = 13$ and $q = 3$ is clear that $N_H \leq 23$. In order to provide a larger margin, i.e., to increase q, the value $N_H = 19$ is selected.



(a) (b)

Figure 4.6: DCT reconstruction of an annotated beat from QTDB (record sel102, first heartbeat) using 13 components (a) segment of interest for detecting Te (b) the original segment (gray continuous line) and the 13-components DCT reconstructed segment (black dash-dotted line).

Post-processing

Due to the fact that the output of both, the neural networks and the FS-LSSVM, are offsets from the reference point, a post-processing is necessary in order to estimate the actual Te. In the case of MLP the output is also in the range [0, 1], so the estimated Te is determined by,

$$\hat{t}_i = \left[R_i + 50 + A\tilde{t}_i\right], \tag{4.8}$$

where $[\cdot]$ means rounding towards the nearest integer, A is a constant which depends on the algorithm, i.e., $A = 100$ for MLP and $A = 1$ for FS-LSSVM and $\tilde{t}_i$ is the output of the regression algorithm.

Experiment I: Clustering + MLP

In this experiment we compare the performance of the neural network for different methods of training set selection. Four approaches, random selection, simple k-means, Trimmed k-means and TCLUST are evaluated. The neural network used in this experiment has the structure 13:19:1 (286 parameters). The number of clusters is fixed to 6. For each method, 50 iterations are performed, and a fixed percentage of 25% is used (one of four heartbeats are selected for

training). For the latter training set size (25%), it is possible to select the α value in the overall interval [0,25]. However, extreme values for α i.e. near to zero or 25 should be avoided because of the loss of diversity of the training set. Thus, a proportion of 3:2 is kept, i.e. the α value is set to 0.15 and the other 10% is available for common (clustered) heartbeats. For heterogeneous clustering the upper bound eigenvalue ratio is $c = 1000$. This value was selected after several simulations using the values $1, 10, 100, 1000, 10000$. The value $c = 1$ corresponds to a weighted version of TKMEANS and $c = 10000$ is a highly heterogeneous algorithm. The training set selection strategy is as follows: all trimmed vectors are used as part of the training set (15%), 10% of the vectors at each cluster selected at random complete the training set.

Experiment II: Best Clustering Methods + MLP

This experiment studies the influence of the training set size (p) and the number of clusters for the best clustering methods. The same (13:19:1) network structure is used. The number of cluster (k) is variable from 2 to 12. For each pair (p, k), 10 iterations are performed. The training set size is sorted from 16% to 30%. The trimmed percentage parameter is selected equal to 0.15 for both TKMEANS and TCLUST methods. The latter uses the same upper bound eigenvalue ratio $c = 1000$. The training set selection strategy is similar to the experiment I. All trimmed vectors are used as part of the training set (15%). The [1,15]% of the beats at each cluster are selected at random in order to complete the training set.

Experiment III: Fixed-Size LSSVM

In this experiment we examine the performance of Fixed-Size LSSVM as a regression method. Here we use random selection and active prototype vector selection (based on Rènyi entropy criterion, see algorithm 3). The training/validation set size varies from 16% to 30%. In the random selection approach, a number of observations corresponding to the percentage are chosen at random. After this first selection, a grid search procedure on this set is implemented in order to determine the parameter capacity (C_p) and the kernel parameter (σ). The search sets are $C_p = \{10, 50, 100, 150, 200\}$ and $\sigma = \{0.1, 0.2, 0.5, 1, 2, 4, 10\}$. After tuning C_p and σ, Rényi's entropy criterion, i.e., active PV algorithm is applied in order to select the final training set according to the capacity determined in the previous step. The bandwidth parameter is chosen as $h_{R2}^m = \sigma$.

In the active PV selection approach, the bandwidth is preselected equal to one ($h_{R2}^m = 1$). The best set according to the Rényi entropy criterion is selected after 10 iterations of the algorithm 3. Once the vectors are chosen, a grid search procedure is performed in order to determine both, the capacity (C_p) and the kernel parameter (σ). This grid search is carried out on the dataset selected in the previous step. The search set for the kernel parameter is the same as above, i.e., $\sigma = \{0.1, 0.2, 0.5, 1, 2, 4, 10\}$. On the other hand, the capacity set is $C_p = \{\frac{2}{15}, \frac{1}{5}, \frac{4}{15}, \frac{1}{3}, \frac{2}{5}\}N_T$, where N_T is the size of the training/validation set. For each pair (C_p, σ) 10 iterations are performed. The best pair (C_p, σ) is selected for constructing the regression algorithm together with the training set.

The last part of the experiment compares MLP and FS-LSSVM as regression algorithms. A fixed number of clusters (6) is selected in the case of both MLP approaches (TKMEANS+MLP and TCLUST+MLP). Then, the best algorithm in terms of precision and accuracy (with priority on the former) is selected and compared with the FS-LSSVM approach.

Experiment IV: Comparison with other T-wave end detection algorithms

In this experiment we compare the performance of the algorithms described above with some of the state-of-the-art methods on detecting Te. Such comparison is not straightforward due to fact that the proposed methods require supervised training. Thus, there will be observations with almost zero error beforehand (those which belong to the training set). Consequently, the real performance will be biased when it is computed using the whole dataset. This limitation can be eliminated if just the test set is considered. However, the test set is a subset of the global set, which implies that the results will be given for different datasets.

Here, we compare the methods by Zhang [138], wavelet-based ECG delineation algorithm [70], [38] and trapezium areas [127] with a Fixed-Size LSSVM using Rényi entropy as selection criterion and 15% of the training set size. The former methods are selected because they are state-of-the-art techniques that are also publicly available on-line, which allows to evaluate the results with the same test sets used by the algorithms studied here. Both, Zhang's method and wavelet-based ECG delineation algorithm are used without tuning up their parameters. On the other hand, the trapezium method requires two parameters, the length of the search window (LEN) in milliseconds and the slope (SLP) of the heartbeat (-1 for positive T-waves and +1 for negative ones). The best pair LEN-SLP is used for each record evaluated. The trapezium method also requires the detection of the T-wave peak (Tm). The Tm points are detected using the wavelet-based ECG delineation algorithm.

In order to avoid an unfair comparison, only the test set is considered. Moreover, the results corresponds to the worst case in 10 iterations of the algorithm. Besides, since the machine learning algorithms were trained with the first leads of each record, it is necessary to extend the procedure to more than one lead. The approach followed here is straightforward and consists of training another FS-LSSVM using the second lead versions of the heartbeats selected in the first lead. Thus, the advantage is that no new selection process is required. It is noticeable that maximum Rényi entropy criterion is in general not longer valid for the second lead. Other approaches that take into account this fact can be evaluated as well. For instance, the training set size can be divided among both leads and the selection procedure can be performed independently. However, the evaluation of the latter approach as well as others is beyond the scope of this study.

Performance assessment and testing

Here two performance measures are used. On one hand, the accuracy is quantitatively assessed by the mean value of the error in the location of Te in milliseconds,

$$\mu_e = \frac{1}{N_S}\sum_{i=1}^{N_S} e_i = \frac{1}{N_S}\sum_{i=1}^{N_S} (\hat{t}_i - Te_i), \tag{4.9}$$

where N_S is the number of patterns in the test set and e_i is the error for the current heartbeat. On the other hand, the precision is quantitatively assessed by the corrected sample standard deviation of the location error in milliseconds,

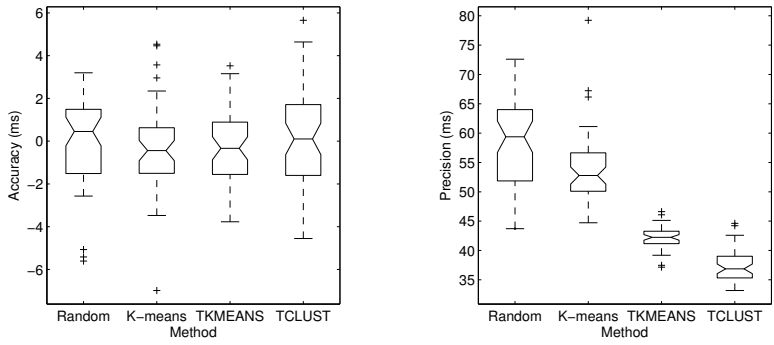
$$\sigma_e = \sqrt{\frac{1}{N_S - 1}\sum_{i=1}^{N_S} (e_i - \mu_e)^2}. \tag{4.10}$$

All the results, except those ones on Tables 4.3-4.6, are given for the test set. Thus, the previous measures are considered as unique set measures.

4.3.2 Results

The Figures 4.7a and 4.7b show the results on accuracy and precision respectively for the experiment I. From the data in Figure 4.7b, it is apparent that the

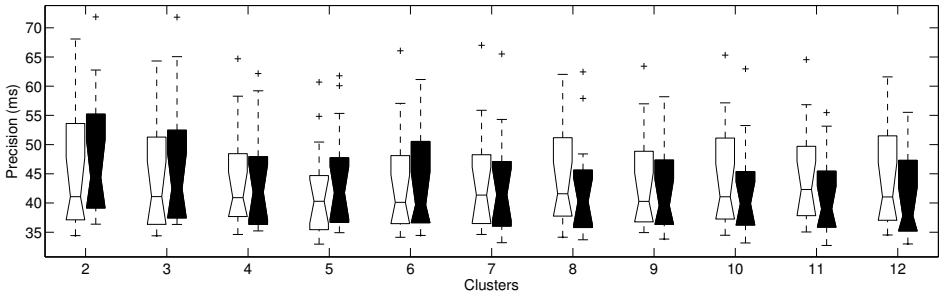
best results were obtained for both trimmed approaches, i.e., TKMEANS and TCLUST.



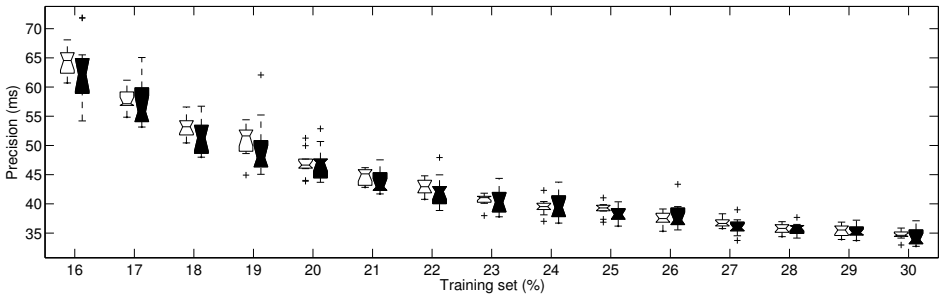
(a) (b)

Figure 4.7: Performance of MLP based Te detection algorithms with random, k-means, trimmed k-means (TKMEANS) and TCLUST training set selection strategies, (a) accuracy and (b) precision.

In the second experiment only the precision parameter is presented for both robust clustering methods. Fig. 4.8 shows the general behavior of the precision with respect to the number of clusters (k) and the training set size (p).

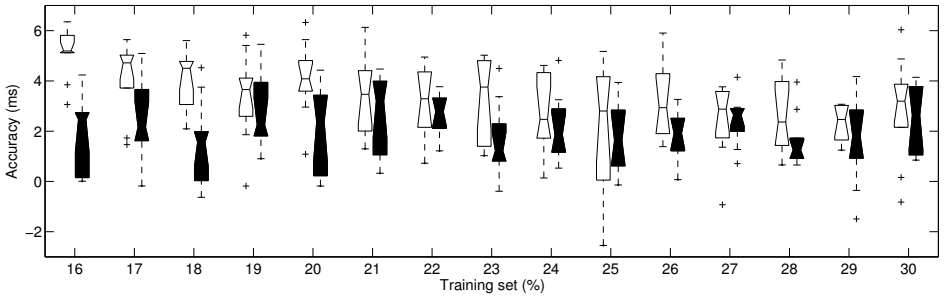


(a)

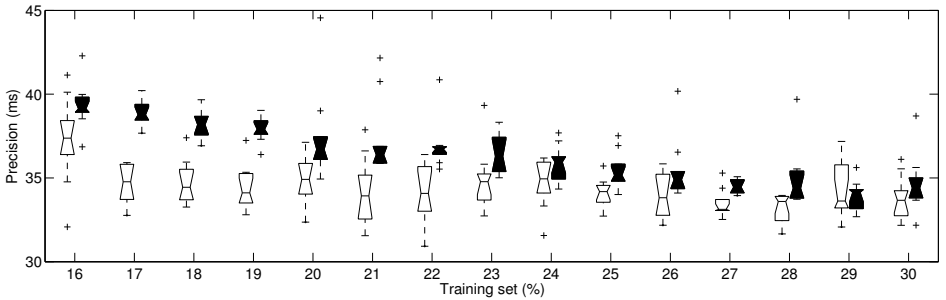


(b)

Figure 4.8: Precision for TKMEANS (white) and TCLUST (black) algorithms with respect to (a) the number of clusters and (b) the training set size.



(a)



(b)

Figure 4.9: Performance indexes for random (white) and Rényi entropy (black) selection strategies, (a) accuracy and (b) precision .

Turning now to the study on the individual influence of each parameter, on one hand the Fig. 4.8a shows the behavior of precision for TKMEANS+MLP and TCLUST+MLP with respect to (k) and independently of (p). On the other hand, the Fig. 4.8b shows the behavior of the precision for both clustering methods with respect to (p) independently of (k).

Fig. 4.9 shows the results for the experiment III using FS-LSSVM. Both parameters, accuracy and precision are considered here. A comparison in terms of accuracy and precision between both MLP-based methods and FS-LSSVM is presented in Figures 4.10a and 4.10b. The graph was obtained by averaging the accuracy and precision of the three methods for each training set size. In the case of MLP-based methods, the k parameters (the number of clusters) were selected using the best performances in term of precision shown in Fig. 4.8a. Thus, $k = 5$ for TKMEANS+MLP and $k = 10$ for TCLUST+MLP.

The results of experiment IV are given in the tables 4.3 and 4.5. The performance measures (μ_e, σ_e) were used. QTDB recording stratification according to Te accuracy and precision are given for the four algorithms. In Table 4.5, the results for each record are classified in one of four groups using the criterion of the CSE Working Party [18]. Group I, records where $\sigma_e < 30.6$ ms and $\mu_e < 15$ ms; Group II, $\sigma_e < 30.6$ ms and $\mu_e > 15$ ms; Group III, $\sigma_e > 30.6$ ms and $\mu_e < 15$ ms and Group IV, $\sigma_e > 30.6$ ms and $\mu_e > 15$ ms.

Table 4.3: Performance comparison using unique set measures and the testing set

Method	**Lead 1**	**Both leads**
	$\mu_e \pm \sigma_e$ (ms)	$\mu_e \pm \sigma_e$ (ms)
Zhang [138]	7.20 ± 60.32	0.68 ± 38.66
Trapezium [127]	-0.36 ± 72.65	-0.97 ± 58.24
Wavelet-ECG [70] [38]	-6.01 ± 65.27	-1.28 ± 59.10
RE + FS-LSSVM 15% **(this study)**	-2.10 ± 42.70	-3.19 ± 29.27

4.3.3 Discussion

Although there were no significant differences between algorithms in the accuracy parameter, experiment I clearly pointed out that trimmed k-means based methods outperform the random and k-means based selection strategies. The median of the accuracy was close to 0 ms for all methods which suggests that this behavior is inherent to the MLP network and it does not depend on the selection of the training set. Both, TKMEANS and simple k-means had almost the same accuracy (TKMEANS is slightly better) while TCLUST was the

Table 4.4: Te detection algorithms performance comparison. The worst case is considered for the proposed approach (bold-faced).

Study	($\mu_e \pm \sigma_e$ (ms))
Madeiro et al., 2013 [64]	2.8 ± 15.3
A. Martínez et al., 2010 [69]	5.8 ± 22.7
Lin et al., 2010 [62]	4.3 ± 20.8
Ghaffari et al., 2009 [35]	0.8 ± 10.7
Zhang et al., 2006 [138]	0.3 ± 17.4
Martínez et al., 2004 [70]	-1.6 ± 18.1
Vila et al., 2000 [128]	0.8 ± 30.3
This study	-3.0 ± 16.9

most disperse approach in terms of accuracy. The precision parameter clearly pointed out the advantages of robust clustering selection over random and simple k-means, see Fig. 4.7b. On the other hand, again TKMEANS shown the lowest inter quartile range (IQR) while TCLUST based selection shows the best precision (median).

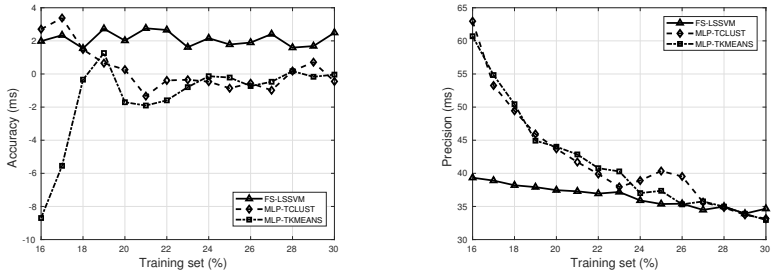
Experiment II compared both trimmed k-means approaches. The findings suggested that generally TCLUST yields better performances in terms of the median of the precision. Notwithstanding, also noticeable results arose with respect to the number of clusters and the training set sizes. TKMEANS based selection seems to have lower dispersion when the number of clusters is in a central range, i.e., from four to seven. On the other hand, TCLUST improves its performance when the number of clusters increases, Fig.4.8a. The median value of precision for TKMEANS is between 40.1 ms and 42.3 ms while TCLUST varies in the range 37.8 ms to 44.4 ms. It is also noticeable that both methods pointed out that small values for the number of clusters (2 and 3) are unsuitable. It is not strange that the performance improves as the training set size increases for both methods, Fig. 4.8b. Nevertheless, for lower percentages (16% - 19%) TCLUST shows a lower median than TKMEANS. This could mean that the scatter structure of the clusters tend to be less spherical for small training sets. Thus, the use of the heterogeneous clustering algorithm offers more advantages than TKMEANS. However, TKMEANS shows lower IQR than TCLUST. The former is also more independent from the number of clusters than TCLUST.

Table 4.5: QTDB Recording stratification according to Te accuracy and precision for Lead 1, (T): amount of records in each group, (%): percentage with respect to the total amount of records (103). Boldfaced values represent the best results for each group

Method	**Group I**		**Group II**		**Group III**		**Group IV**	
	(T)	**(%)**	**(T)**	**(%)**	**(T)**	**(%)**	**(T)**	**(%)**
Zhang [138]	**69**	**67.0**	8	7.8	**15**	**14.6**	11	10.6
Trapezium [127]	59	57.3	5	4.9	24	23.3	15	14.5
Wavelet-ECG [70] [38]	63	61.2	**2**	**2.0**	27	26.2	11	10.6
RE+FS-LSSVM 15% **(this study)**	66	64.1	19	18.4	**15**	**14.6**	**3**	**2.9**

Table 4.6: QTDB recording stratification according to Te accuracy and precision for both leads, (T): amount of records in each group, (%): percentage with respect to the total amount of records (103).

Method	**Group I**		**Group II**		**Group III**		**Group IV**	
	(T)	**(%)**	**(T)**	**(%)**	**(T)**	**(%)**	**(T)**	**(%)**
Zhang [138]	98	96.1	5	3.9	0	0.0	0	0.0
Trapezium [127]	88	85.4	1	1.0	12	11.7	2	1.9
Wavelet-ECG [70] [38]	86	83.5	3	2.9	12	11.7	2	1.9
RE+FS-LSSVM 15% **(this study)**	103	100	0	0.0	0	0.0	0	0.0



(a) (b)

Figure 4.10: Comparison between methods, TKMEANS+MLP, TCLUST+MLP and RE + FS-LSSVM, (a) accuracy and (b) precision.

Although the median precision of TCLUST is slightly better than TKMEANS, these differences are not statistically significant. In order to point out whether a method is overall the best, the use of TKMEANS is recommended rather than TCLUST due to the computational cost increase that implies the use of TCLUST instead of TKMEANS. Finally, from Fig. 4.8b it is clear that the training set size parameter is of more relevance in the performance of the detection algorithm than the number of clusters.

Experiment III evaluated FS-LSSVM as regression functions. In terms of accuracy, the Rényi entropy selection outperforms the random selection, Fig. 4.9a. It is noticeable that for the random selection approach, the precision barely depends on the training set size. This is a direct consequence of the initial randomness of the selection process. The a-posteriori refinement of the training set using Rényi entropy criterion does not allow the possibility to include vectors outside the selected training set which may increase the information potential, i.e., the information potential is upper-bounded beforehand. This also explains the larger values in the accuracy parameter of the random selection approach. The precision parameter analysis pointed out that the random selection had better precision than Rényi entropy based selection. Thus, the random selection strategy yielded also acceptable results, although worser accuracies than in the Rényi entropy strategy might be expected.

The comparison between MLP methods and FS-LSSVM is presented in Fig. 4.10. Except for small training set sizes (16%-18%) the mean accuracies rapidly tends to be in a band between -2 and 2 for both MLP methods. Conversely, RE+FS-LSSVM is always stable around 2 ms of mean error. This could be a consequence of the stronger and more efficient regularization mechanisms of FS-LSSVM approach. On the other hand, the MLP approaches are highly sensitive to the training set size. Thus, performances better than $\sigma_e \leq 40$ ms

are achievable only when the training set sizes are larger than 25% of the whole dataset. The previous discussion points out the FS-LSSVM as the best global approach for detecting the T-wave end for small training set sizes.

Table 4.3 points out that the algorithm based on RE+FS-LSSVM outperforms the other three methods in terms of precision for both cases, i.e. when the first lead in the record is used and when both leads are used. The noticeable differences among both data columns in Table 4.3 are explained by the differences in the method for evaluating the error. Regarding the evaluation using one lead, the error is defined as the difference between the output of the algorithm and the annotated position. However, when both leads are used, the reported error for each beat is given by the smallest difference between the outputs of the algorithm for each lead and the corresponding annotation. In other words, the best Te estimation is selected for each beat. Thus, with this criterion, it is expected that the respective performances of the algorithms increase. This criterion is also known as best-beat-per-cardiac-cycle and it is a standard approach for reporting results of T wave end detection algorithms. This table is given only for the testing set of the algorithm, so there's no influence of the training set in the results and the generalization capabilities of the FS-LSSVM can be clearly appreciated. The mean error value is overall the best only when the first lead is considered. However, it remains below 1 sample (4 ms @250 Hz) which is an expression of the robustness of the method.

Data shown in Tables 4.3-4.6 should be interpreted with caution because the training set output was included for computing those indexes. The main issue is that it is too difficult to compute those indexes without including the training set. Hence, such tables are given as reference because they are two recommended approaches for evaluating Te detection performance algorithms. Thus, they provide a general idea on the performance of the proposed approach with respect to other studies. Besides, it is worth to note that despite the indexes on Tables 4.3-4.6 were computed including the output of the algorithm for the training set, due to the implicit regularization mechanism of FS-LSSVM, no zero output error it is expected for the training set. Considering these facts a brief discussion on these data is presented below.

Tables 4.5 and 4.6 show the performance of the algorithms using the criterion recommended by the CSE Working Party [18]. Regarding this criterion, for the records in Group I the algorithm performs well i.e. the output of the algorithm is comparable to the output produced by a cardiologist. The output of the algorithm for the records in Group II has a large bias and acceptable precision. This is interpreted as the method has a significant systematic error (offset). Conversely, Group III shows a low bias output but high standard deviation, so the algorithm has a significant random error. Finally, Group IV corresponds to records where the output is considered unpredictable (both, the bias and the

standard deviation of the error are large). Using only the first lead (see Table 4.3), Zhang's algorithm is the one which has good performance in the largest number of records (69) followed by the FS-LSSVM approach (67). On the other hand, the algorithm using FS-LSSVM shows the smallest number of records in Group IV (2). This means that the proposed method is very robust since unpredictable output was observed for only 3 records in the database. Table 4.6 confirms the latter showing that for all records FS-LSSVM has a Group I type output if both leads are used by the algorithm. Table 4.4 include several studies on Te detection. As one can see, the proposed method lead to a state-of-the-art Te detection algorithm. Finally, Appendix 1 shows examples of the output of the algorithm for different recordings. The annotations of the database are provided as reference.

4.3.4 Conclusions

This study has shown a novel approach for detecting the end of the T-wave in ECG using neural networks and SVM. It was also shown that training set selection strategies can reduce the amount of patterns required to obtain acceptable performances. The findings suggest that for MLP-based methods the required training set size is around 25% while for FS-LSSVM even a 15% of the global dataset for training is enough to obtain more than acceptable performances. FS-LSSVM shows the best performance on precision parameter (σ_e). It also shows high stability, even for small training set sizes. Another major finding was that robust clustering-based and APV selections of the training set are more effective than others, e.g., random, simple k-means or other *ad-hoc* selections.

Although the algorithms proposed here requires training, the results show an increase in the precision of the output which leads to an increment on the reliability of the algorithm from the point of view of the user. This is especially relevant in the case of a test where a large number of Te points have to be determined. Another interesting property of the proposed approach is that the training set size is the only one parameter which is left to the user choice. The rest of the parameters are internally determined by the algorithm. Thus, the user does not have to deal with a number of difficult-to-understand parameters. Conversely, she/he can decide beforehand the number of heartbeats that she/he is willing to manually annotate and the rest of the process can be done automatically. Although 15% may be seen as a too high percentage, actually this is a relatively small training set size and the proposed method have acceptable performances. Besides, it can be argued that the method has been evaluated considering that all heartbeats, coming from 103 different records (also coming from different original databases) belong to a single record.

In other words, it is unlikely to find the diversity that QTDB presents in a long-term record. Hence, in practice smaller training set sizes can be used with good results. Additionally, the method may be combined with unsupervised approaches such as those ones discussed above. In this hybrid approach, the unsupervised method could be added to the preprocessing stage in order to provide an initial guess of the Te for the heartbeats selected for training. Thus, the expert would have only to check and correct the output of the unsupervised method for a small number of heartbeats. This would lead to a decrease in the time needed for manually annotating the training set.

Despite unsupervised approaches may be more suitable for short-term analysis, this is not the case for long-term recordings where both, signal quality and morphology change. In fact, in long-term analysis, the latter is the common scenario and usually, a considerable amount of time is spent in correcting the T-wave end detection errors of unsupervised approaches. Tuning the parameters of these methods is not always possible neither intuitive. Moreover, when tuning is available, it frequently leads to poorer results. On the other hand, the proposed approach depends on both the cardiologist expertise and the number of heartbeats the user is willing to annotate. So, the main question is... What would the user prefer to do? To correct an unknown number of erroneous detections or to be proactive and to annotate a small number of heartbeats in order to gain in robustness and confidence. The results of this work open a new alternative for cardiologists that prefer to annotate instead of correcting.

4.4 Conclusions

This chapter presented a new approach for detecting the T-wave end in the electrocardiogram (ECG). Both, Multilayer Perceptron (MLP) neural networks and Fixed-Size Least-Squares Support Vector Machines (FS-LSSVM) were used as regression algorithms to determine the T-wave end. After an exploratory study using MLP neural networks, an extended evaluation was performed including FS-LSSVM. Different strategies for selecting the training set including random selection, k-means, robust clustering, and maximum quadratic (Rényi) entropy were evaluated as well. Individual parameters were tuned for each method during training and the results were given for the evaluation set. A comparison between MLP and FS-LSSVM approaches was performed as well. Finally, a comparison of the FS-LSSVM method with other algorithms for detecting the T-wave end was included. Broadly speaking, the experimental results showed that FS-LSSVM approaches are more precise than MLP neural networks for T-wave end detection. The small training sets evaluated suggest that the method can be used in Holter monitoring applications.

Chapter 5

Tool for the analysis of ventricular repolarization

This chapter presents an easy-to-use software tool for QT interval analysis in the electrocardiogram. The software is written in Python 3.6 and among its main features includes signal filtering, Q onset, R peak and T offset detection algorithms, classifiers for premature heartbeat identification and rejection, and tools for easy correction of automatically generated annotations. Moreover, the software includes a signal quality assessment module in order to help the researcher on deciding which lead should be used. The software tool computes and plots the Q and QT dynamicity markers. Since the software is designed for cardiologists and specialists with no programming skills, the graphical user interface (GUI) is intuitive, compact and easy to use. The chapter is structured as follows. Section 5.1 discusses the main features and aims of the tool. Next, the modules that compose the tool are presented in section 5.2. Section 5.3 shows a brief evaluation of the software. Finally, conclusions are drawn in section 5.4. A paper describing the tool presented in this chapter has been accepted for publication in the Cuban Journal of Electronic Engineering, Automation and Communications.

5.1 Introduction

Several software tools have been developed for the analysis of the ECG signal, particularly for HRV analysis. In [118], a software for advanced HRV analysis is presented. This tool is available free of charge on Linux and Windows platforms.

gHRV is an open source tool written in Python for HRV analysis [95]. It is multiplatform software (Linux, Windows and Apple OS X) and provides support for several formats. Other works include a tool for HRV spectral analysis [96], a software for the analysis of cardio-respiratory variability signals [88] and a tool in MATLAB© for the analysis of cardiac inter-beat interval (IBI) data [87]. An extended revision of software tools for HRV can be consulted in [107].

Although heartbeat classification in HRV software is rarely used, it is crucial in QT analysis because most of the indexes are defined for normal heartbeats. Hence, the inclusion of abnormal heartbeats, like premature atrial or ventricular beats, would bias the values of the indexes. Thus, a classification or labeling algorithm is needed for rejecting or identifying such beats. Ecg-kit is a package written in MATLAB© scripting language which focuses on delineation and classification of the ECG signal [26]. However, this tool is intended to be a MATLAB© toolbox, so is not targeted to any specific task, which implies knowledge of the language or programming skills in order to exploit its features.

In spite of the considerable amount of studies in the analysis of ventricular repolarization, QT analysis is not always available in Holter systems and when it is present, the analysis is limited. There is also a lack of tools for computing QTVI using the methodology proposed by Berger [6]. Furthermore, up to the knowledge of the authors, there are no software tools that support research on QT analysis. The reason behind these facts could be that there is still a lot of research to do before including QT indexes in the standard diagnostic protocols. Nevertheless, as more research is needed there is also a need for tools that support such research. Hence, this document proposes an open source software tool that uses advanced algorithms for the analysis of the QT interval in Holter recordings. The software called PyECG, is intended to be a useful tool for cardiologists and researchers with no or little programming skills, so a simple and intuitive graphical user interface is provided. The software is written in Python and supports both, QTVI analysis and QT dynamicity analysis. Future versions may include TWA and QTd analysis.

5.2 Materials and methods

The software has been developed in Python 3.6 using Anaconda 3-5.01 for Linux. The user interface was designed using PyQt5 which is a wrapper in Python of the multiplatform library Qt. Both standard packages, NumPy and SciPy were extensively used as well. NumPy is a basic package for scientific computing with Python. It includes an efficient array object and useful functions for performing linear algebra operations, Fourier transform and random number generation.

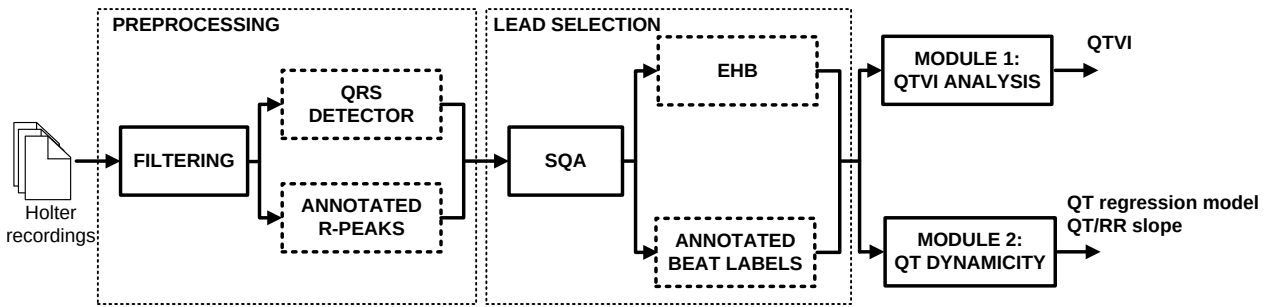


Figure 5.1: PyECG general workflow. Preprocessing and lead selection stages of the software. SQA and EHB are the signal quality assessment and the ectopic heartbeats detection blocks respectively.

Scipy is a collection of algorithms for mathematics, science, and engineering based on Numpy. Graphics generation used PyQtGraph which is a graphics and user interface library for Python intended for use in data acquisition and analysis applications. Other packages such as Scikit-Tensor and Scikit-Learn were also used. Scikit-Tensor is a Python module for multi-linear algebra and tensor analysis whereas Scikit-Learn is a machine learning library for Python [86]. The development environment (IDE) was PyCharm 2017.2.4 from JetBrains. The general workflow of the software is shown in Figure 5.1.

The tool consists of four main phases, see Figure 5.1. Since QT analysis requires a high-quality ECG signal some preprocessing steps are compulsory before doing any analysis. Thus, after loading the signal, the first two modules, namely Preprocessing and Lead selection, perform the signal conditioning, Figure 5.1. The preprocessing stage includes filtering and QRS complex detection whereas the lead selection stage includes a signal quality assessment (SQA) block and an optional premature (ectopic) heartbeats detection block (EHB). Next, the user can select between two types of analysis. On one hand, Module 1 is intended for QTVI analysis in both, single and successive 256-second windows. On the other hand, Module 2 is designed for QT dynamicity analysis in the segment of the signal previously loaded.

The filtering stage includes the following blocks, (1) a second order notch filter for removing 60 Hz power-line interference (2) a baseline drift removing algorithm using median filtering [22] and (3) a bandpass filtering stage. By default, the -3 dB bandwidth of the notch filter was set to 3 Hz which implies a quality factor (Q) of 20. The median filter uses two windows sizes of 200 ms and 600 ms respectively. The first stage, using the 200 ms window, removes the P waves and the QRS complexes of each heartbeat. The second one, using the 600 ms window, eliminates the T waves. After removing the physiological waves, the resulting signal is considered the baseline wander and consequently, it is subtracted from the original ECG signal [22]. The bandpass filtering stage consists of a fourth order forward-backward Butterworth filter with cut-off frequencies of 0.05 and 50 Hz. As an alternative to the latter, a low pass high order FIR filter is also available.

The second stage of the preprocessing is the QRS complex detection. Two QRS complex detection algorithms were provided with the tool, the first one is based on thresholds on the first and second derivatives of the ECG signal [51]. The second one is based on parabolic fitting [65].

The SQA block determines the lead which is more suitable for the further analysis, either QTVI analysis (Module 1) or QT dynamicity analysis (Module 2). In order to assess the quality of the signal, six quality indexes proposed in [59] were implemented in the software:

- The relative power in the QRS complex (pSQI)
- The relative power in the baseline (basSQI)
- The baseline wander check in time domain (bsSQI)
- The relative energy in the QRS complex (eSQI)
- The relative amplitude of high frequency noise (hfSQI)
- The relative standard deviation (STD) of QRS complex (rsdSQI)

In a separate experimental study (unpublished data), we observed that the above indexes increase with the quality of the signal. Since the purpose is to select the lead with the highest quality, a simple majority voting algorithm is proposed as follows. First, a counter is initialized to zero. Then, the first index is computed for both leads. If the index for lead A is greater than the index of lead B the counter is increased, otherwise is decremented. The process is repeated for all indexes. The software recommends one lead or the other one based on the values of the counter (voting index, (VI)), see Figure 5.2.

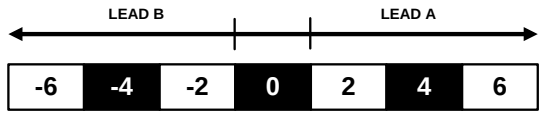


Figure 5.2: Voting index (VI) based on the relative values of the six quality indexes from both leads. The sign indicates the lead as follows, (+) lead A and (-) lead B. The absolute value corresponds to the difference in the voting process, (6) unanimity, (4) majority, (2) minimum majority and (0) tie.

The case where the counter remains equal to zero corresponds to a tie in the voting process, in such case the software will recommend the lead with the highest normalized index defined as follows,

$$\mathrm{NVI}_L = |\mathrm{pSQI}_L| \cdot |\mathrm{basSQI}_L| \cdot |\mathrm{bsSQI}_L| \cdot |\mathrm{eSQI}_L| \cdot |\mathrm{hfSQI}_L| \cdot |\mathrm{rsdSQI}_L| \quad (5.1)$$

where L is the lead (A or B) and the || symbol means the normalized value of the current index with respect to both leads e.g. the normalized $|\mathrm{pSQI}_A|$ for lead A is the ratio between pSQI_A and the maximum among both pSQI_A and pSQI_B. The normalized pSQI_B is computed in a similar way.

In the unlikely case that both NVI_A and NVI_B are equal, the software would recommend using Lead A. It is important to note that the suggestion made

by the software is relative to the current segments of both leads. Thus, from the point of view of the further analyses, it does not mean that the rejected lead is inappropriate nor a guarantee that the suggested one fits the quality requirements.

A key prerequisite in QT analysis is that ectopic heartbeats should be avoided, i.e., the analysis should be carried out on Normal-to-Normal intervals. In the case of QTVI computation, less than the 5% of the labeled heartbeats might be ectopic. In such cases, the procedure recommends interpolating on the resampled instantaneous interval series by using a linear spline approach [6]. For QT dynamicity analysis ectopic heartbeats are not allowed. This fact points out that an premature heartbeat detection block is needed in order to perform the analysis on NN intervals. PyECG provides two tensor-based methods for detecting premature heartbeats. The first method uses an unsupervised approach described in [40]. First, a tensor is constructed from the signal. Next, a rank-1 CPD takes place. Then, the mode-3 loading vector of the decomposition is used for classifying the heartbeats. Here, a threshold is constructed using the median and the standard deviation of the mode-3 loading vector. The second method uses the algorithm described in section 3.2. Both methods can be used either separately or together. However, depending on the length of the segment under analysis it might be more efficient to use the unsupervised approach on short-term analysis. Conversely, the supervised method or the combination of both approaches might be preferable on longer segments. The combination scheme uses the output of the unsupervised classifier as preliminary inputs to the supervised method. This leads to a faster training set generation.

Since Holter systems may provide both, QRS complex detection and heartbeat labeling, it is possible to load such information directly from the recording file. Hence, the user can make use of the tools available on the software or load the corresponding annotations. Any combination of both alternatives can be used as well.

After preprocessing the signal, the tool is ready for performing the required analysis using either Module 1 or Module 2. Previously, the user is motivated to select the lead of interest. This choice should be guided by the suggestion of the software based on the signal quality assessment. However, the user can still perform the analysis on any of the two leads regardless of the software suggestion.

5.2.1 QTVI and QT dynamicity modules

The QTVI module performs the computation of the QTVI marker following the algorithm proposed by Berger [5]. The QTVI algorithm involves the definition of

a single or several 256-second segments (epochs) and a template heartbeat in the segment under analysis. A QT interval template is generated by identifying the start of the QRS complex (Q onset, Qon) and the end of the T-wave (T offset, Toff) on the template heartbeat [5]. Given these requirements, the workflow for the QTVI module is shown in Figure 5.3.

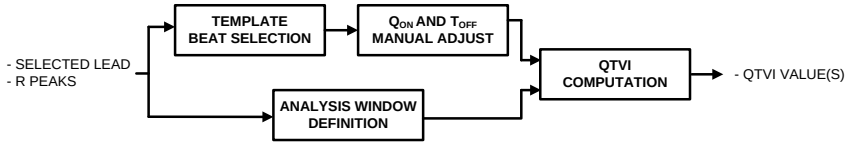


Figure 5.3: QTVI module workflow.

First, a template heartbeat must be manually selected by the user. Then, the software will suggest the Qon and Toff points for the current heartbeat. Both points may be manually adjusted if needed. The analysis windows can be defined by setting the starting sample at any point of the signal. This module allows computing QTVI in a single window or in a sequence of either overlapping or non-overlapping windows.

QT dynamicity analysis requires the detection of the Qon and Toff points for every heartbeat in the segment under analysis. This module includes both Qon and Toff automatic detection algorithms. The Qon detection is based on the method of the maximum triangle area. The Toff detection algorithm uses the method based on the area under the T-wave proposed by Zhang [138]. The Module 2 workflow is shown in Figure 5.4.



Figure 5.4: QT dynamicity analysis module workflow.

Although the software automatically detects Qon and Toff points for every heartbeat, these annotations must be manually corrected in order to guarantee the precision of the points. Hence, the first step is to check the generated points and manually correct them wherever it is needed. The next step is to select an RR profile for the QT analysis. Three profiles are available.

1. QT depends on the previous RR interval (default)
2. QT depends on a history of several previous RR intervals; this relation can be modeled by using a linear weighted (LW) average of preceding RR intervals [91].

3. Idem to the previous one but using an exponentially weighted (EW) profile [91].

The general expression for all profiles is given by the following equation,

$$\overline{RR}_i = \sum_{j=-N_i+1}^{0} \omega_j \cdot \overline{RR}_{i+j}, \quad \forall\, j = -N_i + 1, \ldots, 0 \tag{5.2}$$

where RR_i is the RR interval for the i-th heartbeat, N_i is the number of heartbeats in a time lag window of a pre-defined length and ω_j are the weights of the last N_i RR intervals within the window. Different profiles can be generated by varying the weights dependence on j, e.g. a linear weighting (LW) approach is given by,

$$\omega_j^{LW} = \frac{2(j + N_i - 1)}{N_i(N_i - 1)} \tag{5.3}$$

As mentioned above, another feasible varying law for the weights is the exponential weighting (EW) defined as,

$$\omega_j^{EW} = \frac{\gamma(1-\gamma)^{-j}}{1 - (1-\gamma)^{N_i}} \tag{5.4}$$

where $\gamma = \frac{2}{(1+N_i)}$ [91].

Finally, the QT dynamicity block determines the QT/RR model and their parameters given the RR profile and the QT interval series, see Figure 5.4.

5.3 Results

Figure 5.5 shows the user interface of PyECG. The application includes a Main Menu and a Toolbar in the topmost side of the main screen. Both of them provide access to all the options of the software. Thus, hereinafter only the commands in the Toolbar will be commented. The Toolbar is divided in three sections. The first one includes actions related to the application management. The second and the third sections provide actions which support the general workflow previously discussed.

Section (1) provides the following actions, *Open*, *Save*, *Options* and *Exit*. The *Open* action (1.1) allows the user to load a Holter recording from disk, currently

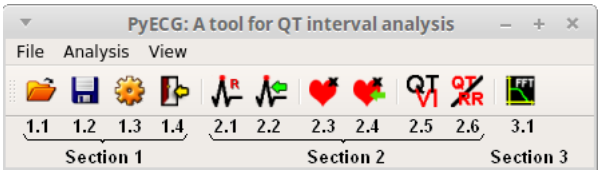


Figure 5.5: PyECG user interface, main menu and toolbar.

the tool supports Excorde E3C and MATLAB© files. This command gives the alternative of loading either a segment of the signal or the whole recording. *Save* (1.2) allows storing the results of the analyses to a file. The button *Options* (1.3) provides access to configuration parameters of the preprocessing stage. Here, the user can select and configure the QRS detector and the ectopic heartbeat detection algorithm. Finally, the *Exit* action (1.4) quits the application.

The analysis section (2) implements both processing modules. The elements on this section will be available after opening a recording. The actions included are: *Detect R*, *Load R annotations from file*, *Detect premature heartbeats*, *Load label annotations from file*, *QTVI* and *QT dynamicity*.

The *Detect R* action (2.1) filters the signal and automatically detects the R peaks on both leads of the record, Figure 5.6. The command shows the detected points directly onto the signal plot. Two panels with possibly missing or incorrectly detected R peaks are available to the right. Both panels show the time positions where the algorithm failed and allow going directly to these positions by clicking on them. This makes easier the manual correction task, Figure 5.6.

The action *Load annotations from file* (2.2) shows the R-peak positions of the signal, but no R-peak detection is executed by the tool. Instead, the R-peak positions are loaded from the recording file. However, still the signal is pre-filtered as was described for the *Detect R* action. After finishing the detection/loading process, the user can manually correct the positions in case of errors. The software provides a very simple interface for correcting the detected points. Essentially, a popup menu with three entries is available for each detected point. The possible actions include *Adjust point*, *Remove point* and *Add point*. *Adjust point* allows moving the current point around the window, *Remove point* deletes the current point and *Add point* includes a new point, Figure 5.6.

Together with preprocessing actions, the user can explore the power spectrum of the signal before and after filtering. Section 3 unique action, namely *Spectrum* (3.1) shows the power spectrum for both leads at any time it is invoked. This action is useful as reference on the effect of the filtering approach implemented

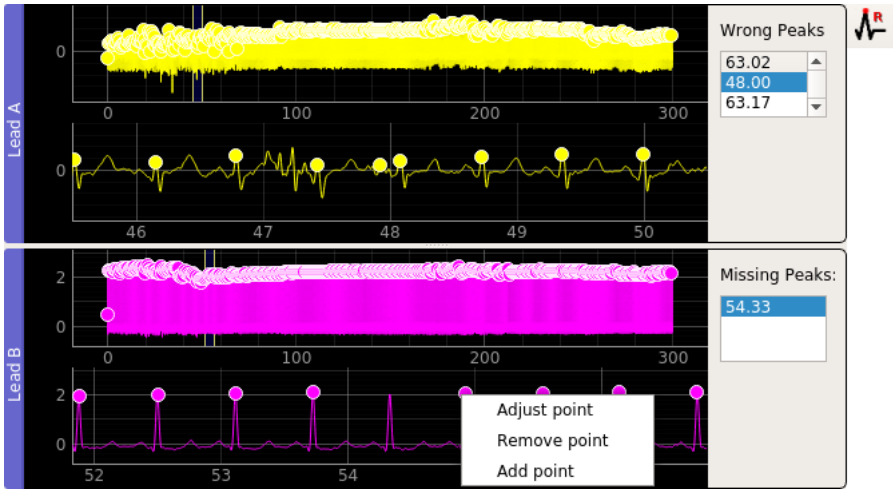


Figure 5.6: R-peak detection results using the built-in algorithm in a 300 s segment. The panels to the right include the time positions of possibly missing or incorrectly detected points. The user can navigate directly to these positions by clicking on them. The popup menu shows the available options for the current point.

in the software.

Both *Detect premature heartbeats* (2.3) and *Load label annotations from file* (2.4) actions show the class label (normal/ectopic) associated to every single heartbeat. The main goal of both actions is to provide information on the number of ectopic heartbeats in the segment under analysis. Thus, the user can judge the pertinence of computing the QT indexes on this interval. The EHB is accessible via action 2.3. It processes the signal and assigns a label to each heartbeat. Depending on the algorithm a guided training process may be needed. Action 2.4 involves loading the label annotations stored on the recording file. Although the software is not intended for annotating records, it is possible to override the automatically generated labels provided by both, the built-in algorithms and the recording file.

QTVI and QT dynamicity buttons implement the Module 1 and Module 2 stages respectively. Clicking on the QTVI button will display a dock with a brief tutorial on computing QTVI. Here, the software gives details on all the necessary steps and suggests a lead for QTVI computation. Then the user should select a lead by clicking on one of the push buttons provided. Once the lead has been selected a new dock is displayed with only the lead of interest,

Figure 5.7.

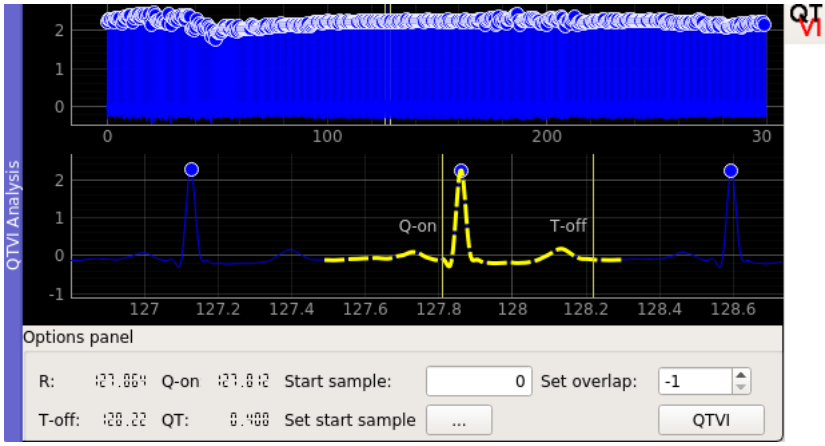


Figure 5.7: QTVI analysis window, the options panel shows information on the current template heartbeat (thick dashed yellow line).

The new dock includes three sections, (1) a global view of the segment of the signal under analysis, (2) a zoomed area of the signal and (3) an information/control panel. The latter, provides the following features, (1) displays information on the current template heartbeat, (2) gives options for defining the analysis window (start and overlapping factor) and (3) allows computing QTVI, Figure 5.7.

The user can define the template heartbeat by clicking on any R peak displayed on the zoomed region. As response to this action, the software will change the color of the current heartbeat. Furthermore, two vertical lines will be displayed suggesting the Q-on and T-off points of the current heartbeat respectively. These lines can be manually adjusted by the user, Figure 5.7.

There are two alternatives for specifying the start of the 256 s analysis window. The first one is by directly writing the time in seconds or the number of the sample on the Start sample input control. The second one is a graphical alternative where the user selects the start by clicking on the push button (...) and moves the start line around the zoomed area. The Set overlap control allows for computing either one or several QTVI values on the current segment, depending on its value. A negative value corresponds to only one QTVI computation. Zero or positive values correspond to the percentages of overlapping among adjacent 256 s windows for computing each QTVI. Finally, the QTVI push button allows the user to compute the QTVI value or values given the defined parameters.

Clicking on the QT dynamicity button follows the same approach as QTVI, i.e. a brief tutorial on QT dynamicity analysis is displayed and the user is motivated to select the lead with the best relative signal quality. After selecting the lead of interest, a new three-panel dock is opened. The first panel shows the whole segment, the second one, is a zoomed version which includes automatically generated Qon and Toff points for every heartbeat on the segment. Finally, the third one is a control panel for managing options, see Figure 5.8.

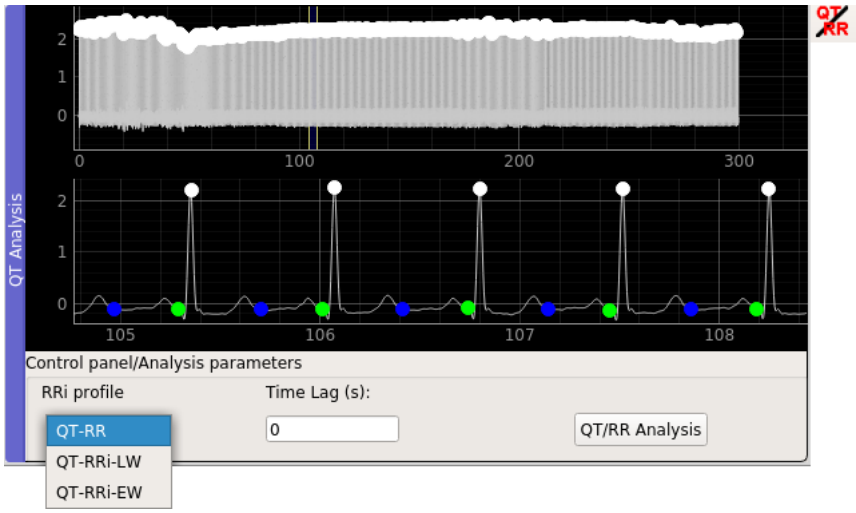


Figure 5.8: QT dynamicity analysis window, the panel at the bottom shows the available parameters. The user can select the profile and a time lag in seconds (only for linear and exponentially weighted profiles).

Every single Qon and Toff point can be manually adjusted by the user on the zoomed panel. The possible actions include, *Adjust point* (the point can be moved around), *Add point* (a new point is included, its position is given by the mean value between the current point and the previous one), *Remove point* (the point is deleted). All these actions are available on a contextual menu accessible by clicking on the point.

The control panel provides options for selecting one of the three available RR profiles through the combo box named RRi profile. LW and EW profiles require a time lag parameter that can be specified in the corresponding control (*Time Lag*), Figure 5.8. The QT dynamicity analysis is performed by clicking on the QT/RR button. As a response to this action, a new panel is displayed with the QT/RR analysis results. The results panel shows a QT-RR scatter plot and the fitted model. Up to 10 models of the relation QT/RR can be evaluated [91].

The parameters of each model are available on demand by clicking on the name of the model.

5.3.1 Tool test

This section shows a brief qualitative and quantitative evaluation of PyECG. Several tests have been performed using both, synthetic signals and recordings from the Excorde 3C Holter [15]. The tests will focus on the main features of the tool i.e. signal quality assessment, premature heartbeats detection and QT analysis. The SQA block was evaluated by using the tutorial feature of both modules. The tutorial explains the steps for performing the further analysis and suggests a lead for doing so. Precisely this suggestion expresses the results of the SQA module by coding the VI absolute value (VIav) in words as follows. The unanimity (VIav=6) corresponds to the words "strongly recommends", the word “recommends” means majority (VIav=4), simple majority (VIav=2) is coded to "slightly recommends" and a tie (VIav=0) corresponds to “suggests”. The sign of VI points out the lead i.e. is positive for lead A and negative for lead B.

The test for SQA block evaluation consists of comparing artificial signals with different SNR. The signals were generated with the synthetic generator proposed in [71]. The parameters for the model are given in Table 5.1. Thus, with this model a noise free signal was generated. Then, this signal was contaminated with uniformly distributed noise with amplitude 0.08 mV. Moreover, a 1 Hz, 0.3 mV baseline drift was added. Both, the contaminated and the clean signals were assembled in a single two channel signal. This two-channel record was loaded into the tool. Here, the contaminated signal corresponds to channel A and the clean one to Lead B. After detecting the R points, the SQA module can be evaluated by clicking on the QTVI action, see Figure 5.9. Since there is a clear difference among qualities of the channels it is expected that the software recommends Lead B, this can be seen in Figure 5.9.

An EHB stage performance evaluation requires annotated records. Thus, eight 15-min segments of different Holter recordings were manually annotated by cardiologists using an independent tool. Table 5.2 shows the main characteristics of these records. The sample intends to cover several heartbeat classes such as normal beats (NORMB), supraventricular ectopic beats (SVEB), paced beats (PB) and ventricular ectopic beats (VEB). Moreover, the recordings include signal quality changes, different types of noise, artifacts and other types of disturbances that normally affect ambulatory signals.

Table 5.3 shows the results of the performance evaluation using the segments of Table 5.2. It is worth to note that a true positive corresponds to the correct

Table 5.1: McSharry et. al. [71] model parameters for two experiments, the SQA evaluation and the QT dynamicity analysis.

Parameter	Unit	Value (SQA)	Value (QT/RR)
Sampling frequency	Hz	250	250
Noise amplitude	mV	0.01	0.01
Number of beats	-	60	3700
Heart rate mean	bpm	75	75
Heart rate standard deviation	bpm	4.667	4.667
LF/LH ratio	-	0.5	0.5
Internal sampling frequency	Hz	250	250

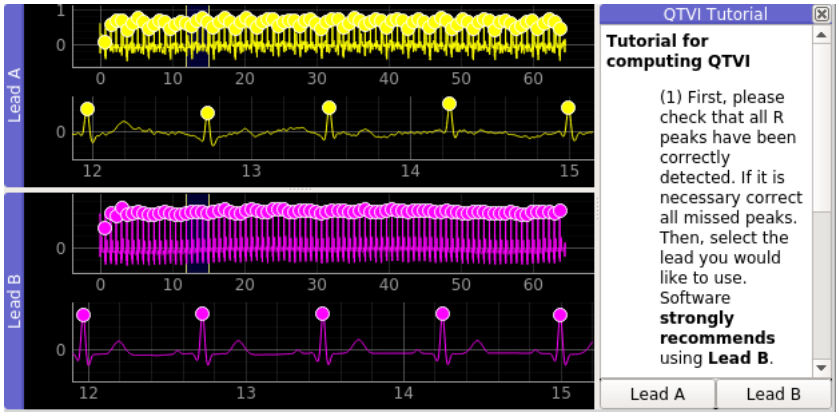


Figure 5.9: SQA block test with synthetically generated signals. Lead A was contaminated with noise and baseline drift (see the text), lead B is the clean signal. To the right, the QTVI tutorial points out lead B as the best one.

detection of an abnormal heartbeat. Excluding the positive predictive value (P+), the performance indexes are all above 96%. The worst performance index is P+ with a 64.4%. This means that the classifier is very sensitive to morphology variations. Indeed, the signal quality changes affect the morphology and consequently the output of the classifier. For instance, in segments 1 and 5 most of the false positives found, correspond to intervals where the signal quality is compromised by an increment in the noise level. We hypothesize that in such cases, better performances can be achieved by using supervised classification because the knowledge of the user can be incorporated into the classification system. However, the proper assessment of the previous hypothesis would require an extensive evaluation, which is beyond the scope of this paper. Furthermore, for the purposes of this tool, this behavior is not too critical

Table 5.2: Segments of 15 min from different Holter recordings for the evaluation of the EHB.

Segment	Characteristics
1	Moderate noise in both leads, PVC and paced beats.
2	Several SVEB. Lead B low amplitude
3	First half of lead A is noisy. Few PVC beats.
4	Low SNR in lead A. Motion artifacts.
5	Very low level signal in both leads, particularly in lead A, where it is almost unreadable. Few artifacts.
6	Low level signal in both leads, particularly in lead B. Few ectopic beats.
7	Severe noise in both leads in the interval 300-500 s. Several paced beats.
8	Lead A clean signal, no abnormal heartbeats. Lead B completely noisy and unusable.

because it is important to avoid low-quality segments. Hence, a very sensitive classifier may notify the user about poor quality segments.

In order to evaluate the performance of the detection algorithms the QT Database (QTDB) [55] was used. QTDB is publicly available in Physionet [38] and was designed for evaluating the performance of algorithms for event detection in ECG. It consists of short segments (15 min) extracted from 105 Holter recordings, each with two channels. The sampling frequency is 250 Hz.

Regarding the evaluation of the Toff detector, the following experiment was designed. First, the output of the original algorithm was obtained for all records in QTDB. This results in 65 records with at least one lead, which satisfies Group I error stratification level according to the CSE Working Party criterion [18]. This level corresponds to the records where the mean error (accuracy) on detecting Toff is below 15 ms and the standard deviation of the error (precision) is below 30.6 ms. When both leads accomplished this criterion, the best one was chosen. Then, 40 recordings were selected at random from this group for the evaluation using PyECG. The results of this evaluation are shown in Table 5.4.

Table 5.3: Evaluation of the ectopic heartbeat detection block using the signals from Table 5.2. Here, R is the number of detected heartbeats, TP, FP, FN and TN are the number of true positives, false positives, false negatives and true negatives respectively. Moreover, sensitivity (Se), specificity (Sp), positive predictive value (P+) and accuracy (Acc) performance metrics are included.

Segment	R	Total	(%)	TP	FP	FN	TN	Se	Sp	P+	Acc
1	1037	1042	99.5	32	52	0	953	100	94.8	38.1	95.0
2	1026	1029	99.7	41	6	4	975	91.1	99.4	87.2	99.0
3	1368	1370	99.9	2	0	1	1365	66.7	100	100	99.9
4	1315	1318	99.8	1	0	0	1144	100	100	100	100
5	977	978	99.9	2	21	1	954	66.7	97.8	8.70	97.8
6	975	981	99.4	4	8	0	962	100	99.2	33.3	99.2
7	888	935	95.0	88	7	0	793	100	99.1	92.6	99.2
8	903	906	99.7	0	0	0	903	-	100	-	100
Total	8489	8559	99.2	170	94	6	8049	96.6	98.8	64.4	98.8

Although the original output is slightly better, both algorithms produce similar results and the overall performance barely changes. Indeed, the absolute differences in the mean accuracy and the mean precision are below one sample at 250 Hz (4 ms). Hence, it is clear that both versions have equal performances so the PyECG implementation is reliable enough and follows the original algorithm.

The Q onset detection algorithm was compared against the output of the wavelet delineator [26] included in the ECG-kit. This is a well-known delineator which is also publicly available in Phyisionet. The original code of the wavelet delineator is written in MATLAB© and a similar methodology was followed for the comparison. Once more, the ground-truth is the set of Q onset annotations available on QTDB. Besides, the previous 40 records were also used and the same lead was considered for both algorithms. Although this approach for evaluating the Q onset detectors will result in lower performances, this choice is based on the fact that for the purposes of the QT/RR and QTVI analysis only one lead is finally available. Thus, all the fiducial points should be detected on the chosen lead, see Table 5.4.

Table 5.4: Evaluation of the Toff and Qon detectors using a subset of the QT database. MAT is the original MATLAB© implementation of the respective algorithms.

No	Record	T offset location error				Q onset location error			
		MAT [138]		PyECG		MAT [70]		PyECG	
		μ	σ	μ	σ	μ	σ	μ	σ
1	sel100	-14.0	16.5	-9.87	17.1	23.3	8.28	3.33	7.80
2	sel103	-7.47	17.1	-3.73	16.7	11.3	9.62	-11.8	14.6
3	sel116	-11.8	17.6	-7.36	17.0	12.1	12.8	-25.2	22.8
4	sel123	-5.73	8.71	-2.00	7.77	33.3	11.7	-10.3	16.2
5	sel14046	-6.84	15.3	-2.45	15.1	-1.60	18.6	-14.9	18.9
6	sel14157	-14.3	8.71	-10.1	8.39	10.4	5.62	4.27	5.65
7	sel16272	4.27	10.0	6.00	11.0	10.8	5.37	-6.80	5.86
8	sel16273	14.9	8.06	-9.87	8.65	10.0	9.38	3.20	8.43
9	sel16420	2.53	11.3	4.67	11.5	6.80	5.05	0.00	4.33
10	sel16483	-2.40	7.32	-3.07	7.62	8.80	6.68	5.47	6.43
11	sel16539	4.13	10.2	7.20	9.82	12.5	7.41	6.00	7.33
12	sel16773	2.67	8.75	7.60	8.75	4.40	8.29	-45.6	12.1
13	sel16786	0.53	10.2	4.13	10.4	-34.5	40.5	-11.7	20.1
14	sel16795	-10.3	11.5	-10.1	12.0	16.7	8.73	-3.07	8.96
15	sel17152	-3.07	16.5	4.67	18.3	6.53	9.48	-38.0	12.1
16	sel17453	8.00	18.7	11.6	18.0	-2.06	11.9	-27.5	13.4
17	sel221	-8.67	14.9	-4.53	14.1	25.8	28.9	-19.6	20.8
18	sel223	4.00	20.7	8.13	21.1	-0.08	7.86	-6.00	6.32

Table 5.4: Evaluation of the Toff and Qon detectors using a subset of the QT database. MAT is the original MATLAB© implementation of the respective algorithms.

No	Record	T offset location error				Q onset location error			
		MAT [138]		PyECG		MAT [70]		PyECG	
		μ	σ	μ	σ	μ	σ	μ	σ
19	sel230	-2.88	17.2	-1.04	17.5	13.8	6.79	20.7	12.7
20	sel231	-10.6	15.6	-6.64	15.8	13.7	8.32	-8.13	7.24
21	sel306	-4.11	10.8	8.89	9.80	9.87	8.19	14.9	21.5
22	sel803	-2.27	12.6	-5.73	12.5	3.20	15.0	-45.7	14.5
23	sel808	-13.6	19.1	-14.5	19.9	3.87	12.3	-12.3	9.57
24	sel811	-6.80	11.2	-10.4	12.2	15.9	9.92	-25.9	11.5
25	sel821	7.73	15.4	12.3	16.8	-9.07	24.7	-25.9	12.7
26	sel840	0.23	13.5	1.31	14.3	18.0	7.11	-4.80	7.00
27	sel847	-5.21	13.9	-0.61	14.2	14.5	6.99	-9.21	5.79
28	sel853	-8.80	14.9	-11.7	16.6	11.2	9.88	-6.00	11.7
29	sel871	-2.00	22.4	-1.14	15.7	24.4	4.62	1.20	4.35
30	sel872	-0.80	9.12	-2.40	10.5	9.73	5.63	-19.3	16.3
31	sel873	7.27	19.2	11.4	18.8	7.07	5.43	-11.6	4.97
32	sel883	-5.07	12.6	-3.60	12.4	8.93	4.54	-10.5	4.26
33	sel891	4.79	13.3	4.23	17.7	8.13	8.69	-2.13	7.26
34	sele0106	7.07	15.3	12.0	14.7	2.67	20.1	-9.73	10.0
35	sele0110	-12.8	27.3	-8.53	27.4	1.33	4.50	-18.1	13.2
36	sele0111	-6.40	8.76	-2.00	9.32	0.67	12.2	-32.0	23.0
37	sele0114	7.73	20.9	12.4	20.6	17.3	6.67	-3.60	6.75
38	sele0121	10.5	8.17	14.8	8.15	2.53	7.54	1.47	4.98
39	sele0122	8.27	6.21	2.27	6.38	19.1	11.7	-0.40	7.96
40	sele0133	-0.67	9.10	3.60	9.70	9.73	8.51	-4.80	5.70
	μ (ms)	-1.79	13.7	0.14	13.9	9.03	10.6	-10.3	10.9
	μ (samples)	-0.45	3.43	0.04	3.47	2.26	2.66	-2.56	2.72

From Table 5.4, it is noticeable that there are significant differences among algorithms. The method implemented tends to estimate the Q onset points before their real positions whereas the wavelet delineator tends to estimate the Qon points after their true location. In terms of the QT interval and assuming an exact Toff, the former method would overestimate the QT interval. Conversely, the wavelet delineator would underestimate it. Nevertheless, in terms of the absolute value of the accuracy, both methods have approximately the same mean accuracy. This is also the case of the precision parameter where the absolute difference is negligible (0.3 ms). Hence, the Q onset detector based

on trapezium area has almost the same precision as the wavelet delineator; however, it is simpler and faster than the wavelet approach.

Finally, a brief test of the QT dynamicity block was performed as follows. Using the McSharry model a 3700 s signal was generated. The parameters for the model are shown in Table 5.1. Two signals were generated A signal with 0.01 mV of noise amplitude and a clean signal which is used as reference. This free-noise reference is used for determining the positions of the Qon and Toff points. These positions were determined outside of the tool using MATLAB©. Then the QT/RR slope and y-intercept were computed using the previous points and the first profile (QT depends on the previous RR). The values of both, the slope and the y-intercept are taken as ground truth, see Figure 5.10.

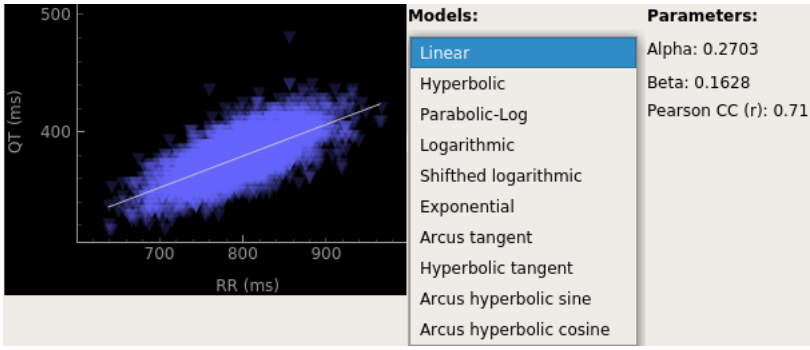


Figure 5.10: Results of the QT dynamicity analysis on the synthetic signal generated with the model (see Table 5.1). Scatter plot QT/RR and results panel of the QT dynamicity analysis. The first profile (QT depends on the previous RR) was used, so blue triangles represent the coordinates (RR_{i-1}, QT_i) for the i-th heartbeat. Ten models are accessible through the combo box. The model parameters (alpha and beta) are shown below the QT/RR scatter plot. Here, alpha is the slope of the regression line (in white) and beta is the y-intercept. The Pearson correlation coefficient is also available. The parameters for the linear model are given to the right.

The noise-contaminated signal was loaded into the tool. The QT dynamicity analysis module was launched after filtering and R peak detection and correction processes. Since it is known that the model generates QT intervals linearly related to the RR intervals [71], the linear model for regression was used. The results for the linear model using the first profile and the relative errors with respect to the reference are given in Table 5.5. It is noticeable that no manual correction to the automatically generated Qon and Toff points was used. In spite of the latter, low relative errors were obtained, see Table 5.5. Figure 5.10

shows the results for this analysis using PyECG and the QT-RR scatter plot. Besides, the regression line is also visible.

Table 5.5: QT analysis on synthetic signals using the linear model and the profile where the QT depends on the previous RR interval. QT/RR regression line parameters given for both, contaminated and clean signals. Here α is the slope, β is the y-intercept and R.E. stands for relative error.

Clean signal (ground-truth)		Contaminated signal		R.E	
α	β	α	β	α (%)	β (%)
0.2728	0.1598	0.2703	0.1628	-0.9121	1.9052

5.4 Conclusions

This chapter presented a software tool for the analysis of the QT interval on Holter recordings. The main contribution of this work is that this is the first public software tool that allows to compute indexes that have been pointed out as markers of repolarization instability. Besides, premature heartbeats can be detected and rejected. This feature, together with a block for signal quality assessment allows for an easy, reliable and fast evaluation on the feasibility of the current segment for the QT analysis. It can be used by cardiologists and specialists with no programming skills as a tool for research on QT interval analysis. Moreover, the software has been tested with records from the Excorde 3C Holter system which is widespread throughout hospitals in Cuba.

Chapter 6

Conclusions and future work

6.1 Conclusions

This research presented different machine learning based algorithms for processing the ambulatory electrocardiographic (AECG) signal. The main challenge for ambulatory ECG studies is the loss of relevant information caused by noise and artifacts. Thus, it is needed to improve the methods for processing the ambulatory signal in order to enhance its diagnostic capabilities. Inspired by this problem, we focused this dissertation on the following topics

- A new approach for ectopic heartbeat detection using tensors and machine learning.
- A new method for T wave end detection using machine learning
- Development and evaluation of a tool for QT analysis

Besides noise and artifacts, isolated ectopic heartbeats may occur in an ambulatory recording. Premature heartbeats disrupt the sinoatrial node firing rate which may affect HRV/QT analysis. Therefore, it is relevant to accurately detect these beats in order to exclude them from the analysis. The main findings in this topic are

- Two novel tensor-based algorithms were proposed for detecting ectopic heartbeats.

- The use of tensors and tensor decompositions in combination with supervised machine learning, particularly, support vector machines, is feasible for detecting ectopic heartbeats.
- The tensor approach has the advantage to directly deal with multi-lead ECG, this allows focusing on the integral analysis of the signal rather than any specific lead.
- Since features were extracted through a tensor decomposition or approximation, only one classifier is required. This implies an added value by saving training time.

The increase in the performance of ectopic heartbeat detection algorithms has also a positive economical impact. It saves time and expenses in salary for medical staff because more ectopic beats can be accurately detected without a time-consuming beat-to-beat visual inspection.

Apart from the study on classifiers, a novel machine learning approach for detecting the end of the T-wave was presented in this work. Both, neural networks and least-squares support vector machines were evaluated as T-wave end detectors. Along with both algorithms, several methods for extracting features and selecting the training set were evaluated as well. The main findings are summarized as follows:

- The suport vector machine approach reported the best performance. Besides, this method combined with active prototype vector selection outperformed other state-of-the-art T-wave end detectors.
- The method is easy to tune since the size of the training set is the unique parameter that should be adjusted beforehand.
- The main disadvantage of the proposed algorithm is that a training period is required. This can be solved, for instance, by using hybrid approaches that combine this algorithm and unsupervised methods minimizing the time required for traininig. Moreover, the proposed aproach showed high performances using small training sets.
- QT interval analyses can be improved with the proposed approach. QT interval analysis often requires the accurate detection of the T-wave end. Thus, as better the method for doing so is as more reliable is the result of the QT analysis. Consequently, a better diagnostic is possible having a positive impact on patients.

The last contribution of this research is a software tool for the analysis of the QT interval in the AECG. The need for this tool relies on the lack of software

that allows computing the QTVI and QT adaptation markers easily. The software was developed for cardiologists and specialists. The built-in GUI is intuitive, compact and easy to use. Furthermore, no programming language knowledge is needed. It is a useful tool for encouraging and supporting the research on ventricular repolarization analysis. Several studies have reported QT analysis techniques as promising methods for assessing the risk of suffering life-threatening arrhythmias and sudden cardiac death. AECG enhances the diagnostic value of the ECG. Therefore, providing tools for accurately computing QT markers is relevant for tackling challenges such as those sudden cardiac death risk stratification impose.

In a nutshell, this work focused on improving the processing methods of AECG. The AECG is a cheap and non-invasive method for assessing cardiovascular function. Thus, empowering the diagnostic capabilities of the AECG has a positive impact on both, society and economy. One one hand, often an AECG test might provide enough diagnostic information, so invasive and expensive tests can be avoided. On the other hand, invasive tests might be uncomfortable or cause stress in patients. Thus, they affect the life-quality of patients and relatives.

6.2 Future work

The possible extensions and future directions of this research are summarized below.

- Regarding premature heartbeat detection using tensors and machine learning two main directions of further research can be identified. On one hand, the differentiation between ectopic heartbeats generated in the atria and ventricular ectopic beats can be addressed. On the other hand, the combination of tensor methods and unsupervised learning approaches can be further evaluated. Furthermore, the classifier that uses least-squares support vector machines might be implemented in the QT analysis tool.
- In relation to T-wave end detection, this research may further derive in two directions. First, the extended evaluation of the proposed algorithm in long-term recordings could be addressed since so far the evaluation was performed using records from international databases.
- In close alliance with medical doctors, it will be possible to evaluate transfer learning methods and evolutionary algorithms in the context of any fiducial point extraction. Thus, future research might address the evaluation of emergent machine learning tools like deep-learning as well as

the combination of supervised and unsupervised approaches. This might lead to intelligent and powerful systems for processing AECG.

- Regarding the proposed tool for QT interval analysis, it is crucial to validate it with the leadership of the medical staff. Further actions may include the extension of the tool to other types of analysis such as T wave alternans, QT dispersion or Heart Rate Turbulence.
- The long-term goal regarding the tool is to expand the capabilities of the software in a flexible and scalable product that allows performing several types of analyses. The latter would demand a design where the new processing methods can be easily plugged into the main software as add-ons.

Appendix A

Examples of T-wave end detection in QTDB

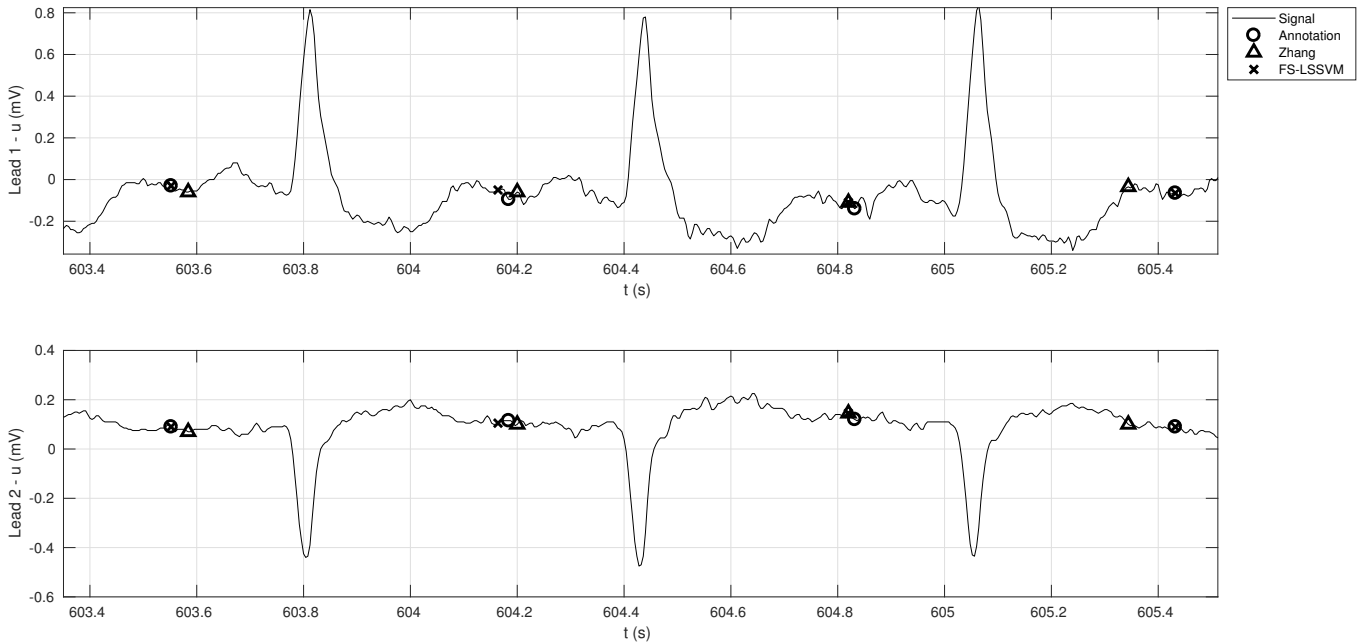


Figure A.1: T-wave end detection in a noisy recording, the interval corresponds to the recording "sel48.dat" from QTDB.

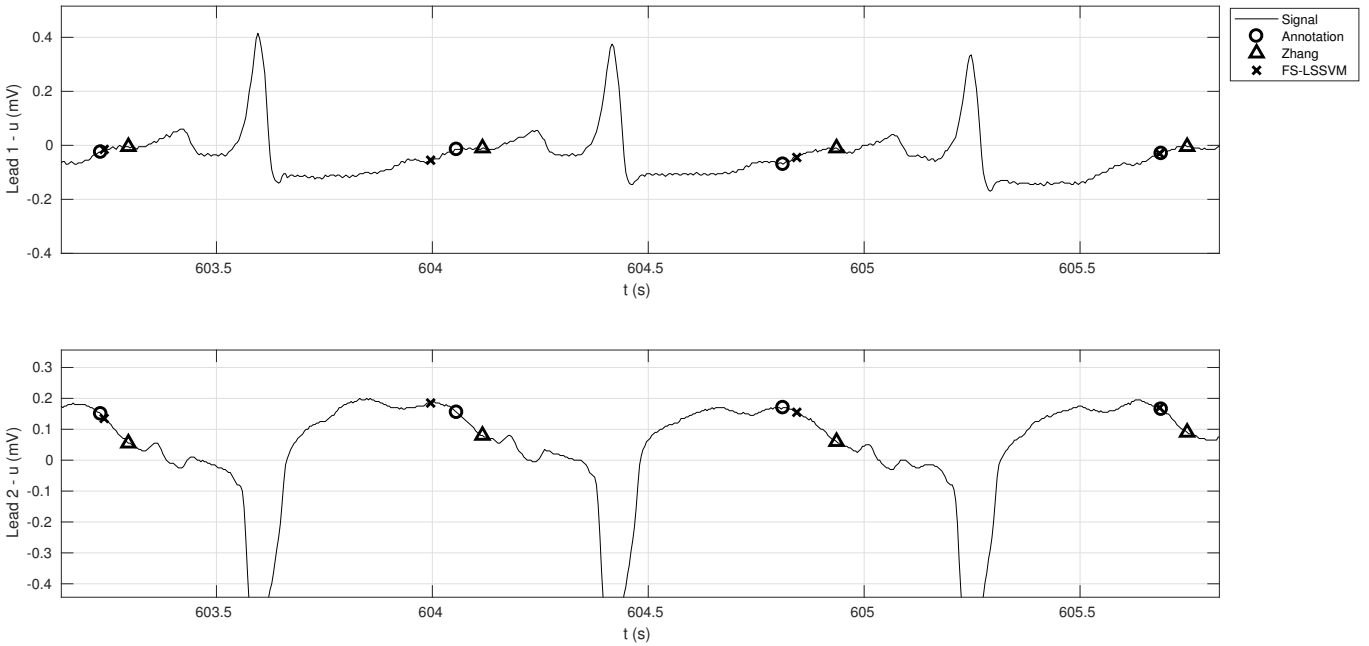


Figure A.2: T-wave end detection for a low amplitude T-wave, the interval corresponds to the recording "sel31.dat" from QTDB.

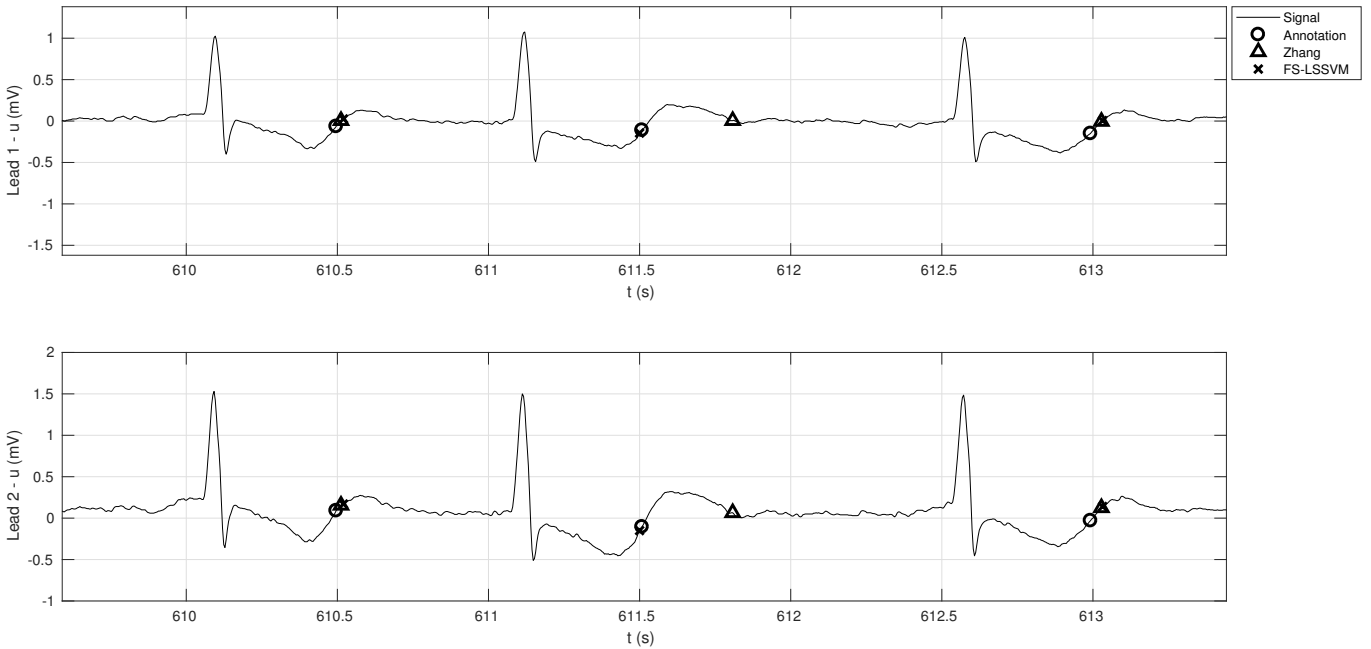


Figure A.3: T-wave end detection where U-wave is present, the interval corresponds to the recording "sel50.dat" from QTDB.

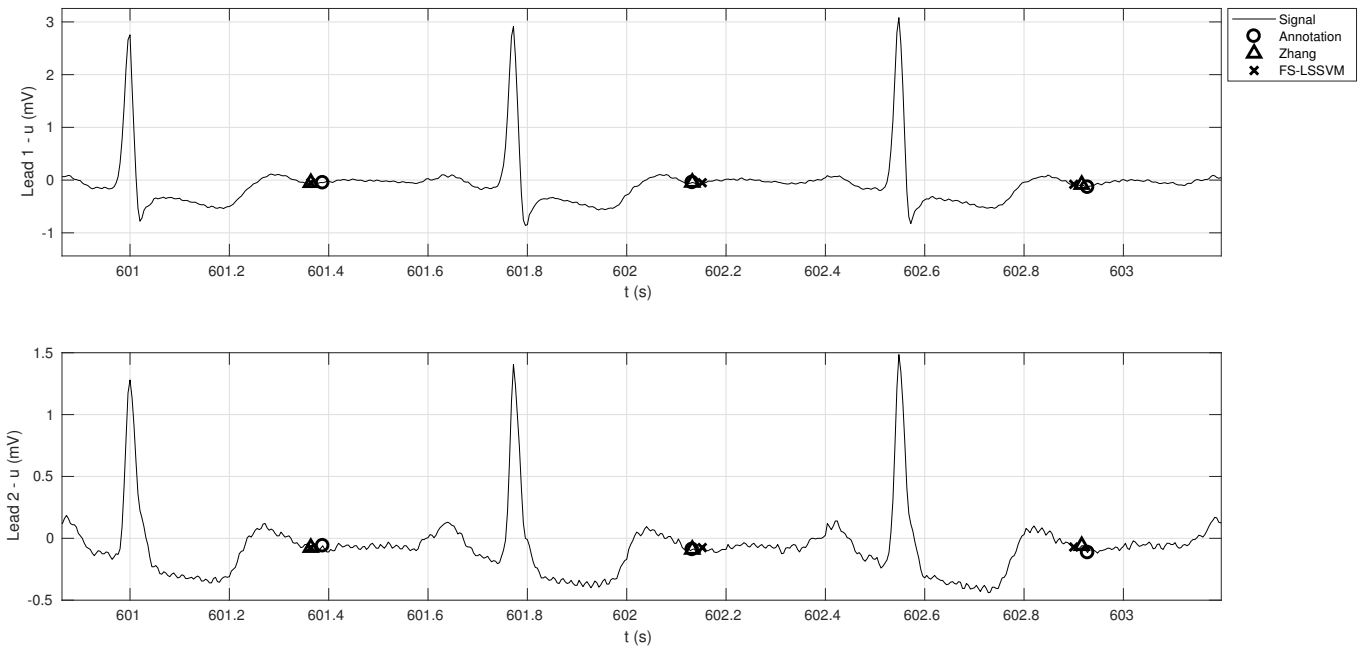


Figure A.4: T-wave end detection for biphasic waves, the interval corresponds to the recording "sel301.dat" from QTDB.

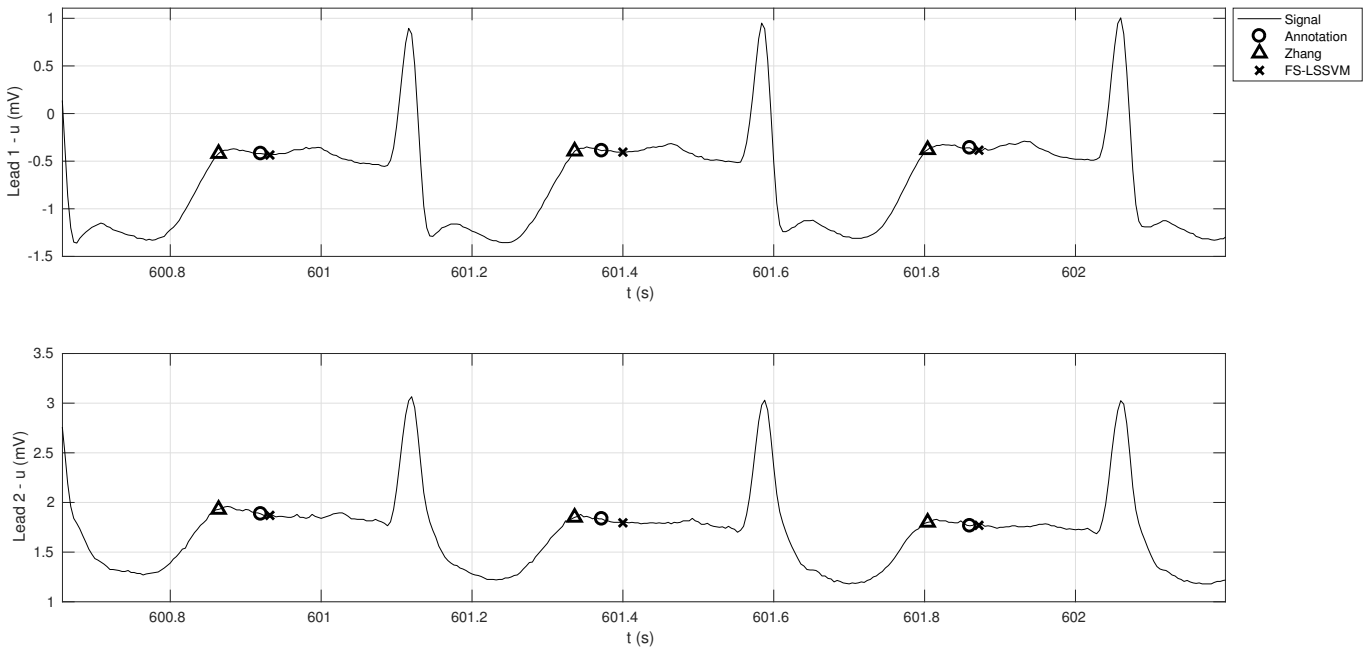


Figure A.5: T-wave end detection in an "unintuitive" case, the interval corresponds to the recording "sele0409.dat" from QTDB.

Bibliography

[1] Acharya, U. R., Fujita, H., Adam, M., Lih, O. S., Sudarshan, V. K., Hong, T. J., Koh, J. E., Hagiwara, Y., Chua, C. K., Poo, C. K., et al. Automated characterization and classification of coronary artery disease and myocardial infarction by decomposition of ECG signals: A comparative study. *Information Sciences 377* (2017), 17–29.

[2] Ahmed, N., Natarajan, T., and Rao, K. R. Discrete cosine transform. *IEEE transactions on Computers 100*, 1 (1974), 90–93.

[3] Bahaz, M., and Benzid, R. Efficient algorithm for baseline wander and powerline noise removal from ecg signals based on discrete fourier series. *Australasian physical & engineering sciences in medicine 41*, 1 (2018), 143–160.

[4] Benarroch, E. E. The autonomic nervous system: basic anatomy and physiology. *CONTINUUM: Lifelong Learning in Neurology 13*, 6, Autonomic Disorders (2007), 13–32.

[5] Berger, R. D. QT Variability. *Journal of Electrocardiology 36*, Supplement (2003), 83–87.

[6] Berger, R. D., Kasper, E. K., Baughman, K. L., Marban, E., Calkins, H., and Tomaselli, G. F. Beat-to-beat QT interval variability: novel evidence for repolarization lability in ischemic and nonischemic dilated cardiomyopathy. *Circulation 96*, 5 (1997), 1557–1565.

[7] Biswas, U., and Maniruzzaman, M. Removing power line interference from ecg signal using adaptive filter and notch filter. In *Electrical Engineering and Information & Communication Technology (ICEEICT), 2014 International Conference on* (2014), IEEE, pp. 1–4.

[8] Brateanu, A. Heart rate variability after myocardial infarction: what we know and what we still need to find out. *Current medical research and opinion 31*, 10 (2015), 1855–1860.

[9] Budoff, M. J., and Shinbane, J. S. *Cardiac CT imaging: diagnosis of cardiovascular disease*. Springer, 2016.

[10] Bystricky, W., and Safer, a. Modelling T-end in Holter ECGs by 2-layer perceptrons. In *Computers in Cardiology* (2002), no. 2, pp. 105–108.

[11] Ceylan, R., and Özbay, Y. Comparison of FCM, PCA and WT techniques for classification ECG arrhythmias using artificial neural network. *Expert Systems with Applications 33*, 2 (2007), 286–295.

[12] Chang, C.-C., and Lin, C.-J. LIBSVM: a library for support vector machines. *ACM transactions on intelligent systems and technology (TIST) 2*, 3 (2011), 27.

[13] Choudhry, M. S., Puri, A., and Kapoor, R. Removal of baseline wander from ecg signal using cascaded empirical mode decomposition and morphological functions. In *Signal Processing and Integrated Networks (SPIN), 2016 3rd International Conference on* (2016), IEEE, pp. 769–774.

[14] Cichocki, A., Mandic, D., Phan, H. A., Caiafa, C., Zhou, G., Zhao, Q., and De Lathauwer, L. Tensor decompositions for signal processing applications: From two-way to multiway component analysis. *IEEE Signal Processing Magazine 32*, 2 (2015), 145–163.

[15] COMBIOMED. *Excorde 3C Holter manual (in spanish)*, 2009.

[16] Corinna, C., and Vapnik, V. Support vector machine. *Machine learning 20*, 3 (1995), 273–297.

[17] Crawford, M. H., Bernstein, S. J., Deedwania, P. C., DiMarco, J. P., Ferrick, K. J., Garson, A., Green, L. A., Greene, H. L., Silka, M. J., Stone, P. H., et al. ACC/AHA guidelines for ambulatory electrocardiography: a report of the American College of Cardiology/American Heart Association Task Force on Practice Guidelines (Committee to revise the guidelines for ambulatory electrocardiography) developed in collaboration with the North American Society for Pacing and Electrophysiology. *Journal of the American College of Cardiology 34*, 3 (1999), 912–948.

[18] CSE Working Party. Recommendations for measurement standards in quantitative electrocardiography. *European Heart Journal 6*, 10 (1985), 815–825.

[19] Cuesta-Albertos, J. A., Gordaliza, A., and Matrán, C. Trimmed k-means: An attempt to robustify quantizers. *Annals of Statistics 25*, 2 (1997), 553–576.

[20] Day, C. P., McComb, J. M., and Campbell, R. QT dispersion: an indication of arrhythmia risk in patients with long QT intervals. *Heart 63*, 6 (1990), 342–344.

[21] De Brabanter, K., De Brabanter, J., Suykens, J. A., and De Moor, B. Optimized fixed-size kernel models for large data sets. *Computational Statistics and Data Analysis 54*, 6 (2010), 1484–1504.

[22] de Chazal, P., Heneghan, C., Sheridan, E., Reilly, R., Nolan, P., and O'Malley, M. Automated processing of the single lead electrocardiogram for the detection of obstructive sleep apnoea. *IEEE Trans. Biomed. Eng. 506*, 6 (2003), 205–227.

[23] de Chazal, P., O'Dwyer, M., and Reilly, R. Automatic classification of heartbeats using ECG morphology and heartbeat interval features. *IEEE Transactions on Biomedical Engineering 51*, 7 (jul 2004), 1196–1206.

[24] de Chazal, P., and Reilly, R. B. A patient-adapting heartbeat classifier using ECG morphology and heartbeat interval features. *IEEE Transactions on Biomedical Engineering 53*, 12 (2006), 2535–2543.

[25] De Lathauwer, L., De Moor, B., and Vandewalle, J. A multilinear singular value decomposition. *SIAM Journal on Matrix Analysis and Applications (SIMAX) 21*, 4 (2000), 1253–1278.

[26] Demski, A., and Soria, M. L. ecg-kit: a matlab toolbox for cardiovascular signal processing. *Journal of Open Research Software 4*, 1 (2016).

[27] Dobson C, P., Kim, A., and Haigney, M. QT Variability Index. *Progress in Cardiovascular Diseases 56* (2013), 186–194.

[28] Elhaj, F. A., Salim, N., Harris, A. R., Swee, T. T., and Ahmed, T. Arrhythmia recognition and classification using combined linear and nonlinear features of ecg signals. *Computer methods and programs in biomedicine 127* (2016), 52–63.

[29] Erdogmus, D., and Principe, J. C. Generalized information potential criterion for adaptive system training. *IEEE Transactions on Neural Networks 13*, 5 (2002), 1035–1044.

[30] Fernanda, A., Bernardo, B., Vanderlei, L. C. M., and Garner, D. M. HRV Analysis : A clinical and diagnostic tool in chronic obstructive pulmonary disease. *International scholarly research notices 2014* (2014).

[31] Florea, V. G., and Cohn, J. N. The autonomic nervous system and heart failure. *Circulation research 114*, 11 (2014), 1815–1826.

[32] Fujita, H., Acharya, U. R., Sudarshan, V. K., Ghista, D. N., Sree, S. V., Eugene, L. W. J., and Koh, J. E. Sudden cardiac death (SCD) prediction based on nonlinear heart rate variability features and SCD index. *Applied Soft Computing 43* (2016), 510–519.

[33] García-Escudero, L. Á., and Gordaliza, A. Robustness properties of k-means and trimmed k-means. *Journal of the American Statistical Association 94*, 447 (1999), 956–969.

[34] García-Escudero, L. A., Gordaliza, A., Matrán, C., and Mayo-Iscar, A. A general trimming approach to robust cluster analysis. *Annals of Statistics 36*, 3 (2008), 1324–1345.

[35] Ghaffari, A., Homaeinezhad, M. R., Akraminia, M., Atarod, M., and Daevaeiha, M. A robust wavelet-based multi-lead electrocardiogram delineation algorithm. *Medical Engineering and Physics 31*, 10 (2009), 1219–1227.

[36] Gillet, R., Teixeira, P., Meyer, J.-B., Rauch, A., Raymond, A., Dap, F., and Blum, A. Dynamic CT angiography for the diagnosis of patients with thoracic outlet syndrome: Correlation with patient symptoms. *Journal of cardiovascular computed tomography* (2017).

[37] Girolami, M. Orthogonal series density estimation and the kernel eigenvalue problem. *Neural computation 14*, 3 (2002), 669–688.

[38] Goldberger, A. L., Amaral, L. A. N., Glass, L., Hausdorff, J. M., Ivanov, P. C., Mark, R. G., Mietus, J. E., Moody, G. B., Peng, C.-K., and Stanley, H. E. Physiobank, physiotoolkit, and physionet : Components of a new research resource for complex physiologic signals. *Circulation 101*, 23 (2000), e215–e220.

[39] Goldenberg, I., Moss, A. J., Zareba, W., et al. QT interval: how to measure it and what is "normal". *Journal of cardiovascular electrophysiology 17*, 3 (2006), 333–336.

[40] Goovaerts, G., De Wel, O., Vandenberk, B., Willems, R., and Van Huffel, S. Detection of irregular heartbeats using tensors. In *Computing in Cardiology Conference (CinC), 2015* (2015), IEEE, pp. 573–576.

[41] Hall, J. E. *Guyton and Hall textbook of medical physiology e-Book*. Elsevier Health Sciences, 2015.

[42] Harshman, R. A. Foundations of the PARAFAC procedure: Models and conditions for an "explanatory" multimodal factor analysis.

[43] Hashemi, A., Rahimpour, M., and Merati, M. R. Dynamic gaussian filter for muscle noise reduction in ecg signal. In *Electrical Engineering (ICEE), 2015 23rd Iranian Conference on* (2015), IEEE, pp. 120–124.

[44] Hurst, J. W. Naming of the waves in the ECG, with a brief account of their genesis. *Circulation 98*, 18 (1998), 1937–1942.

[45] Ince, T., Kiranyaz, S., and Gabbouj, M. A generic and robust system for automated patient-specific classification of ECG signals. *IEEE Transactions on Biomedical Engineering 56*, 5 (May 2009), 1415–1426.

[46] Jaiswal, M., Divers, J., Urbina, E. M., Dabelea, D., Bell, R. A., Pettitt, D. J., Imperatore, G., Pihoker, C., Dolan, L. M., Liese, A. D., et al. Cardiovascular autonomic neuropathy in adolescents and young adults with type 1 and type 2 diabetes: The search for diabetes in youth cohort study. *Pediatric diabetes 19*, 4 (2018), 680–689.

[47] Jayasekera, G., Crowe, T., Mackenzie, A., Church, C., Johnson, M., Radjenovic, A., and Peacock, A. Left atrial function by cardiac MRI in idiopathic pulmonary arterial hypertension (IPAH) and pulmonary hypertension due to heart failure with preserved ejection fraction (PH-HFpEF). In *C106. MONEY DON'T MATTER TONIGHT: PULMONARY HYPERTENSION ASSESSMENT, PROGNOSTICATION, AND TREATMENT*. American Thoracic Society, 2017, pp. A6903–A6903.

[48] Jobbágy, Á., Majnár, M., Tóth, L. K., and Nagy, P. Hrv-based stress level assessment using very short recordings. *Periodica Polytechnica. Electrical Engineering and Computer Science 61*, 3 (2017), 238.

[49] Jørgensen, R. M., Abildstrøm, S. Z., Levitan, J., Kobo, R., Puzanov, N., Lewkowicz, M., Huikuri, H., Peltola, M., Haarbo, J., Thomsen, P. E. B., et al. Heart rate variability density analysis (dyx) and prediction of long-term mortality after acute myocardial infarction. *Annals of Noninvasive Electrocardiology 21*, 1 (2016), 60–68.

[50] Jumutc, V., and Suykens, J. A. K. Weighted coordinate-wise pegasos. In *Pattern Recognition and Machine Intelligence* (Berlin, Heidelberg, 2013), P. Maji, A. Ghosh, M. N. Murty, K. Ghosh, and S. K. Pal, Eds., Springer Berlin Heidelberg, pp. 262–269.

[51] Köhler, B. U., Hennig, C., and Orglmeister, R. The principles of software QRS detection. *IEEE Engineering in Medicine and Biology Magazine 21*, 1 (2002), 42–57.

[52] Kohno, R., Abe, H., and Benditt, D. G. Ambulatory electrocardiogram monitoring devices for evaluating transient loss of consciousness or other related symptoms. *Journal of arrhythmia 33*, 6 (2017), 583–589.

[53] Kolda, T. G., and Bader, B. W. Tensor decompositions and applications. *SIAM review 51*, 3 (2009), 455–500.

[54] Lagarias, J. C., Reeds, J. A., Wright, M. H., and Wright, P. E. Convergence properties of the Nelder–Mead simplex method in low dimensions. *SIAM Journal on optimization 9*, 1 (1998), 112–147.

[55] Laguna, P., Mark, R., Goldberg, A., and Moody, G. A database for evaluation of algorithms for measurement of QT and other waveform intervals in the ECG. In *Computers in Cardiology 1997* (1997), IEEE, pp. 673–676.

[56] Lang, R. M., Badano, L. P., Mor-Avi, V., Afilalo, J., Armstrong, A., Ernande, L., Flachskampf, F. A., Foster, E., Goldstein, S. A., Kuznetsova, T., et al. Recommendations for cardiac chamber quantification by echocardiography in adults: an update from the American Society of Echocardiography and the European Association of Cardiovascular Imaging. *Journal of the American Society of Echocardiography 28*, 1 (2015), 1–39.

[57] Lederman, Y. S., Balucani, C., Lazar, J., Steinberg, L., Gugger, J., and Levine, S. R. Relationship between QT interval dispersion in acute stroke and stroke prognosis: a systematic review. *Journal of Stroke and Cerebrovascular Diseases 23*, 10 (2014), 2467–2478.

[58] Lee, S. C. Using a translation-invariant neural network to diagnose heart arrhythmia. In *Advances in neural information processing systems* (1990), pp. 240–247.

[59] Li, Q., Rajagopalan, C., and Clifford, G. D. A machine learning approach to multi-level ECG signal quality classification. *Computer methods and programs in biomedicine 117*, 3 (2014), 435–447.

[60] Limaye, H., and Deshmukh, V. Ecg noise sources and various noise removal techniques: a survey. *International Journal of Application or Innovation in Engineering & Management 5*, 2 (2016), 86–92.

[61] Lin, C., Mailhes, C., and Tourneret, J.-Y. P-and T-wave delineation in ECG signals using a Bayesian approach and a partially collapsed Gibbs sampler. *IEEE Transactions on Biomedical Engineering 57*, 12 (2010), 2840–2849.

[62] Lin, C., Mailhes, C., and Tourneret, J.-y. T-wave Alternans Detection Using a Bayesian Approach and a Gibbs Sampler. *IEEE Engineering in Medicine and Biology Magazine 57*, 12 (2011), 5868–5871.

[63] Ma, Y., and Guo, G. *Support vector machines applications*. Springer, 2014.

[64] Madeiro, J. P., Nicolson, W. B., Cortez, P. C., Marques, J. A., Vázquez-Seisdedos, C. R., Elangovan, N., Ng, G. A., and Schlindwein, F. S. New approach for T-wave peak detection and T-wave end location in 12-lead paced ECG signals based on a mathematical model. *Medical Engineering and Physics 35*, 8 (2013), 1105–1115.

[65] Manriquez, A. I., and Zhang, Q. An algorithm for QRS onset and offset detection in single lead electrocardiogram records. In *Engineering in Medicine and Biology Society, 2007. EMBS 2007. 29th Annual International Conference of the IEEE* (2007), IEEE, pp. 541–544.

[66] Marek, M., and John, C. A. Task Force of the European Society of Cardiology: Heart rate variability standards of measurement, physiological interpretation, and clinical use. *Eur Heart J 17* (1996), 354–381.

[67] Maron, B. J., Friedman, R. A., Kligfield, P., Levine, B. D., Viskin, S., Chaitman, B. R., Okin, P. M., Saul, J. P., Salberg, L., Van Hare, G. F., et al. Assessment of the 12-lead Electrocardiogram as a Screening Test for Detection of Cardiovascular Disease in Healthy General Populations of Young People (12–25 years of age): A Scientific Statement From the American Heart Association and the American College of Cardiology. *Journal of the American College of Cardiology 64*, 14 (2014), 1479–1514.

[68] Martinek, R., Kahankova, R., Jezewski, J., Jaros, R., Mohylova, J., Fajkus, M., Nedoma, J., Janku, P., and Nazeran, H. Comparative effectiveness of ica and pca in extraction of fetal ecg from abdominal signals: Towards non-invasive fetal monitoring. *Frontiers in Physiology 9* (2018), 648.

[69] Martínez, A., Alcaraz, R., and Rieta, J. J. Application of the phasor transform for automatic delineation of single-lead ECG fiducial points. *Physiological measurement 31*, 11 (2010), 1467.

[70] Martínez, J. P., Almeida, R., Olmos, S., Rocha, A. P., and Laguna, P. A wavelet-based ECG delineator: evaluation on standard databases. *IEEE Transactions on Biomedical Engineering 51*, 4 (apr 2004), 570–581.

[71] Mcsharry, P. E., Clifford, G. D., Tarassenko, L., and Smith, L. A. A dynamical model for generating synthetic electrocardiogram signals. *Annual International Conference of the IEEE 0*, 2 (mar 2011), 5686–5689.

[72] Mehmet, Ü., Abdulkadir, S., Muammer, G., and Fikret, A. Performance comparison of wavelet thresholding techniques on weak ECG signal denoising. *Przeglad Dermatologicznyd Elektrotechniczny 89*, 5 (2013), 63–66.

[73] Monasterio, V., Laguna, P., Cygankiewicz, I., Vázquez, R., Bayés-Genís, A., Bayés De Luna, A., and Martínez, J. P. Average T-wave alternans activity in ambulatory ECG records predicts sudden cardiac death in patients with chronic heart failure. *Heart Rhythm 9*, 3 (2012), 383–389.

[74] Monitillo, F. Ventricular repolarization measures for arrhythmic risk stratification. *World Journal of Cardiology 8*, 1 (2016), 57.

[75] Moody, G. B., and Mark, R. G. The impact of the MIT-BIH arrhythmia database. *IEEE Engineering in Medicine and Biology Magazine 20*, 3 (2001), 45–50.

[76] Nachimuthu, S., Assar, M. D., and Schussler, J. M. Drug-induced QT interval prolongation : mechanisms and clinical management. *Therapeutic Advances in Drug Safety 3*, 5 (2012), 241–253.

[77] Nagueh, S. F., Smiseth, O. A., Appleton, C. P., Byrd, B. F., Dokainish, H., Edvardsen, T., Flachskampf, F. A., Gillebert, T. C., Klein, A. L., Lancellotti, P., et al. Recommendations for the evaluation of left ventricular diastolic function by echocardiography: an update from the American Society of Echocardiography and the European Association of Cardiovascular Imaging. *European Journal of Echocardiography 17*, 12 (2016), 1321–1360.

[78] Nelder, J. A., and Mead, R. A simplex method for function minimization. *The computer journal 7*, 4 (1965), 308–313.

[79] Nielsen, J., Wang, F., Graff, C., and Kanters, J. K. QT dynamics during treatment with sertindole. *Therapeutic Advances in Psychopharmacology 5*, 1 (2015), 26–31.

[80] Opie, L. H. *Heart physiology: from cell to circulation*. Lippincott Williams & Wilkins, 2004.

[81] Padierna, L. C., Carpio, M., Rojas, A., Puga, H., Baltazar, R., and Fraire, H. *Hyper-Parameter Tuning for Support Vector Machines by Estimation of Distribution Algorithms.* Springer International Publishing, Cham, 2017, pp. 787–800.

[82] Pandit, D., Zhang, L., Liu, C., Aslam, N., Chattopadhyay, S., and Lim, C. P. *Noise Reduction in ECG Signals Using Wavelet Transform and Dynamic Thresholding.* Springer Singapore, Singapore, 2017, pp. 193–206.

[83] Parsaei, H., Faraz, M., and Mortazavi, S. A multilayer perceptron neural network–based model for predicting subjective health symptoms in people living in the vicinity of mobile phone base stations. *Ecopsychology 9*, 2 (2017), 99–105.

[84] Pasala, T., Dettmer, M., Leo, P. J., Laurita, K. R., and Kaufman, E. S. Microvolt T-wave alternans amplifies spatial dispersion of repolarization in human subjects with ischemic cardiomyopathy. *Journal of Electrocardiology 49*, 5 (2016), 733–739.

[85] Pathak, A., Curnier, D., Fourcade, J., Roncalli, J., Stein, P. K., Hermant, P., Bousquet, M., Massabuau, P., Sénard, J. M., Montastruc, J. L., and Galinier, M. QT dynamicity: A prognostic factor for sudden cardiac death in chronic heart failure. *European Journal of Heart Failure 7*, 2 (2005), 269–275.

[86] Pedregosa, F., Varoquaux, G., Gramfort, A., Michel, V., Thirion, B., Grisel, O., Blondel, M., Prettenhofer, P., Weiss, R., Dubourg, V., Vanderplas, J., Passos, A., Cournapeau, D., Brucher, M., Perrot, M., and Duchesnay, É. Scikit-learn: Machine Learning in Python. *Journal of Machine Learning 12*, Oct (2011), 2825–2830.

[87] Perakakis, P., Joffily, M., Taylor, M., Guerra, P., and Vila, J. Kardia: A matlab software for the analysis of cardiac interbeat intervals. *Computer methods and programs in biomedicine 98*, 1 (2010), 83–89.

[88] Pichot, V., Roche, F., Celle, S., Barthélémy, J.-C., and Chouchou, F. Hrvanalysis: a free software for analyzing cardiac autonomic activity. *Frontiers in physiology 7* (2016), 557.

[89] Plas, G. J., Bos, J., Velthuis, B. O., Scholten, M. F., den Hertog, H. M., and Brouwers, P. J. Diagnostic yield of external loop recording in patients with acute ischemic stroke or tia. *Journal of neurology 262*, 3 (2015), 682–688.

[90] Podd, S. J., Sugihara, C., Furniss, S. S., and Sulke, N. Are implantable cardiac monitors the 'gold standard'for atrial fibrillation detection? a prospective randomized trial comparing atrial fibrillation monitoring using implantable cardiac monitors and dddrp permanent pacemakers in post atrial fibrillation ablation patients. *EP Europace 18*, 7 (2015), 1000–1005.

[91] Pueyo, E., Smetana, P., Caminal, P., De Luna, A. B., Malik, M., and Laguna, P. Characterization of QT interval adaptation to RR interval changes and its use as a a risk-stratifier of arrhythmic mortality in amiodarone-treated survivors of acute myocardial infarction. *IEEE Transactions on Biomedical Engineering 51*, 9 (2004), 1511–1520.

[92] Quesada, G. P., Ortega, A. M., López, L. A., Martínez, E. P., Torralba, M., Gutiérrez, C. H., Hernández, J. M., Aranda, P. H., Zapata, M. R., and De Tena, J. G. Lower heart rate variability assessed by 24-hour ambulatory blood pressure monitoring is associated with left ventricular hypertrophy. *Journal of Hypertension 34* (2016), e208.

[93] Rao, K. R., and Yip, P. *Discrete cosine transform: algorithms, advantages, applications*. Academic press, 2014.

[94] Riad, F. S., Davis, A. M., Moranville, M. P., and Beshai, J. F. Drug-Induced QTc Prolongation. *American Journal of Cardiology 119*, 2 (2017), 280–283.

[95] Rodríguez-Liñares, L., Lado, M., Vila, X., Méndez, A., and Cuesta, P. gHRV: Heart rate variability analysis made easy. *Computer Methods and Programs in Biomedicine 116*, 1 (2014), 26–38.

[96] Rodríguez-Liñares, L., Méndez, A., Lado, M., Olivieri, D., Vila, X., and Gómez-Conde, I. An open source tool for heart rate variability spectral analysis. *Computer Methods and Programs in Biomedicine 103*, 1 (2011), 39–50.

[97] Romigi, A., Albanese, M., Placidi, F., Izzi, F., Mercuri, N. B., Marchi, A., Liguori, C., Campagna, N., Duggento, A., Canichella, A., et al. Heart rate variability in untreated newly diagnosed temporal lobe epilepsy: Evidence for ictal sympathetic dysregulation. *Epilepsia 57*, 3 (2016), 418–426.

[98] Sankar, P., and Cyriac, M. A non-invasive approach for the diagnosis of Type 2 diabetes using HRV parameters. *International Journal of Biomedical Engineering and Technology 26*, 1 (2018), 71–83.

[99] Sassi, R., Cerutti, S., Lombardi, F., Malik, M., Huikuri, H. V., Peng, C.-K., Schmidt, G., Yamamoto, Y., Reviewers:, D., Gorenek, B., et al. Advances in heart rate variability signal analysis: joint position statement by the e-cardiology esc working group and the european heart rhythm association co-endorsed by the asia pacific heart rhythm society. *EP Europace 17*, 9 (2015), 1341–1353.

[100] Savas, B., and Eldén, L. Handwritten digit classification using higher order singular value decomposition. *Pattern recognition 40*, 3 (2007), 993–1003.

[101] Sharif, H., O'Leary, D., and Ditor, D. Comparison of QT-interval and variability index methodologies in individuals with spinal cord injury. *Spinal Cord 55*, 3 (2017), 274–278.

[102] Sidiropoulos, N. D., Bro, R., and Giannakis, G. B. Parallel factor analysis in sensor array processing. *IEEE transactions on Signal Processing 48*, 8 (2000), 2377–2388.

[103] Sidiropoulos, N. D., De Lathauwer, L., Fu, X., Huang, K., Papalexakis, E. E., and Faloutsos, C. Tensor decomposition for signal processing and machine learning. *IEEE Transactions on Signal Processing 65*, 13 (2017), 3551–3582.

[104] Sidiropoulos, N. D., Giannakis, G. B., and Bro, R. Blind PARAFAC receivers for DS-CDMA systems. *IEEE Transactions on Signal Processing 48*, 3 (2000), 810–823.

[105] Simakov, A., and Webster, J. Motion artifact from electrodes and cables.

[106] Simova, I., Christov, I., and Bortolan, G. A review on electrocardiographic changes in diabetic patients. *Current diabetes reviews 11*, 2 (2015), 102–106.

[107] Singh, B., and Bharti, N. Software tools for heart rate variability analysis. *International Journal of Recent Scientific Research 6*, 4 (2015), 3501–3506.

[108] Sörnmo, L., and Laguna, P. *Bioelectrical signal processing in cardiac and neurological applications*, vol. 8. Academic Press, 2005.

[109] Stein, P. K., Barzilay, J. I., Chaves, P. H., Domitrovich, P. P., and Gottdiener, J. S. Heart rate variability and its changes over 5 years in older adults. *Age and ageing 38*, 2 (2009), 212–218.

[110] Stoickov, V., Ilic, M. D., Stoickov, M., Tasic, I., Nikolic, M., and Mitic, S. The impact of hypertension on QT dispersion and echocardiographic parameters in patients with angina pectoris. *Journal of Hypertension 35* (2017), e117–e118.

[111] Suárez-León, A., Varon, C., Goovaerts, G., Vázquez-Seisdedos, C., and Van Huffel, S. Irregular heartbeat detection using sequentially truncated multilinear singular value decomposition. In *Computing in Cardiology* (2017), vol. 44.

[112] Suárez-León, A., Varon, C., Willems, R., Van Huffel, S., and Vázquez-Seisdedos, C. T-wave end detection using neural networks and Support Vector Machines. *Computers in Biology and Medicine 96* (2018), 116–127.

[113] Suárez León, A. A., Goovaerts, G., Seisdedos, C. R. V., and Van Huffel, S. Irregular heartbeats detection using tensors and support vector machines. In *Computing in Cardiology Conference (CinC), 2016* (2016), IEEE, pp. 1037–1040.

[114] Suárez León, A. A., Molina, D. M., Vázquez Seisdedos, C. R., Goovaerts, G., Vandeput, S., and Van Huffel, S. Neural network approach for T-wave end detection: A comparison of architectures. In *Computing in Cardiology* (2015), vol. 42, IEEE, pp. 589–592.

[115] Suji, R. J., and Rajagopalan, S. A novel hybrid system for diagnosing breast cancer using Fuzzy Rough Set and LS-SVM. *Research Journal of Applied Sciences, Engineering and Technology 10*, 1 (2015), 49–55.

[116] Suykens, J. A. K., Gestel, T. V., Brabanter, J. D., Moor, B. D., and Vandewalle, J. *Least Squares Support Vector Machines*. World Scientific Pub. Co., 2002.

[117] Suykens, J. A. K., and Vandewalle, J. Least Squares Support Vector Machine Classifiers. *Neural Processing Letters 9 9*, 3 (1999), 293–300.

[118] Tarvainen, M. P., Niskanen, J.-P., Lipponen, J. A., Ranta-Aho, P. O., and Karjalainen, P. A. Kubios HRV–heart rate variability analysis software. *Computer Methods and Programs in Biomedicine 113*, 1 (2014), 210–20.

[119] Teresa, G. M. Maximum likelihood clustering with outliers. In *Classification, Clustering, and Data Analysis*. Springer, 2002, pp. 247–255.

[120] Teresa, G. M., and Gunter, R. A robust method for cluster analysis. *Annals of Statistics* (2005), 347–380.

[121] Tong, D., Bartels, K., and Honeyager, K. Adaptive reduction of motion artifact in the electrocardiogram. In *Engineering in Medicine and Biology, 2002. 24th Annual Conference and the Annual Fall Meeting of the Biomedical Engineering Society EMBS/BMES Conference, 2002. Proceedings of the Second Joint* (2002), vol. 2, IEEE, pp. 1403–1404.

[122] Trimmel, K., Sacha, J., and Huikuri, H. V. *Heart rate variability: Clinical applications and interaction between HRV and heart rate*. Frontiers Media SA, 2015.

[123] Übeyli, E. D. ECG beats classification using multiclass support vector machines with error correcting output codes. *Digital Signal Processing: A Review Journal 17*, 3 (2007), 675–684.

[124] Van Gestel, T., Suykens, J. A. K., Lanckriet, G., Lambrechts, A., De Moor, B., and Vandewalle, J. Bayesian framework for least-squares support vector machine classifiers, Gaussian processes, and kernel Fisher discriminant analysis. *Neural computation 14*, 5 (2002), 1115–1147.

[125] Vannieuwenhoven, N., Vandebril, R., and Meerbergen, K. A New Truncation Strategy for the Higher-Order Singular Value Decomposition. *SIAM Journal on Scientific Computing 34*, 2 (2012), A1027–A1052.

[126] Vázquez-Seisdedos, C., Suárez-León, A., and Evangelista-Neto, J. *A comparison of different classifiers architectures for electrocardiogram artefacts recognition*, vol. 8259 LNCS. 2013.

[127] Vázquez-Seisdedos, C. R., Neto, J. E., Marañón Reyes, E. J., Klautau, A., and Limão de Oliveira, R. C. New approach for T-wave end detection on electrocardiogram: Performance in noisy conditions. *BioMedical Engineering Online 10*, 1 (2011), 1.

[128] Vila, J. A., Gang, Y., Rodríguez Presedo, J. M., Fernández-Delgado, M., Barro, S., and Malik, M. A new approach for TU complex characterization. *IEEE Engineering in Medicine and Biology Magazine 19*, 3 (2000), 764–772.

[129] Wiens, J., and Guttag, J. V. Active learning applied to patient-adaptive heartbeat classification. In *Advances in neural information processing systems* (2010), pp. 2442–2450.

[130] Wilkins, L. ECG interpretation made incredibly easy, 2005.

[131] Williams, C., and Seeger, M. W. Using the Nyström method to speed up kernel machines. In *NIPS Proceedings* (2001), vol. 13, pp. 682–688.

[132] World Health Organization, W. Top 10 Cause of Death Worlwide, jan 2017.

[133] Wulsin, L. R., Horn, P. S., Perry, J. L., Massaro, J. M., and D'agostino, R. B. Autonomic imbalance as a predictor of metabolic risks, cardiovascular disease, diabetes, and mortality. *The Journal of Clinical Endocrinology & Metabolism 100*, 6 (2015), 2443–2448.

[134] Xavier-de Souza, S., Suykens, J. A. K., Vandewalle, J., and Bollé, D. Coupled Simulated Annealing. *IEEE Trans. On Systems, Man, And Cybernetics-Part B: Cybernetics 40*, 2 (2010), 320–335.

[135] Yap, Y. G., and Camm, A. J. Drug induced QT prolongation and torsades de pointes. *Heart 89*, 11 (2003), 1363–1372.

[136] Yperzeele, L., van Hooff, R.-J., Nagels, G., De Smedt, A., De Keyser, J., and Brouns, R. Heart rate variability and baroreceptor sensitivity in acute stroke: A systematic review. *International Journal of Stroke 10*, 6 (2015), 796–800.

[137] Zaręba, W. Drug induced QT prolongation. *Cardiology Journal 14*, 6 (2007), 523–533.

[138] Zhang, Q., Manriquez, A. I., Médigue, C., Papelier, Y., and Sorine, M. An algorithm for robust and efficient location of t-wave ends in electrocardiograms. *IEEE Transactions on Biomedical Engineering 53*, 12 (2006), 2544–2552.

[139] Zifan, A., Saberi, S., Moradi, M. H., and Towhidkhah, F. Automated ECG segmentation using piecewise derivative Dynamic Time Warping. *International Journal of Biological and Life Sciences 1*, 3 (2005), 181–185.

Curriculum

Alexander Alexeis Suárez León received the degree in automation engineering and the M.Sc. degree on biomedical engineering both from the Universidad de Oriente, Santiago de Cuba, Cuba in 2008 and 2013 respectively. He started the PhD at KU Leuven in January 2016. His research interests include machine learning and tensor methods applied to biomedical signal processing.

List of publications

Papers in international journals

Suárez-León A.A, Varon C., Willems R., Van Huffel S. and Vázquez-Seisdedos C.R. (2018) T-wave end detection using neural networks and Support Vector Machines. Computers in Biology and Medicine, 2018, 96, 116-127.

Suárez-León A.A, Varon C., Willems R., Van Huffel S. and Vázquez-Seisdedos C.R. (2018) PyECG: A software tool for the analysis of the QT interval in the electrocardiogram, Cuban Journal of Electronic Engineering, Automation and Communications (RIELAC in spanish) (accepted for publication).

Papers in proceedings of international conferences

Suárez-León A. A., Matos Molina D., Goovaerts G., Vazquez Seisdedos C. R., Vandeput S. and Van Huffel S. Neural network approach for T-wave end detection: A comparison of architectures. Proceedings Computing in Cardiology, vol 42, 2015, Nice, France, Sept 6-9, IEEE.

Suárez-León A. A., Goovaerts G. , Vazquez Seisdedos C. R. and Van Huffel S. Irregular Heartbeats Detection Using Tensors and Support Vector Machines. Proceedings Computing in Cardiology, vol 43, 2016, Vancouver, Canada, Sept 11-14, IEEE.

Suárez-León A.A, Varon C., Goovaerts G., Vázquez Seisdedos C.R. and Van Huffel S. Irregular Heartbeats Detection Using Sequentially Truncated Multilinear Singular Value Decomposition, Proceedings Computing in Cardiologyy, vol 44, 2017, Rennes, France, Sept 24-27, IEEE.



FACULTY OF ENGINEERING SCIENCE
DEPARTMENT OF ELECTRICAL ENGINEERING
STADIUS
Kasteelpark Arenberg 10 box 2446
B-3001 Leuven
aasl@uo.edu.cu